1-1-2012

3-Dimensional Intracortical Neural Interface For The Study Of Epilepsy

Jessin Koshy John
Wayne State University,

3-DIMENSIONAL INTRACORTICAL NEURAL INTERFACE FOR THE STUDY OF EPILEPSY

by

JESSIN KOSHY JOHN

DISSERTATION

Submitted to the Graduate School

of Wayne State University,

Detroit, MI

in partial fulfillment of the requirements

for the degree of

DOCTOR OF PHILOSOPHY

2014

MAJOR: ELECTRICAL ENGINEERING

Approved by:

_____

Advisor Date

_____

_____

_____

_____

DEDICATION

To my Savior,
To whom I owe everything,
Jesus, the Son of God

and

to my wife, Soumya, and all of my family who always supported me with their never ceasing encouragement and prayer

ACKNOWLEDGEMENTS

I am grateful beyond words for my advisor, Dr. Yong Xu, for his encouragement, support, and discipline at times. His constant motivation and his immense expertise in the field have always been an inspiration to me. He continues to be my role model in whom I would like to evolve into as a researcher. I also sincerely appreciate the advice and assistance of all my committee members, Dr. Jeffrey Loeb, Dr. Amar Basu, Dr. Mark Ming-Cheng Cheng, and Dr. Hazem Eltahawy. Their wisdom and insight truly helped refine my research strategies and develop a good project. I express my sincere gratitude to all my lab mates, Dr. Yuefa Li, Hongen Tu, Eric Kim, Yating Hu, and Qinglong Zheng, Daniel Barkmeier, and Danielle Senador. Throughout the years they have assisted me in my research in countless ways and were always willing to give me advice. Thanks to all the DLAR staff as well, especially Susie, for all their care and assistance.

I am filled with gratitude for my friends and family for their love, prayers, and support throughout the years. Regardless of the challenges that I faced, I never faced them alone. I am grateful to my parents, Koshy and Annamma John, for their constant devotion throughout my life. I am grateful to my wife's parents, Sunny and Susan Mathews, for supplying joy and hope in the midst of my challenges. I am grateful to my siblings, Jobin, Becky, Justin, and Selina John, for their constant support and encouragement. I am grateful for my best friends, Alan and Ann Thomas, for bringing laughter and joy in the midst of my trials. Most importantly, I am grateful to my wife, Soumya John. She has strengthened me, motivated me, enlightened me, and unconditionally loved me throughout our relationship. Without her, I am nothing. To her, I owe everything. I am excited to see what comes along in our journey together.

TABLE OF CONTENTS

LIST OF FIGURES

CHAPTER 1: BACKGROUND

Of all the most powerful computing tools available to man, none surpasses the power of the human brain. Even to the current day, no technology has been created which matches the complexity and speed at which the human brain operates. The computing power of the brain comes from cells within the brain known as neurons. Although various categories of neurons exist, they are common in an important respect – they all receive and send signals via changes in membrane potential (voltage). In spite of this generalization, just one neural signal may be passed through countless associated neuronal connections. Given the sheer complexity of the human brain, diseases related to the brain are often among the most difficult to treat. In spite of the challenges, mankind has made and continues to make great strides towards building understanding of the various functional regions and interconnections of the brain. New technologies are allowing observation of brain function at the molecular and sub-molecular level. As technology continues to improve, so improves the opportunity for elucidation of the underlying causes of neurological diseases. One such disease that has yet to be fully understood is the disease known as epilepsy.

1.1 About Epilepsy

Epilepsy is a disorder of the central nervous system which is characterized by recurrent, unprovoked seizures. Seizures are abnormal central nervous system events in which groups of neurons suddenly fire synchronously, often impairing the individual. Patients with epilepsy carry a significant burden as seizures often occur unexpectedly.

10% of the population is affected by convulsive disorders and the incidence of epilepsy is as high as 3% of the population [1]. Single gene defects in ion channels or neurotransmitter receptors have been shown to be associated with some inherited forms of epilepsy [2-4]; however the majority of epilepsy cases are idiopathic. In epilepsy patients with partial complex seizures, seizures are often found to originate at focal brain regions that often have no histopathological abnormalities [5]. Of these patients, those who are not successfully treated with medications often find great benefit in resection of the epileptic focus. While in young patients the epileptic focus is usually found within the neocortex, in adults the epileptic focus is often within the hippocampus [6]. Why these often normal-appearing regions become or remain epileptic is still largely undetermined. However, cases with neocortical foci are often characterized by a similar electrophysiological pattern of localized, often rhythmic, electrical discharges which can spread to other brain regions, thus resulting in clinical seizures. Between clinical seizures (also known as ictal events), the epileptic foci generate unique, localized "interictal" discharges that often, but not always correspond to regions of seizure onset and therefore can sometimes allow neurologists and neurosurgeons to identify the abnormal epileptic regions [7]. Clinical studies are being undertaken to determine the electrical and spatial relationship between the latency and frequency of interictal discharges in relation to ictal-onset zones as well as their relationship to post-surgical outcome. As a means to understand the molecular underpinnings of focal epilepsy, genes have been identified which are consistently induced at these foci, regardless of the underlying cause [8]. Induction of these genes has been found to be highly activity-dependent and the magnitude of induction seems to correlate more with interictal activity rather than ictal

activity [9]. These observations have led to the desire to investigate interictal activity and how these regions become epileptic.

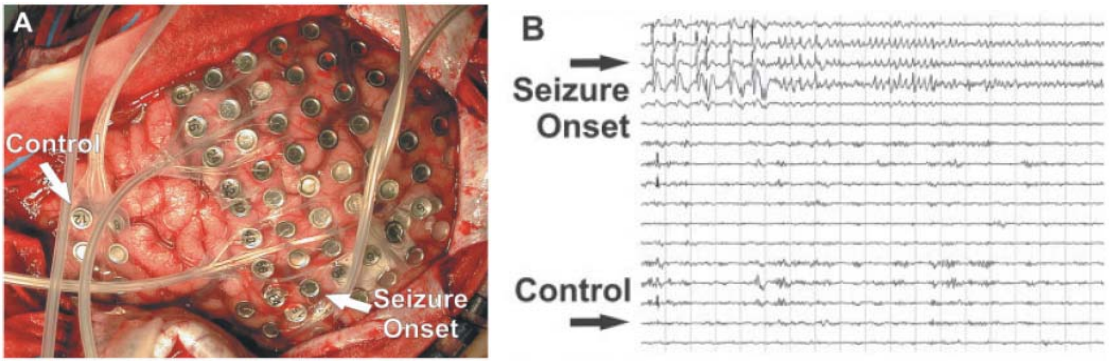

Figure 1-1: Electrocorticogram (ECoG) recording of epileptic cortex. (A) flat 1cm diameter electrodes arranged in an evenly spaced grid are placed on the suspected epileptogenic region of cortex with a control electrode placed at a region of non-epileptic cortex; (B) the respective neural signals acquired by the electrodes demonstrate high spiking activity at the seizure onset electrode and lack of high spiking neural signals at the control electrode [8]

1.2 Rat Model of Epilepsy

In human epileptic tissue studies, genes encoding neurotransmitter receptors, ion channels, transcription factors, and neurotrophic factors have been found to have altered expression patterns in comparison to normal neural tissue [10-18]. Many of these molecular markers can be identified through immunoflourescence studies thus allowing visualization of the spatial progression and development of an epileptic focus. These markers have been identified to be activated specifically in cortical lamina II and III with sharp lateral borders within the cortex. These findings suggests that increased lateral connectivity, known to be prominent within cortical layers II and III, may be the structural basis of the epileptic discharge in human neocortex. In an effort to correlate these molecular changes to real-time electrical potentials, rat models of epilepsy have been designed and utilized. In the animal model of epilepsy described by Jefferys and others [19-21], tetanus toxin is injected into the somatosensory cortex of the rat to

produce a minimally damaging lesion with predominantly interictal spikes, and occasional seizures. In the study in Figure 1-2 [22], tetanus toxin (100ng dissolved in 1 microliter of .01M Sodium Phosphate) was injected into the somatosensory cortex and screw electrodes were implanted along both hemispheres (Figure 4a). Within one week, interictal discharges were seen at the injection site (Figure 4b). Over a span of 20 days, interictal spike frequency and amplitude increased selectively (when compared to vehicle injections) at the location of the cortex treated by tetanus toxin (Figure 4c). Eventually, the interictal activity transformed into secondarily generalized focal seizures. Rats were sacrificed and analyzed histologically for activation of CREB (Cyclic AMP Response Element Binding protein) and NARP (a synaptic organizing protein), which demonstrated increased activation of both molecules in layers 2/3 (Figure 4d and Figure 4e) as seen in human studies.

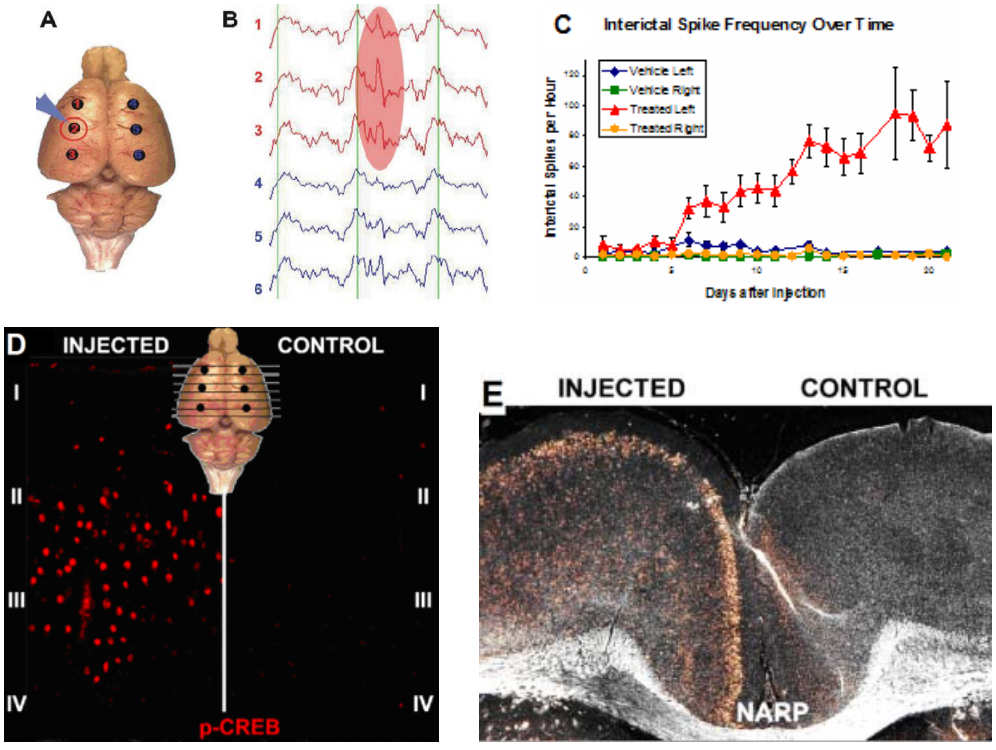

Figure 1-2: (A) Injection of tetanus toxin into the left somatosensory cortex (blue arrow) is followed by the placement of 6 skull-based screw electrodes at the indicated positions. (B) Within one week, small

interictal discharges can be detected with an expected electrical field centered over the injections site (pink oval). (C) The interictal discharge frequency increases selectively at the injection site. (D) Induction of pCREB on the left, spiking side is seen in layers 2/3 just as in human epiletpic neocortex. (E) NARP activation is seen in these same neuronal lamina, but does not cross the midline [22].

Although much information has been gained from the rat model of epilepsy and the corresponding molecular studies, much is still to be understood. The screw electrodes utilized to record interictal discharges have provided lateral information on the spread of epilepsy, thereby allowing correlation between the spread of interictal discharges and associated changes for molecular markers. Due to the rat model of epilepsy, it is now known that areas of interictal activity have increases in synaptic plasticity molecules such as CREB and NARP along layers 2 and 3 of the cortex. It is now important to know how interictal spiking actually changes from single to poly spiking to focal generalized seizures within these focal regions of interictal activity. Based on the prior studies of molecular markers, it is hypothesized that interictal activity at least initiates propagation to adjacent layers of cortex through layers 2/3 of the cortex. From layers 2/3, interictal spiking may then spread upward toward the surface of the cortex or downwards to deeper cortical layers. To demonstrate this, a new technology must be designed that will allow elucidation of the interictal spiking region to map out the spread of ictal activity. Using Microelectromechanical Systems (MEMS) technology, devices can be designed that will allow more in-depth analysis of cortical signals in the epileptic rat model.

1.3 MEMS Technology

Microelectromechanical Systems (MEMS) are micro-scale devices that have the capability to perform electrical and mechanical functions. MEMS devices have revolutionized the analytical chemical industry with the advent of micro total analysis

system (μTAS) microchips, also known as "lab on a chip", which is a device that is able to perform chemical reactions, separation, and chemical analysis on a single microchip. One of the earlier demonstrations of such a miniaturized analytical microfluidic device was developed in 1975 in an effort to create a portable gas chromatography device [23]. This first device included an injector valve, a separation column, and a thermal detector. Later, in the late 80's and early 90's, various groups started to develop micropumps, microvalves, and microreserviors [24]. The "lab on chip" technology later extended to the fields of the life sciences through DNA isolation functions, protein preparation, cell sorting, and even cell culturing [25, 26].

Extending further, devices have been made across all fields of medicine including an artificial "pancreatic tooth" design [27] and an artificial nephron system [28]. For a comprehensive review of various artificial devices created using MEMS technology, refer to a review article published by Dr. Mark Staples in the journal of pharmaceutical research [29]. Along this trend to develop devices suited toward the fields of medicine, many groups have desired to create artificial neural prosthesis devices. MEMS (Microelectromehcanical Systems) technology has several unique advantages for the fabrication of neural probes. First, photolithography enables precise definition of electrode size, shape, and position. With MEMS technology, multiple recording/stimulation sites can be fabricated on a single probe shank. MEMS also enable the integration of other microstructures, such as microchannels for direct chemical delivery to neural tissues. In addition, the batch fabrication capability of MEMS may lower the unit-cost of neural probes. These are some of the reasons why MEMS neural

probes, including the well-known Michigan probes and Utah electrodes, have been extensively researched in the last two decades [30-52].

1.4 Neural Devices

Two of the more common modalities of neural probes include KCl-filled glass micropipette probes and metal-wire probes [52]. Both have been used extensively within the neurological sciences resulting in leaps in our understanding of the nervous system. However, both technologies have limitations. The glass micropipette probes have characteristic high impedances, resulting in poor recording potential, and are limited in ability to generate multiple recording sites. The metal-wire probes, which are used in deep brain stimulation, are limited to only one electrode per wire. Although wire bundles can be produced, the possible configurations are limited and 3D configurations are poorly reproducible. MEMS-based neural probes are a more recently developed modality of neural probe design. Many current studies on MEMS-based neural probes address the concept of restoring sensation and motor function to patients with spinal cord lesions. Unlike other neural probe designs such as metal-wire probes [52], MEMS probe electrodes can be produced via photolithography, thereby allowing multiple electrodes on multiple shanks of various shapes, positions, and dimensions. In addition, MEMS processes are Integrated-Chip (IC) compatible allowing for the integration of various chip components such as on-board amplifiers and multiplexers. This can allow for recording of numerous arrays of electrodes and high signal-to-noise ratios. Microchannels can also be integrated via MEMS processes to allow for chemical delivery of various compounds.

MEMS devices can be batch fabricated thus lowering costs and enhancing reproducibility.

The initial Michigan probe developed in 1990 was a single probe shank with multiple stimulating sites [53]. The goal of the probe was to improve upon the conventional wire electrode. The probe was fabricated using MEMS development techniques such as a micromachined silicon substrate and deposition of dielectric thin films. The exposed stimulating sites were composed of Iridium oxide, a material which is biocompatible, capable of delivering high charge densities, and compatible with the probe production process. A long term goal of this project was to develop this probe for use in neural prostheses.

Along with the goal of developing a neural prosthesis, a device was desired that would allow high density recording or stimulation of deeper structures of the brain. With this desire in mind, the Utah group developed the Utah probe in 1991 [36]. The initial Utah probe was composed of 100 penetrating electrodes which were each 1.5 mm long and sharpened at their tips (to facilitate cortical penetration). In addition, the sharpened tips were coated with platinum to facilitate charge transfer to the neural tissue. In contrast to the development of the Michigan probe, the Utah probe is produced from a silicon block through a process of thermomigration (alters the organization of the silicon material atomic structure) and guided chemical etching.

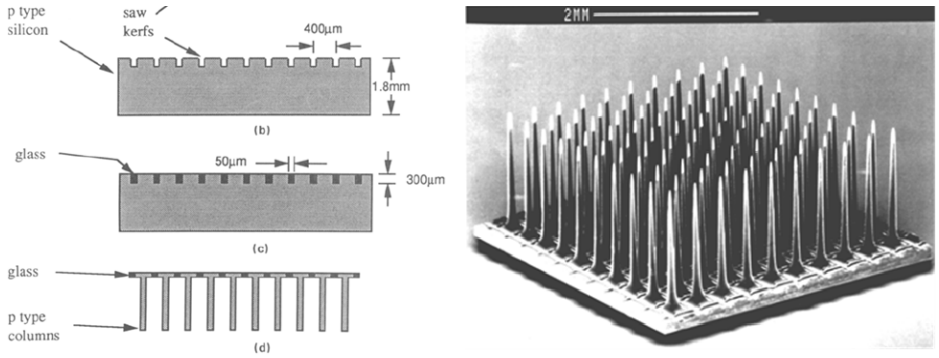

Figure 1-3: Utah Electrode Array Fabrication Scheme [54] and SEM image [55]

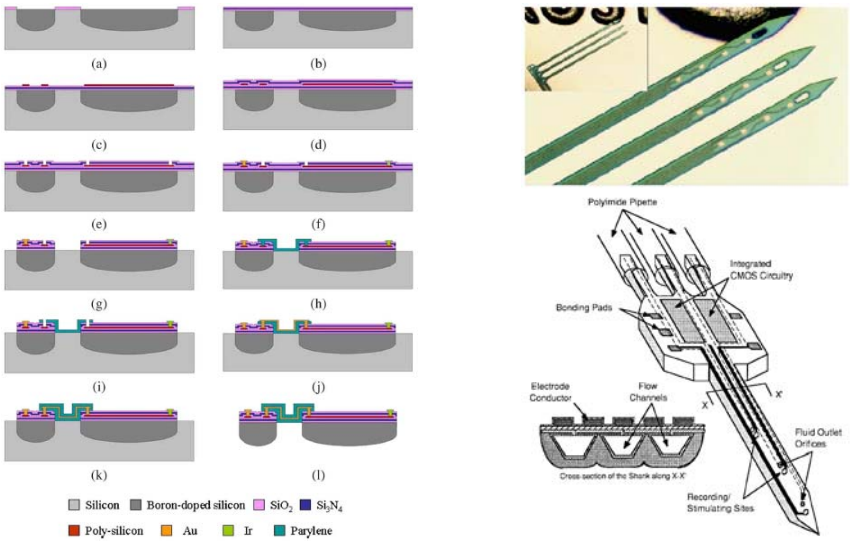

Figure 1-4: Michigan Electrode Array fabrication scheme [56], optical microscope image [56], and design layout for microfluidic Michigan electrode array [57].

In later works, the Michigan group continued to add features to their neural probe design. One important feature that was added was the application of microfluidic channels to their probes [57]. The microfluidic channels are constructed through wet anisotropic etching and sequential boron doping, thermal oxidation, and dielectric thin film deposition. Further improvements Michigan has worked on include integrated in-line flow meters (via an integrated thermal sensor) for detection of the rate of drug release [58] and the concept of hydrogel-filled microwells as a short-term alternative to microchannel delivery of drugs [59]. In addition to drug delivery, studies have been

conducted to develop flexible neural devices. In 2001 developed a completely flexible polyimide-based intracortical electrode array [48]. Due to its flexible nature, the probe was capable of folding into a 3-dimensional structure. Unfortunately, the drawback of this ultra-flexible probe design was that the probes were too soft to penetrate the pia mater thereby requiring the pia mater to be cut before insertion of the probe. In addition, although the probe was incorporated with microwells, additional design capabilities were limited due to the ability to utilize silicon-based MEMS fabrication techniques.

1.5 Smart Skins

Utilizing the flexible nature of polyimide, Dr. Tai and Dr. Jiang in 1997 demonstrated a flexible MEMS technology that incorporated the idea of several silicon islands connected by a polyimide film (skin) [60]. It was developed for use in aerodynamics studies as a shear stress sensor. The process starts with wet etching of the backside of a silicon wafer to reduce the silicon to a desired thickness. Then, aluminum is evaporated onto the front side of the wafer followed by polyimide spin coating which completely covers the aluminum layer. Next a process known as reactive ion etching (RIE) is performed on the backside of the wafer to completely remove the underlying silicon substrate at locations defined by a mask. Finally, polyimide is spin coated on the backside of the wafer thereby surrounding the exposed aluminum layer with polyimide on both sides. To release the probes from the wafer, the probe is simply cut off with a razor blade.

Unlike current technologies at the time, this flexible sensor was capable of being folded and taped to a semi-cylindrical delta wing [61, 62]. The capabilities of the device were further extended by combining the sensor skin with an integrated circuit (IC) containing on-skin bias circuits, amplifiers, and multiplexers [63]. Entering into the medical field, in 2003 a tactile sensor skin was produced using the smart skin technology [64]. This device, which also uses strain sensors, was produced with the aim of providing a sensation of touch. Another medical application of the smart skin technology was the development of wearable respiratory rate sensors. The respiratory rate was detected using integrated accelerometers located on the silicon islands [65]. Through these smart-skin studies, it was understood that flexible devices could be created by starting with silicon based devices coated with a polymer, and etching away the silicon leaving a device with a polymer base. These studies paved the concept behind the modality for creation of a true 3D neural device.

1.6 3D Neural Devices

There is an increasing need for 3D arrays of high-density electrodes because of the 3D nature of the nervous system. However, practical 3D neural probes have not yet been realized. The micro-wire and Utah array neural probes are both 2-dimensional by nature and the 3D Michigan probe is complicated and difficult to reproduce. As mentioned before, the 3D versions of Michigan probes were realized by microassembling multiple planar chips on a silicon platform with the help of vertical and horizontal spacers [56]. 3D neural probes were also constructed by stacking discrete 2D devices [52, 66]. Polymer 3D electrode arrays were developed by bending the polymer shanks out of the

plane [47, 48]. The NeuroProbes consortium of the European Union reported a 3D technology by slotting planar 2D devices into cavities on a silicon backbone [67]. The electrical contact was made using gold clips hanging over the edge of the cavities. In spite of the multiple studies done to develop 3D devices, the use of 3D devices is limited due to challenges in assembly and packaging of the devices. A reliable 3D device package is difficult to reproduce thus making mass production expensive and burdensome.

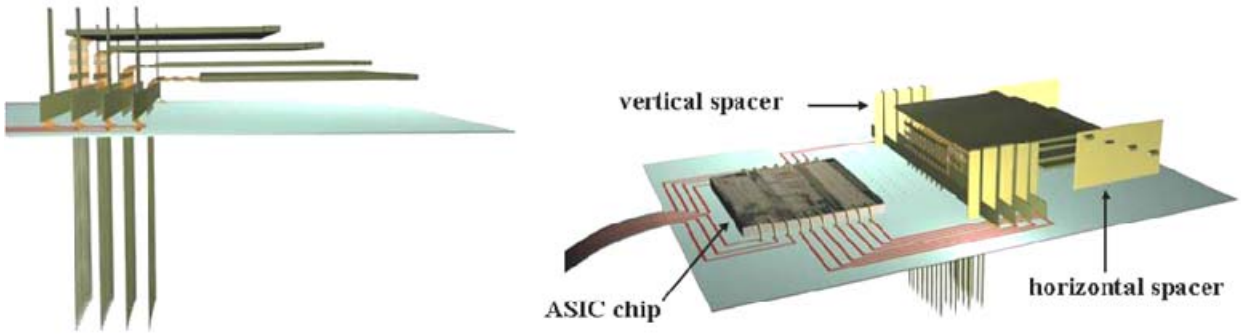

Figure 1-5: 3D stacking of Michigan electrode array design schematic [56]

In addition to the desire to produce reliable 3D neural devices, many groups are realizing the need to have microfluidic channels which are integrated with the neural electrode sites to allow for targeted fluidic drug delivery. As a result, many attempts have been made to implement microfluidic channels along with electrodes. One group demonstrated electrodes and solid state channels using anisotropic silicon etching, boron etch stop, and thermal oxidation/LPCVD (low pressure chemical vapor deposition) sealing [57]. This device was implanted in the guinea pig superior/inferior colliculus in an effort to acutely monitor electrical reaction of neurons to various chemicals. Another group demonstrated microfluidic channels on silicon-on-insulator (SOI) wafers [68].

Other groups have demonstrated polymer microchannels [49, 69]. However, 3D microfluidic channel implementation has not been demonstrated most likely due to the fact that routing of microchannels in 3D space is difficult to achieve.

In this work, a novel technology for developing 3D neural probes based on a silicon island structure and a simple folding procedure has been developed. Some preliminary results have been presented in prior works [70-72]. This technology enables several highly desirable features. First, it provides a simple and reliable method to fabricate and assemble high-density 3D arrays of electrodes. Second, this technology enables the integration of microchannels with 3D arrays of electrodes for localized fluidic drug delivery. In addition, this technology allows the easy incorporation of a flexible cable between probe shanks and the interfacing die, which leads to very low-profile implants and helps to reduce the movement between brain tissue and probes [30]. In addition, the flexible cable allows production of a more stable 3D neural device package. The fabrication process is also post-CMOS compatible, allowing the monolithic integration of CMOS (complementary metal oxide semiconductor) circuits with neural probes using economic post-CMOS process. These important features will make the developed devices a valuable tool for various neural prostheses and neural disorder studies/treatments.

CHAPTER 2: DESIGN

2.1 Introduction

The design of the neural probe devices was a multi-step approach consisting of several different device designs with a variety of desirable features. As the project progressed, better ideas and new features were implemented to enhance the functionality of the devices. The various designs will be discussed in addition to the rationale behind the design and problems encountered with each design. Device fabrication and packaging results including optical images of the various devices will be discussed in more detail in later chapters.

2.2 Folding Neural Probe Technology

The basic premise of this new technology is that devices can be created in such a way that portions of the device can be made completely flexible via etching away of any rigid portions of the device (such as silicon) while leaving the flexible portions of the device (such as Parylene or thin layers of gold). The new neural probe technology is schematically illustrated in Fig. 4. First, planar devices consisting of multiple silicon islands are fabricated on a Si (silicon) wafer using conventional MEMS technology and a flexible skin process [73-75]. Note that in addition to electrodes and microchannels, other microstructures such as reservoirs, valves, and pumps can all be fabricated using conventional MEMS processes. In Fig. 4, the top three silicon islands are actually 2D neural probe devices, each of which carries a 2D electrode array and drug delivery ports.

The electrodes and microchannels on different islands can be accessed by the bonding pads and inlet ports on the bottom silicon island. These silicon islands are connected by a parylene C layer, in which metal interconnects and microchannels are embedded. Parylene C is widely used for implantable devices due to its good biocompatibility.

The procedure of assembling the planar device into 3D probes is shown in Figure 2-1. First, island 1 is folded to island 2 back to back. Next, island 3 is folded to island 2 face to face. Note that a spacer is inserted between islands 2 and 3 to adjust the distance between probes in row 2 and row 3. During this assembly process, epoxy is used to glue all pieces together. Compared with the stacking method which utilizes discrete electrode arrays, the major difference here is the built-in interconnects between the 2D devices. This feature is especially desirable if a reservoir is integrated for on-chip drug delivery or circuits are integrated for on-chip signal processing or wireless communication. The built-in interconnection will significantly reduce the system complexity. In this model, the folding of three silicon islands results in a 3×3×2 3D array of electrodes. More islands or denser electrodes can be integrated to develop larger 3D arrays of electrodes. A 3D model of the assembled neural probe is illustrated in Figure 2-1(c).

2.3 Device Parameters

As this is a batch fabrication process, a wide variety of devices can be designed and created simultaneously. Although each device has its own features and characteristics, they have a few common characteristics. The fabricated device probe shanks are typically 2800 μm long, 100 μm wide, 100 - 200 μm thick, and are spaced 650 μm from

each other. The open electrode area is 40×40 μm^2, with the most distal electrode typically being 300μm from the tip of the shank. The electrode size is appropriate for the study of field potentials, which is important for certain neurological studies including the study of epilepsy [22]. Devices vary in regards to distance of electrodes from each other along a probe shank. For example, some devices with two electrodes per shank have electrodes spaced 500μm from each other and other devices with three electrodes per shank have electrodes spaced 250μm from each other. All device parameters were chosen based on the anatomical structure of the rat cortex, typically 1.5 – 2.5mm in thickness and several mm in length and width [22]. The interfacing die is connected to the shank island with a flexible 10 μm thick parylene cable, which allows the shank island to be positioned out of plane from the interface island. It should be clear that the parylene cables bend while silicon islands remain rigid.

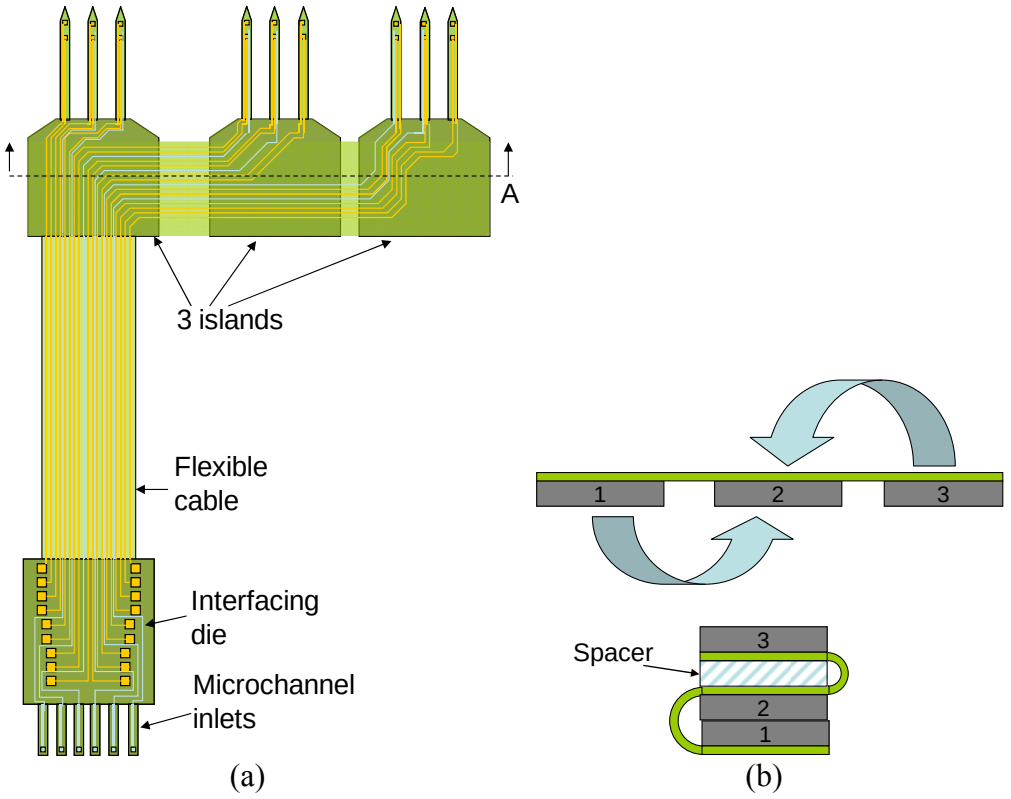

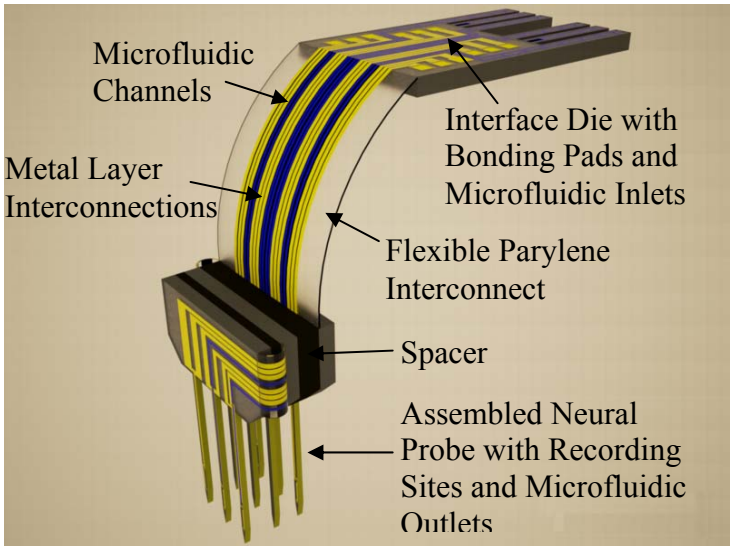

(c)

Figure 2-1: (a) Schematic of the planar device consisting of multiple silicon islands before folding. (b) Assembly method of the 3D probes (cross sectional view). (c) 3D illustration of the assembled neural probes.

2.4 1st Generation Proof of Concept Devices

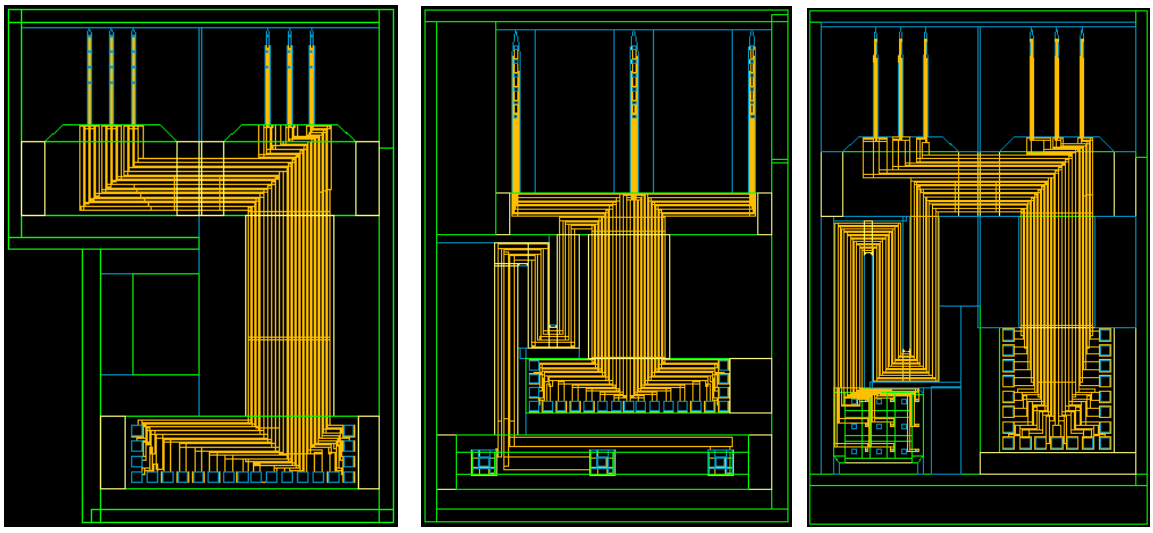

(a) (b) (c)

Figure 2-2: Prototypic devices including (a) a two-island device with a flexible interconnect, (b) a 2D planar/penetrating device, and (c) a 3D planar/penetrating device

The first set of prototypic devices included various designs of electrode-only devices including devices with 3 to 4 sets of electrode sites per probe shank and devices with

fold-over electrode islands. These prototypes were designed and created with the assistance of Dr. Yuefa Li, a postdoctoral researcher in our lab. These devices have a variety of features. The device of Figure 2-2(a) has two three-probe islands, with one island having 3 sets of electrodes per shank and the other island having 4 sets of electrodes per shank. This demonstrated the concept of having two islands of electrodes which could be folded to create a 3-dimensional array of electrodes and varying numbers of electrodes per shank. The device of Figure 2-2(b) demonstrated the ability to have an island which could be flexed in such a way that the probe island could be inserted through a planar (no shank) electrode island. This would enable the assembly of a device package with electrodes on the shanks (penetrating) and electrodes at the base of the shanks. Such a device could be used in comparison to the commonly used electrocorticography (ECOG) electrodes, which are cortex surface electrodes which are currently used to measure electrical activity of groups of neurons from the surface of the cortex. The device of Figure 2-2(c) combines concepts of the other two devices in that it contains two foldable three-probe islands and a planar (no shank) electrode islands. As before, the probe islands can be inserted through the planar island, however in this case the fully packaged device is a 3-dimensional array with surface electrodes. This would allow measurement of a 3-dimensional region of electrical activity including activity at the surface of the cortex. These prototypic devices demonstrated the flexibility in design of this technology in the creation of customized 3-dimensional neural electrode arrays. Other prototypic devices were created that demonstrated functionality of microfluidic channel integration along with electrodes.

2.5 2nd Generation Neural Probe Devices

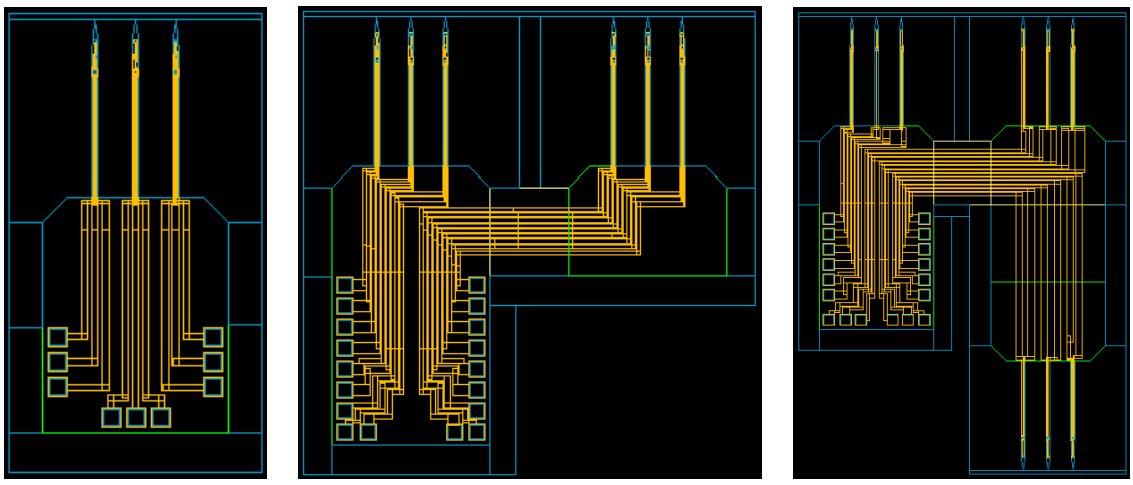

(a) (b) (c)

Figure 2-3: (a) Rigid single-island device, (b) rigid two-island device, (c) rigid three-island device

The 2nd generation of device design involved modification of previous design parameters such that the devices could be utilized in a specific application – the study of neural signals within the cortex. As has already been discussed in the background, activated phospho-CREB and NARP had been identified along layers 2 and 3 of the cortex in both human and animal models of epilepsy. This knowledge formed the basis for the design parameters of the 2nd generation neural probes. Using a rat brain atlas [76] with the assumption that the skull/subarachnoid space is 1mm [77, 78], the location of the most superficial 40µm x 40µm electrode was centered at a depth of **2.0mm** from the top surface of the skull for the electrode to be located within layers 2 and 3. Probe depth was designed to be greater than 2mm but less than 3.5mm so as not to damage underlying subcortical structures. For signal acquisition at deeper layers, a second electrode was placed in layer 4 at a depth of **2.25mm** and a third electrode was placed in layer 6 at a depth of **2.5mm** [79]**.** With these design parameters in mind, the devices were designed

to have probe shanks with a length of 2.85mm and a width of 100µm. Each design has three probe shanks for each probe island and an interface island with wire bonding pads. Devices with three electrodes per shank had electrodes for recording from layers 2/3, 4, and 6. Devices with two electrodes per shank had electrodes for recording from layers 2/3 and 6. The probe shanks are spaced 650µm from each other. Each 260µm x 260µm wire bonding pad on the interface island corresponds to a specific electrode site on the probe shanks. Six device designs were created including features such as multiple islands, flexible interconnections, and integrated microfluidic channels.

A rigid single-island device was created with three shanks and three electrodes per shank (Figure 2-3(a)). The purpose of this design was to simplify the complexities of the device to a simple 2D array of electrodes with no microchannels and no flexible interconnects. Previous prototypes of devices with flexible interconnections were seen to be very fragile with the interconnection being easily torn adjacent to the rigid islands. In addition, previous packaging techniques along with the ultra-flexible (difficult to handle) interconnects made implantation with flexible interconnects challenging. Two additional 3D rigid devices were designed including a two-island package with three electrodes per shank (Figure 2-3(b)) and a three-island package with two electrodes per shank (Figure 2-3(c)). An integrated microfluidic device was designed having two probe islands, three shanks per probe island, and two electrodes per shank, with each shank having a microfluidic outlet just proximal to the electrode at layer 2/3 (Figure 2-4(a)). The six microfluidic outlets were connected by microchannels to four inlets, with the right most and left most inlets each being connected to two outlets. The patterns for the

microchannels were arrays of 150µm x 8µm rectangles. During fabrication of these devices, the microchannels were to have an inner diameter of 30µm. Lastly, two devices with flexible interconnections were designed in an effort to improve upon previous iterations of flexible interconnect devices. Both devices have two probe islands, three shanks per probe island, and three electrodes per shank, with one of the probe islands being connected via a flexible interconnect to the wire bonding island. As opposed to the sharp, right-angle interface between rigid and flexible regions of the previous iteration of flexible interconnects, these devices have flanked interfaces which reduce the susceptibility of developing a cut at the interface. One of the flexible interconnect devices has an interconnect which spans about 8mm in length (Figure 2-4(b)), while the other flexible interconnect device has an interconnect which spans a length of 45mm (Figure 2-5).

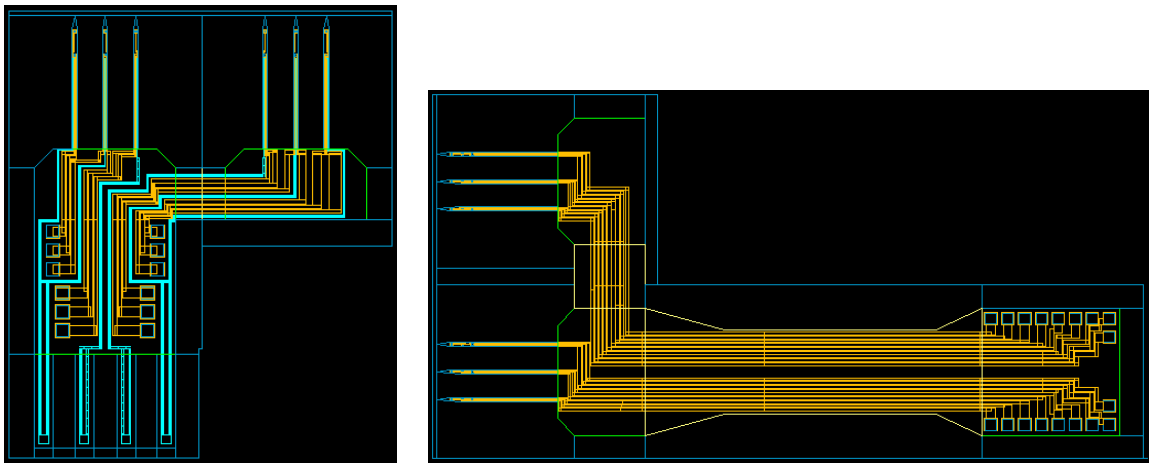

(a) (b)

Figure 2-4: (a) a microfluidic device, (b) a prototype long interconnect device

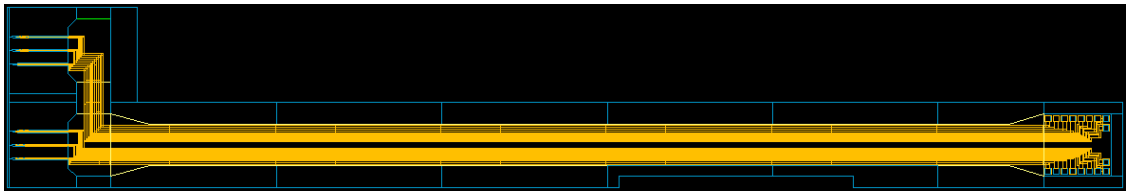

Figure 2-5: Prototypic extra-long interconnect device

2.6 Device Design Modifications

After development and testing of the 2nd generation neural probes, a variety of additional features were desired to improve the device design. One such feature was a modified microchannel pattern (Figure 2-6). The 2nd generation microfluidic channels often had blocked channels due to either microchannel collapse or due to material entering the large inlets during wafer processing. As a means to solve the issue of microchannel collapse, microchannel patterns were modified to have smaller rectangular patterns (8µm x 15µm) in an effort to create silicon microbridges over the microchannels to enhance their structural stability. In addition, the large microfluidic inlet was replaced with a three smaller, joined inlets with one of the inlets positioned perpendicular to the direction of the microchannels. The smaller inlets and the third perpendicular inlet would serve as barriers to the flow of processing material entering and clogging the microchannels. In addition, microchannel interconnections were placed between parallel (same inlet and same outlet) microchannels to serve as a failsafe if one of the parallel channels were to become clogged along the length of the channel. Finally, a dual microchannel array pattern was compared to a single microchannel array pattern to determine which pattern would be more reliable. It was later observed that the dual pattern resulted in a higher possibility of incompletely sealed channels.

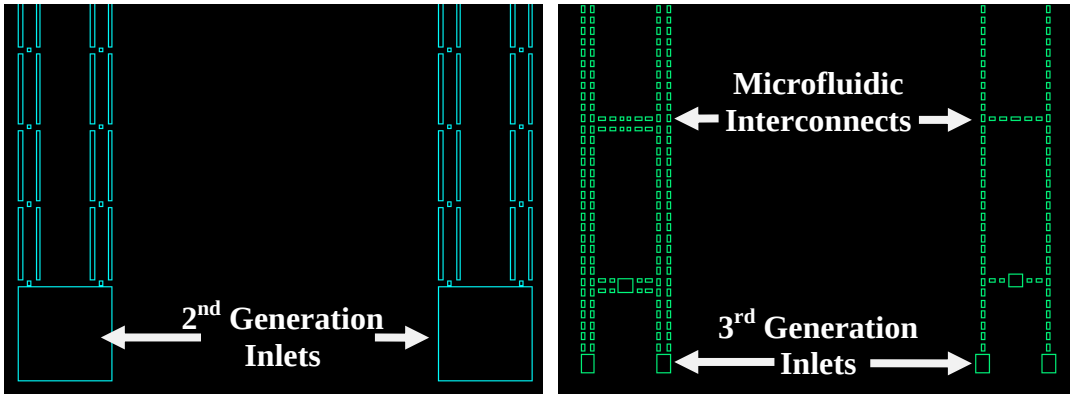

Figure 2-6: Microchannel patterns with (a) 2nd Generation microchannels and (b) 3rd Generation microchannels

Another important modification to the device design was the implementation of a trench pattern that surrounds the device shanks (Figure 2-7). Although parylene is biocompatible, parylene only covered the top surface of the 2nd generation neural devices. The other three surfaces were exposed silicon, effectively decreasing the biocompatibility of the devices. In addition, during implantation of the 2nd generation neural devices, the insulating parylene layer was seen to easily peel off during implantation in spite of use of adhesion promoter prior to parylene deposition (see Fabrication chapter). In an effort to improve the biocompatibility of the shanks and improve the adhesion of the insulative top parylene layer, the initial strategy was to deposit parylene conformally over the devices and then etch directionally using an oxygen plasma etch, so that only the sidewalls would be coated with parylene (see Fabrication chapter). Unfortunately, the directional etch was not uniform in removing parylene between shanks resulting in undesirable "parylene links" between adjacent probe shanks. The modified strategy involved the development of a trench pattern which outlined the perimeter of the probe shanks. This trench pattern would be only 8μm in width and would be at least 80μm in depth. Once the trench is

made, it would be filled with parylene. At the end of device processing, the parylene trenches would remain as the sidewalls of the probe shanks.

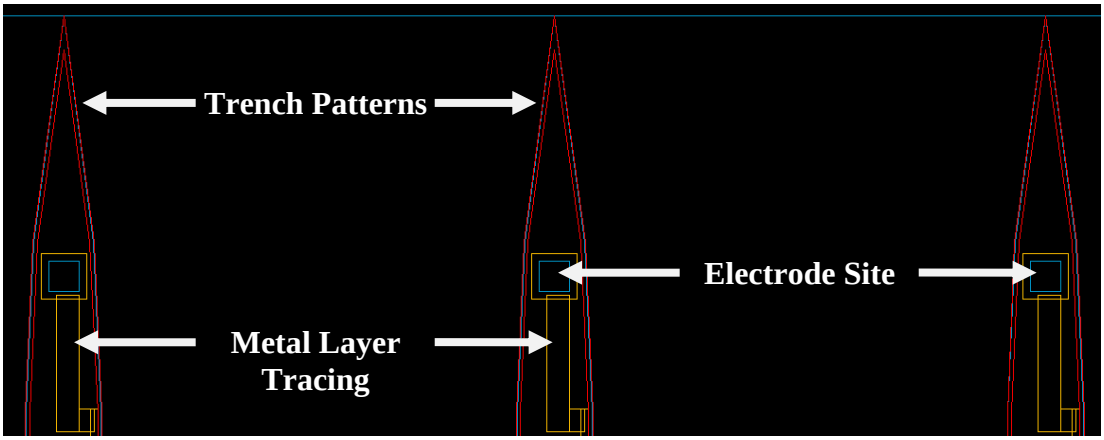

Figure 2-7: Trench Pattern

The final modification made to the 2nd generation neural devices was the development of partly flexible and completely flexible probe shanks. According to comments made in previous literature [48, 69], rigid shanks could cause more trauma to neural tissue than flexible devices. However, completely flexible devices would need to be inserted through guide holes, thereby complicating the surgical procedure [80]. Flexible devices were created by spring-boarding off the trenches made in the preceding modification. Since the trenches were reasonably deep (~100µm), it was conceived that completely flexible devices could be made by over-etching channels until all of the silicon material within the shanks were etched. The deep trenches would serve as an etch stop, preventing further etch of silicon laterally. Processing would then continue as before until device release, where the devices would be released with no silicon over the flexible areas of the probe shanks. As a means to determine the best balance of flexible and rigid regions of probe shanks, a batch of prototypic flexible devices were created with varying flexible regions. Additionally, non-functional channels were added along flexible

interconnect regions in an effort to adjust the flexibility/stiffness and enhance the durability of the flexible interconnects. Previous flexible interconnects were too flexible and easily friable, making implantation of the probe islands difficult.

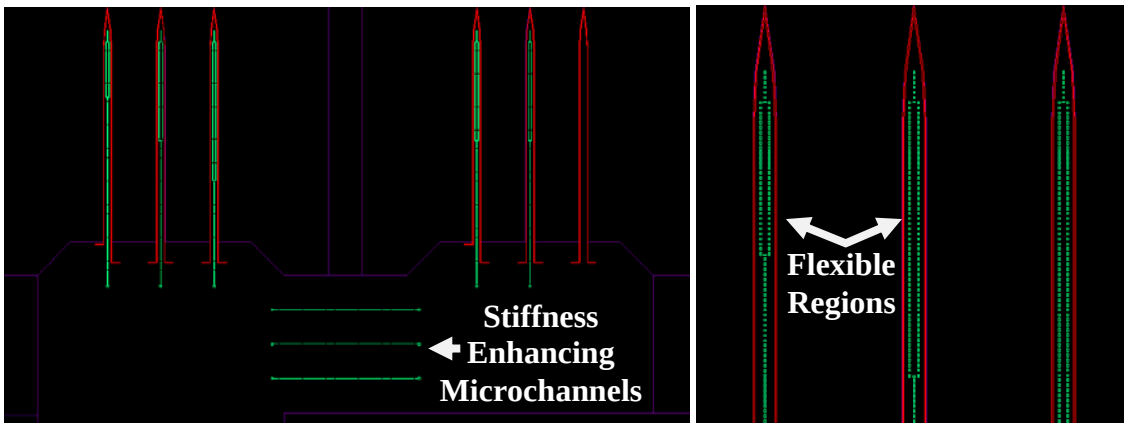

Figure 2-8: Flexible shank devices

2.7 Chronic Device Printed Circuit Board

During prior attempts of chronic animal surgeries, it was promptly understood that the entire chronic implantation package needed to be as small as possible in order to minimize animal suffering and preserve functionality of the device. As a means to achieve the smallest possible package while allowing for the largest number of channels, Altium designer was used to design and optimize a customized printed circuit board (PCB). It was decided that the printed circuit needed a variety of components including a connector interface area, a wire bonding area, and soldering pads.

From chronic package designs from other groups, it was apparent that the most commonly used connectors were the Omnetics connectors. These connectors are small in size, mass produced, and utilized universally by many neural interface groups around the

country [52, 81]. The Omnetics connectors chosen were the female NPD-18-DD and the male NSD-18-WD. Both connectors had a total of 18 channel and 2 guide post locations. Aside from the interface between each other, the female connector had straight thru-hole tails and the male connector had 18" 34 AWG lead wires. The female connector tails could be fed through and soldered to thru-holes within the PCB. The male connector lead wires could be easily interfaced with any external recording equipment. According to specifications provided by the Omnetics Corporation, the tails of the female connector were for 13mil diameter thru-holes that were spaced (center-to-center) 25mils from each other vertically and 30mils from each other horizontally.

The wire bonding area needed to be an appropriate size that it would comfortably fit a neural device bonding pad, while maintaining a high density of channels without making wire bonding too difficult. A bonding pad diameter of 8mils with bonding pads space at 8mils diagonal from neighboring bonding pads seemed to be the best configuration, balancing between ease of wire bonding and density of channels. The bonding pads were arranged around the perimeter of a 3.5mm x 3.5mm square, where the device bonding island would be fixed. It is important to note that a total of 40 bonding pads were placed, even though the Omnetics connectors only allowed for a total of 36 possible channels. To connect to the remaining 4 channels, 8 soldering pads were also incorporated into the PCB design. In this manner, 8 channels could potentially be recorded from the neural devices without the need for connection to the Omnetics connectors. These soldering pads could also be utilized in referencing to the circuit board.

After determining necessary components and component parameters, it was important to determine capabilities of various PCB manufacturing companies. The chosen company, Hughes Circuits Inc., specified a minimum trace/space size of 3mils, a minimum hole/via size of 0.1mm, and a minimum thickness of 21 mils. To improve the flexibility of the PCB in utilizing one or two Omnetics connectors (depending on number of channels needed), the inner wire bonding pads were connected to one connector and the outer wire bonding pads were connected to the other connector. With these restrictions in mind, Altium designer software was utilized to design and optimize the configuration and arrangement of all components. Once the component positions and connection tracings had been finalized, the design files were sent along with material specifications to Hughes Circuits Inc. for production. The board material was set as Polyclad 370 HR (a non-conductive, rigid material) with a thickness of 21mils. Due to the complexity of the connections, two conductive layers were necessary to minimize board size. Electroless Nickel Immersion Gold (ENIG) was utilized for all exposed conductive surfaces such as the bonding pads, thru-holes, and soldering pads. The final board design length and width were .51” x .458”, respectively.

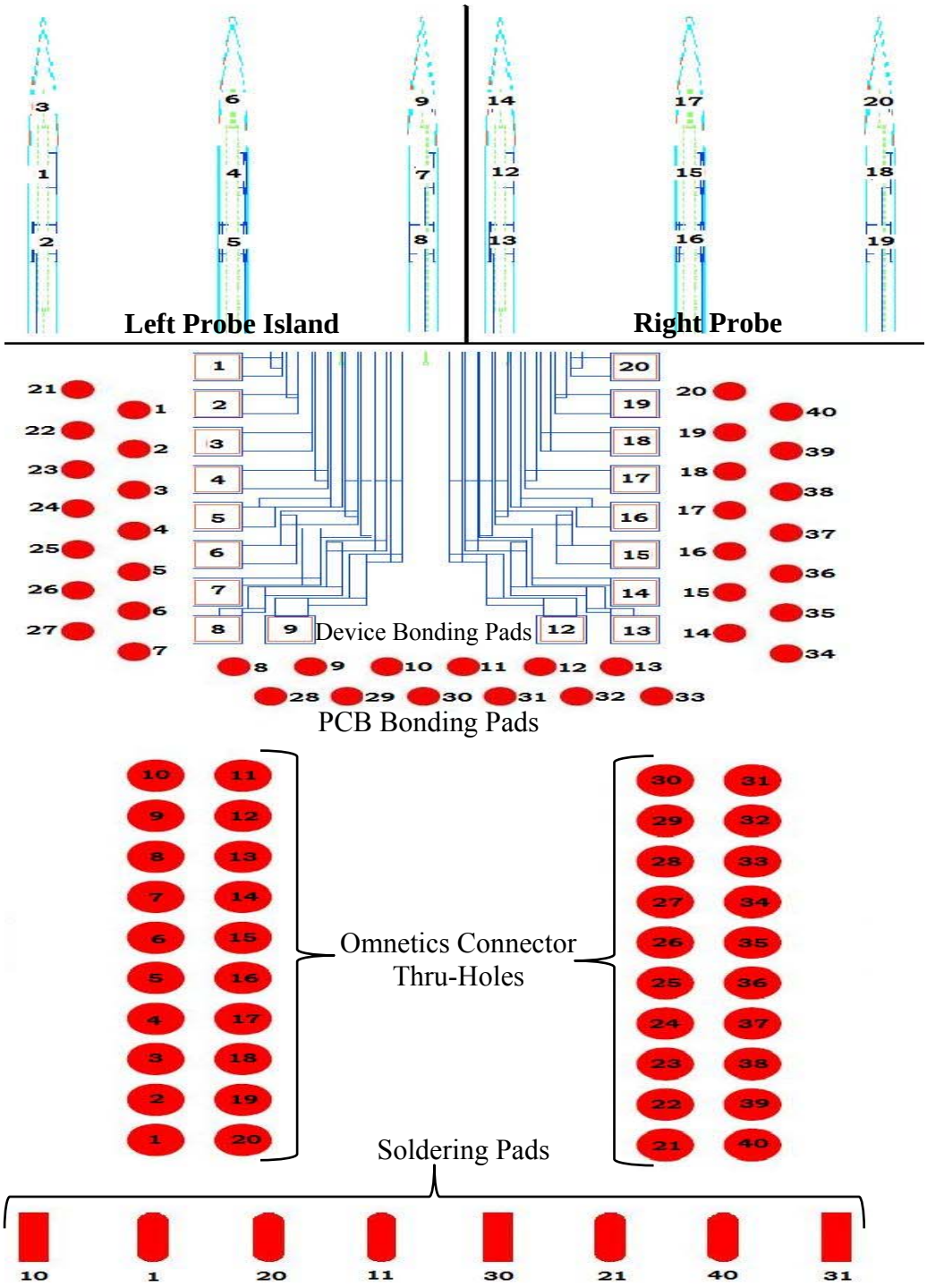

Figure 2-9: Connection schematic for the printed circuit board including the Omnetics connectors, the soldering sites, the wire bonding pads, the wire bonding islands, and the probe islands

2.8 Chronic Devices

Utilizing lessons learned from the previous animal surgery attempts and the modified device designs, chronic neural devices were designed in an effort to realize the goal of observing change in electrical signals across the various cortical layers. Previous neural devices were only appropriate for measuring neural signals during implantation (acute neural signal recording). Chronic surgeries were attempted, however the bulky packaging of the assembly resulted in 100% failure rates, with the assembly breaking from the animals head in less than a week. As mentioned in the preceding section, great strides were accomplished in miniaturizing the package assembly through development of the chronic device PCB. The next step was development of the chronic neural device. During prior animal surgeries, it was realized that the most stable implantation setup would be such that the package is parallel to the plane of the skull, with only the probe islands being perpendicular to the skull implanted into the cortex. In order achieve this, the flexible interconnect design was utilized with the wire bonding island being fixed along with the package to the skull. Via the flexible interconnect between the wire bonding island and the probe islands, the probe islands could be positioned and implanted within the cortex. Additional features were also included. Two types of chronic devices were designed: electrode-only chronic devices and integrated microfluidic chronic devices.

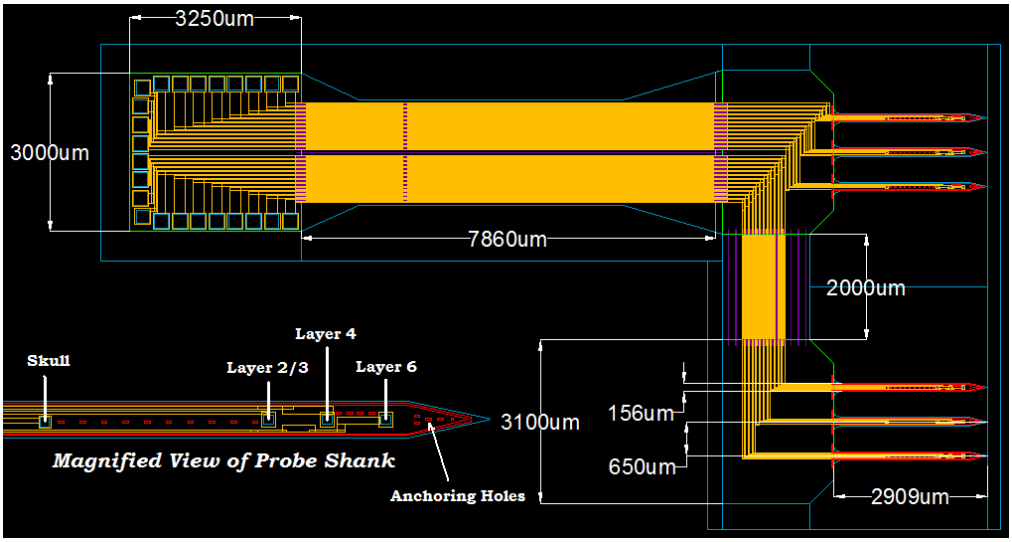

Figure 2-10: Electrode-Only Chronic Device

The electrode-only device (Figure 2-10) featured four electrode sites per probe shank. As with previous device parameters, electrodes were positioned at layers 2/3, layer 4, and layer 6 of the cortex. However, an additional fourth electrode was positioned more superficially at a depth of 1mm – just below the surface of the skull. The purpose of this electrode was to serve as a reference to previous animal studies which utilize screw electrodes as discussed in the background section. In addition to the fourth electrode, this device featured anchoring holes which were placed at different areas along the probe shanks. In spite of the trench patterns, the parylene layer would still have a tendency to peel off from the silicon substrate. The anchoring holes, which were 8µm x 24µm rectangles, were etched and sealed along with the trench patterns. Another added feature was embedded microchannels underneath the gold tracings of the flexible interconnects. A common problem with the longer flexible interconnects was peel off of the gold tracings underneath the parylene layer. During processing of the previous designs of devices, a very thin layer of silicon dioxide would be the only layer covering the thin

metal layers running the flexible interconnects, thus the thin metal layers of the flexible interconnect would often be peeled off resulting in loss of channels. For the electrode-only chronic device, electrode tracings within the flexible interconnect regions would be split into two thinner electrode tracings with a microchannel between the two tracings. During processing, the microchannel would be etched to the extent that the electrode tracings would become freestanding. At this point, parylene would be deposited within the microchannels, thereby fully encapsulating the electrode tracings with parylene. Additional improvements to the device design included thicker shanks (200µm thick) to improve the durability of the devices and additional microchannels within the flexible interconnects to enhance the strength and adjust the stiffness of the interconnects.

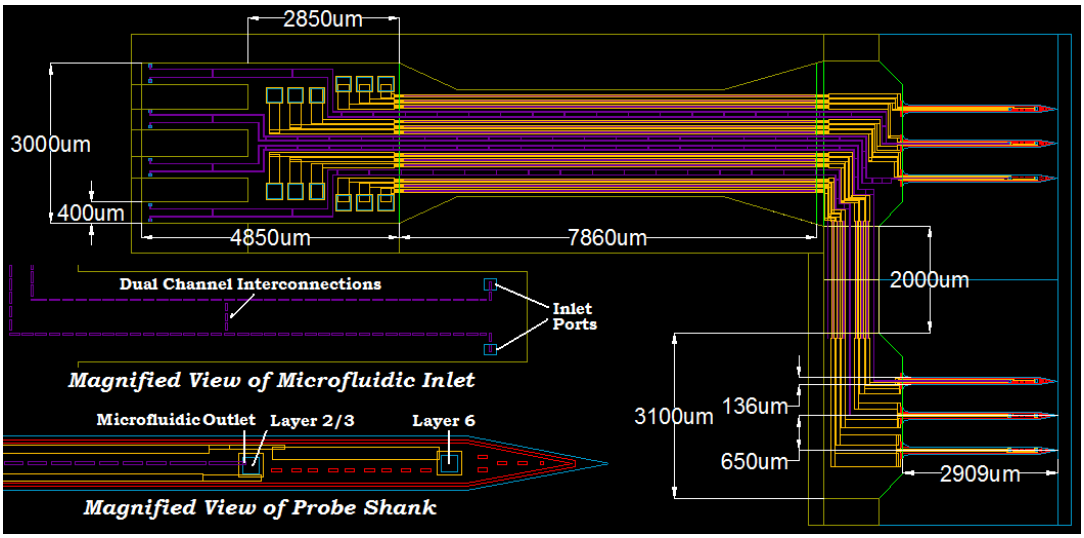

Figure 2-11: Integrated Microfluidic Chronic Device

The integrated microfluidic device featured two electrode sites per probe shank, with 4 of the 6 probe shanks having a microfluidic outlet. The two electrodes of the probe shanks were positioned at layers 2/3 and layer 6 of the cortex. In contrast to the electrode-adjacent microfluidic outlets of previous designs, the outlet for this design was

integrated within the electrode positioned at layers 2/3. In previous design iterations, processing material would often enter and clog the microchannels at the inlets and outlets. This was believed to be due to the microfluidic channels being open during wafer processing. As a means to prevent material influx into the channel, the outlets and inlets were designed such that the microfluidic inlet and outlet ports would be sealed until the electrode sites were opened via oxygen plasma RIE (see Fabrication chapter). No additional inlet/outlet patterning steps would be necessary. Oxygen plasma RIE used to open the electrode sites would continue until the inlet/outlet sites were fully open. As described for the electrode-only devices, the integrated microfluidic devices also included parylene anchoring sites, microchannels underneath gold tracings in flexible regions, 200μm-thick shanks, and stiffness/durability enhancing microchannels within the flexible interconnects.

CHAPTER 3: FABRICATION

Development of the devices was a multi-step approach consisting of several different layers and processing steps. The results are summarized in Figure 3-1.

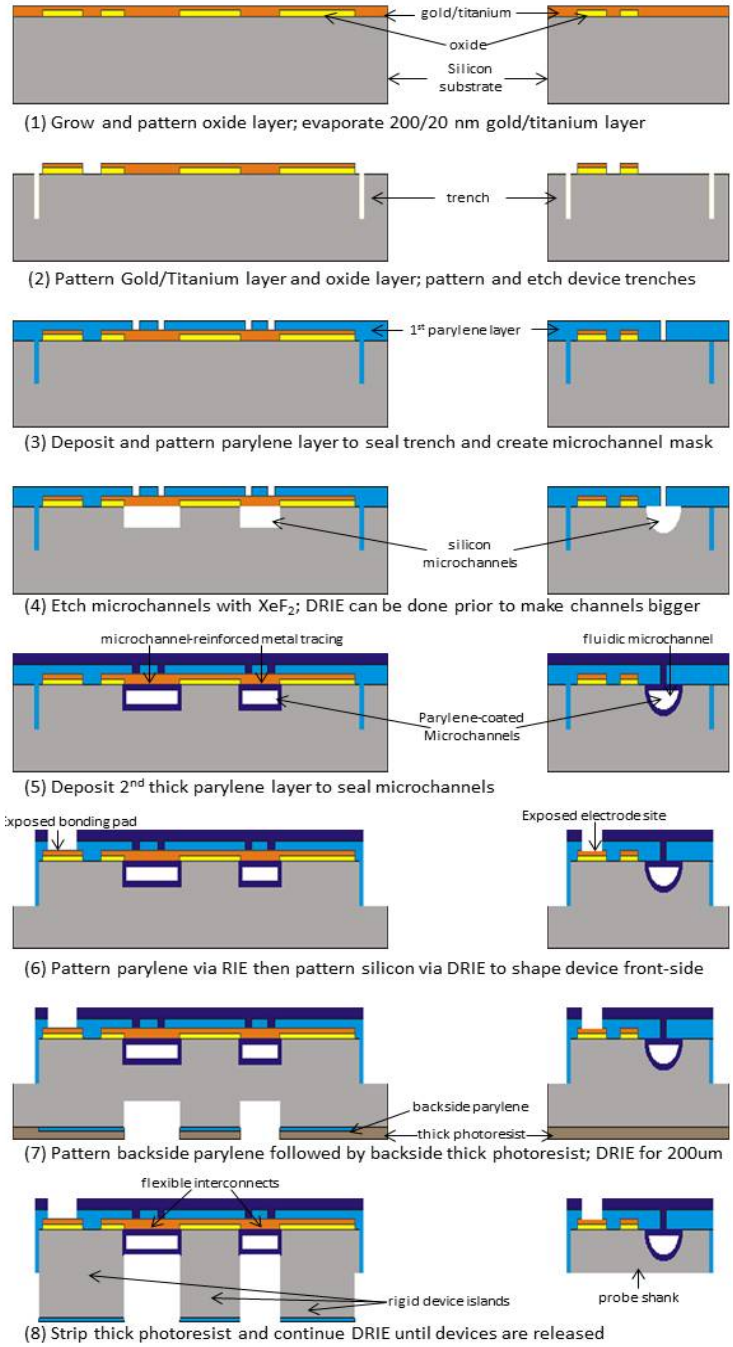

Figure 3-1: Simplified fabrication process of neural probes with integrated microchannels. Left column: cross sectional view of silicon islands. Right column: cross sectional view of one probe shank.

The process starts with a 512μm thick 4 inch diameter (1 0 0) double side polished silicon wafer.

3.1 1st Step: Thermal Oxidation

The first step is thermal oxidation in which a silicon dioxide layer is formed on the surface of the silicon wafers. This silicon dioxide layer provides insulation for the metal traces. In preparation for thermal oxidation, the silicon surfaces are first cleaned using the standard RCA clean process, which involves a sequential ionic clean (1:1:5 $NH_4OH:H_2O_2:H_2O$ at 80°C for 10 minutes) and organic clean (1:1:6 $HCl:H_2O_2:H_2O$ at 80°C for 10 minutes) baths in which organic and ionic contaminants are removed from the surface. The wafers are then immediately placed in the PWS thermal oxidation furnace with a wet oxide growth recipe, where the silicon dioxide layer is formed via wet oxidation at 1100°C for 25 minutes to achieve an oxide thickness of 300 nm. After oxidation is complete, the silicon dioxide layer thickness is measured using an UltraClean100 Nanospec optical analyzer.

Lessons/Potential Pitfalls: During thermal oxidation with the PWS oxidation furnace, oxidation is dependent on location of the wafers in the chamber. Wafers deeper inside the chamber will have a thicker, more uniform silicon dioxide layer than wafers which are located closer to the opening. For this reason, usually not more than 12 wafers are oxidized in one thermal oxidation run (12 wafers per wafer boat).

3.2 2nd Step: Oxide Patterning

After removing the wafers from the chamber, the oxide layer is patterned using SPR220 photoresist using standard photolithography techniques. This step is important for removing any underlying oxide underneath the flexible areas of the devices. To increase adhesion of the photoresist layer, hexamethyldisilazane (HMDS) can be pipetted and spun on the wafer at a speed of 2000rpm. The SPR220 photoresist is spun at 3500 revolutions per minute for 30 seconds after which the photoresist is soft baked at 115 ^{o}C for 90 seconds. Using a chrome photomask with our desired oxide patterns, the photoresist is exposed for 6 seconds using a MA6 Mask Aligner. The exposed wafers are then developed in AZ300 developer solution for 90 seconds after which they are rinsed and nitrogen dried. The patterned wafers are then inspected using an optical microscope for signs of improper photolithography. To ensure that there is no photoresist residue, the wafers are descummed using a Drytek Reactive Ion Etching (RIE) system. Oxygen plasma is generated with a flow rate of 30sccm O_2 gas with a power of 100 Watts and a threshold pressure of 200 mTorr. The wafers undergo descumming for 30 seconds each to ensure no photoresist residue remains. The wafers are then immersed in a buffered oxide etch solution (100:1 DI Water:HF) for 10 minutes. Oxide etch patterning can be observed via optical microscope through observation of the pattern coloration from a bluish hue to a gray coloration. However, completeness of oxide etch can be determined using the Nanospec optical analyzer. Once oxide patterning is complete, photoresist can be stripped using immersion in PRS2000 solution at 60^{o}C for 10 minutes. After photoresist strip, wafer should be observed under optical microscope to ensure there are no observed photoresist residues. Wafers can be descummed in oxygen plasma with a

flow rate of 30sccm O_2 gas, a power of 150 Watts, and a threshold pressure of 200 mTorr for 90 seconds or as needed to remove any residues.

Lessons/Potential Pitfalls: Before spin-coating with photoresist, wafers must be as clean as possible to avoid streaking of the photoresist. For the purposes of spin-coating after PWS thermal oxidation, surface contaminants should be minimal, so nitrogen blow may be sufficient. If wafers are dirty, wafers can be rinsed and dried in the Verteq wafer washer/dryer. In some cases, streaking may be unavoidable due to deformities and non-uniformities in the oxide layer. In this case, photolithography may still be successful, however patterning should be carefully observed before hard baking to ensure no short circuits or open circuits are observed. Additionally, mask should be kept clean before and after exposing the wafer. If any impurities are seen, mask can be cleaned in mask cleaner solution. During exposure and development, caution should always be used to avoid over-development and over-exposure of the patterns. For oxide patterning, various dilutions of buffered HF exist which can affect the rate of oxide etching. It should be noted that a faster HF etch will result in corresponding decrease in oxide etch precision.

3.3 3rd Step: Gold/Titanium Deposition

The third step is deposition of the titanium/gold metal layer on top of the silicon dioxide layer. This is achieved using an Enerjet Electron Beam (E-Beam) Evaporator. The machine generates a high powered electron beam which strikes the metal target, thereby releasing the metal vapors for deposition onto the wafers. The deposition rate is controlled by the power of the electron beam. For our deposition, the deposition rate was

set to 5Å/sec for both layers. Titanium is deposited first to a thickness of 200Å. The titanium layer serves as an adhesion layer between the silicon dioxide layer and the gold layer. Titanium was chosen as the adhesion layer because it is known to be more biocompatible than other possible adhesion metals. Next gold is deposited to a final thickness of 2000Å. After metal deposition is complete, the entire chamber is allowed to cool down for 10 minutes in order to avoid cracking of the thin films upon exposure to cold air.

Lessons/Potential Pitfalls: Since deposition rate is dependent on the power of the electron beam, it is also dependent on location of the beam in striking the target. The location must be adjusted as needed during the initial preparative stages of deposition (rise and soak stages) where the beam is visible. Deposition rate should be consistent to allow for a more uniform deposition of metal layers. It is also important to let the wafers cool before the chamber is vented. If this step is skipped, there is a high possibility that the heat exchange between the hot wafers in the chamber and the cool nitrogen air entering the chamber will cause the wafers to have many cracks along the metal layers.

3.4 4th Step: Electrode/Bonding Pad Patterning

After removing the wafers from the chamber, the metal layers are patterned using SPR220 photoresist using an electrode pattern chrome mask and photolithography techniques presented in the oxide patterning section. After proper photolithography is confirmed through optical microscopy, the wafers are descummed as described in preceding sections. Next, the wafers are placed in a gold etch bath at room temperature

until gold etching is complete (typically ~8 minutes if the temperature of the bath is at room temperature). After gold etch is complete, the wafers are rinsed, dried, and optically inspected for completion and accuracy of gold patterning. The wafers are then placed in the titanium etch bath at room temperature until titanium etching is complete (typically ~1 minute if the temperature of the bath is at room temperature). Again, the wafers are rinsed, dried, and optically inspected. Next, the photoresist on the wafers is stripped and descummed via immersion in PRS2000 solution and oxygen plasma RIE as described previously. Lastly, the oxide layer is removed via dry etching in a LAM9400 RIE system. The LAM9400 etching system differs from the Drytek RIE system in that this tool uses timed inductively coupled plasma generation and a DC bias source to create a higher density, more directional plasma. This results in a faster, more precise etch of the oxide layer. The recipe used utilizes a mixture of C_2F_6 and Argon gases. The Dektak profilometer can be utilized to observe completion of the oxide etch by referencing to the electrode tracings and measuring the depth to the silicon layer. Etching is complete when the depth no longer changes and the surface is observed to be gray instead of bluish. Final verification of oxide etch completion can be done as before using the Nanospec optical analyzer.

Lessons/Potential Pitfalls: During metal etching, care must be used as over-etching can results in a significant undercut of the metal patterns. The metal baths have hot plates which heat the baths up to room temperature (25 or 28 ^{o}C) to allow for faster etching, however faster etching also means a higher chance of accidental over-etching. This is why it is better at this step to use bath temperature without using the hot plates to

heat the solutions. Still, the wafers should be checked in the bath solution at least every 2 minutes for the gold etch and every 15 seconds for the titanium etch, with more frequent checks as time progresses. It is also important to note that Buffered Oxide Etchant solution exhibits similar titanium etching rates in comparison to Titanium Etchant solution and can be used interchangeably when Titanium Etchant solution is not available. In the oxide etching step, wet etching was observed to require a long duration Buffered Hydrofluoric acid immersion, thus putting the thin titanium layer at risk of etchant attack. For this reason, dry etching via the LAM9400 was chosen to remove the oxide layer. The Drytek RIE can also be used to etch the oxide layer as well. In this method, 40 sccm C_2F_6 (seen on the dial as 200) and 3 sccm Ar are pumped to the chamber with a power of 200 Watts and a threshold pressure of 200 mTorr with duration of about 15 minutes.

3.5 5th Step: Trench Patterning

After the oxide layer has been removed, silicon should be the surface material exposed on the wafer (aside from the gold/titanium tracings developed in the preceding step). This step involves patterning of the silicon substrate with deep trenches. To achieve this, the substrate surface was primed with HMDS and then use SPR220 photoresist with a spin rate of 2000rpm for 20 seconds. This should result in a photoresist thickness of approximately 4μm. The wafer is then soft baked at 115 ^{o}C for 90 seconds. Using a photomask with our desired trench patterns, the photoresist is exposed for 9 seconds using a MA6 Mask Aligner. The exposed wafers are then developed in AZ300 developer solution for 90 seconds after which they are rinsed and

nitrogen dried. The patterned wafers are then inspected using an optical microscope for signs of improper photolithography. The wafers are then descummed for 90 seconds in Oxygen plasma RIE as described previously. To ensure no residual oxide has grown on the silicon substrate from the oxygen plasma RIE, the wafers can be immersed in a buffered oxide etch solution (100:1 DI Water:HF) for 1 minute. After the wafers are washed and dried, each wafer is placed within an STS Pegasus Deep Reactive Ion Etching (DRIE) system and is subjected to a timed BOSCH process. The BOSCH process is an alternating etching process involving isotropic etching via reactive SF6/O2 plasma and sidewall passivation using C4F8 which protects the sidewalls from further etching [82]. In this manner, DRIE is often used to create very deep features with relatively straight sidewalls. At the Lurie Nanofabrication Facility (LNF) within the University of Michigan, a variety of BOSCH process recipes have been designed which allow for various etch rates for a variety of feature sizes. The etch recipe which was seen to work well with thin trenches requiring high resolution was LNF recipe #1. This recipe was used for approximately 40 minutes to achieve 150 - 200μm deep trenches.

Lessons/Potential Pitfalls: In contrast to previous patterning steps, extra care must be taken to observe proper patterning of trench patterns as the trench patterns are very long (over 200μm) but very thin (less than 10μm), which results in increased difficulty of properly patterning the trenches especially with lower resolution masks. If underdevelopment occurs, very thin or incomplete trenches could be created resulting in incomplete trenches within the silicon. If overdevelopment occurs, this could result in a wider trench which effectively leads to a deeper trench and a wider undercut. This could

cause later issues such as incompletely filled parylene trenches resulting in two separate layers of parylene within the silicon trench.

3.6 6th Step: Parylene Deposition

The next step is deposition of the biocompatible polymer, Parylene C. This layer serves multiple different purposes including sealing of the deep trenches and anchor points, insulation of the metal layers, as a mask for the microfluidic channel patterns, and to enhance the biocompatibility of the exposed areas of the device. In order to improve adhesion between the Parylene and the silicon substrate, the wafers are first soaked in a solution of A-174 polymer deposition adhesion complex in IPA (A-174:IPA:DI water – 1:100:100 respectively) for 45 minutes after which they are rinsed in IPA for 15 seconds and air dried for 2 minutes (no need for nitrogen blow). Next, the wafers are placed in a wafer holder along with a clean glass slide within the clean parylene deposition chamber. The Parylene C dimer (corresponding to the desired end thickness of parylene) is placed inside an aluminum foil "boat" and placed within the vaporizer chute. In order to seal a trench, it is important to understand that a thickness of parylene must be deposited that is at least half of the width of the trench to be sealed. Deposition of Parylene is a conformal coating process, which means that parylene deposits on every exposed surface at an equal deposition rate. For a 10μm wide trench, as the thickness of the parylene reaches 5μm, the trench sidewalls will each have 5μm thick parylene (total thickness of 10μm as the two sidewall parylene layers meet) thereby sealing the 10μm wide trench. For this stage of the process, 8 grams of parylene C dimer is used for a thickness of approximately 5 microns in order to seal 10μm wide trenches. The chamber is then pumped down with

the cryo-pump until it reaches 11 – 12 mTorr and the furnace heats up to 670^{o}C . At this point, the vaporizer is turned on and the process is allowed to run to completion. After deposition, the chamber is vented, the wafers and glass slide are removed, the chamber is pumped down again, and the system is shut off. Lastly, the glass slide is scratched and measured using the Dektak profilometer to verify the thickness of the parylene. The trenches should also be observed under microscope to verify that the trenches are completely sealed. If needed, additional parylene should be deposited to completely seal the trenches.

Lessons/Potential Pitfalls: Parylene deposition is done in a non-clean environment, however in order to ensure uniform parylene layer, the chamber must checked for debris and other material that may result in chamber leaks or unwanted material deposition. Razor blades are used gently to peel off excessively thick parylene layers deposited on the inside of the chamber after which Micro-90 cleaning solution is used to clean the particulate matter in the entire chamber. Care must be taken not to allow parylene debris to enter the pyrolysis baffle. If parylene enters the baffle, the debris may burn causing black debris to be deposited throughout the chamber and on the wafers. Even with extreme care, Parylene deposition often results in small bubbles which may appear throughout the parylene layer. Although this is usually harmless to the rest of the process, parylene should be checked optically to ensure layer is not excessively dirty or full of bubbles as this could lead to adhesion problems in later parts of the process.

3.7 7th Step: Parylene Patterning for Microfluidics

The first parylene pattern will be the pattern for the microfluidic channels. Similar to the trench patterning described earlier, the substrate surface is primed with HMDS after which SPR220 is spun at a speed of 1800rpm for 30 seconds to achieve a thickness of 5µm. The wafer is then baked at 115^{o}C for 90 seconds. The exposure time for the channel patterns is still 9 second s as with the trench patterns, however it is important that the mask aligner utilizes direct, hard contact between the mask and the wafer to ensure full transference of microfluidic channels. As such, the chrome mask should be checked for any residual photoresist and cleaned often to avoid loss of patterns. The patterns are then developed for 90 seconds in AZ300 developer solution. The microfluidic patterns should be checked thoroughly to ensure accuracy of photolithography. Next, the exposed parylene sites are etched away using the LAM9400 with a fast isotropic parylene etching recipe for 1200 seconds (20 minutes). Alternatively, Drytek RIE oxygen plasma can be used with 30sccm O_2 gas, 150 Watts, threshold pressure of 200 mTorr, for duration of 25 – 30 minutes. Regardless of the tool used, the parylene should be etched enough such that the exposed parylene is fully etched and the underlying silicon is exposed. Since the deposited parylene was approximately 5 microns, it is expected that the photoresist will be completely etched away by the time the exposed parylene is etched through. Extra etching time is suggested to ensure no parylene residue remains on the exposed silicon. Dektak profilometry and optical inspection (scratch an area where parylene should be removed and observe if parylene is readily apparent) are both utilized to ensure parylene patterning. After completion of parylene etching, the channel patterns should have either exposed silicon or exposed metal. The wafers are dipped in gold etchant solution for 1

minute, followed by titanium etchant for 10 seconds, followed by 49% Buffered Hydrofluoric acid (BHF) solution for 1 minute in an effort to remove any exposed layers within the channel patterns on the silicon surface. The wafers are immediately rinsed and dried (optionally, wafers can be baked at 105 ^{o}C for 6 minutes to remove any residual water). The channel patterns should be observed optically to ensure that silicon is exposed at all points within the channel patterns. Metal/Oxide etchant should be repeated if any metal/oxide material remains within the patterns.

Lessons/Potential Pitfalls: Before the SPR220 5μm mask was chosen as the masking layer for the microfluidic patterns, 8 micron thick photoresist (AZ 4620) was attempted as the masking layer. Unfortunately, due to the size of the features (8 μm x 15 μm), the non-uniformity of the thick photoresist layer, the long exposure/development time, and the power of the mask aligner, thick photoresist photolithography resulted in hexagonal and rounded patterns instead of the desired rectangular patterns. According to literature, this effect is due to a variety of factors including but not limited to over/under-exposure, over/under-development, and lamp non-uniformity. If this is unavoidable, an aluminum mask can be utilized for the microfluidic patterning. To improve adhesion between the aluminum mask and the parylene layer, the parylene layer is first roughened in the Drytek RIE. Oxygen plasma with 30sccm O_2 gas, 100 Watts, threshold pressure of 200 mTorr, and duration of 30 seconds should be sufficient. Next, the aluminum is deposited using the E-beam evaporator with a final thickness of 200nm at a deposition rate of 3.5Å/sec (a higher deposition rate is acceptable here because the aluminum is just a masking layer). After deposition of the Aluminum layer, patterning occurs as described above with the

exception that after photolithography, the aluminum is etched away in an aluminum etch bath. Whichever masking method is used for creating the channel patterns, the patterns must be checked for accuracy. One of the leading reasons for blocked channels in this process is incomplete patterning. The latest device design with dual channels and channel interconnections accommodates for some flaws in patterning, but certain areas of the device are very sensitive to incomplete patterning. Specifically in areas with single channels such as appears within the probe shank itself, one missing channel pattern will result in a completely blocked channel. Extra care must be taken to identify flaws in these regions. Although the parylene can be somewhat over-etched in this step, excessive over-etching may result in wider channel patterns since the oxygen plasma etch (regardless of using either the LAM9400 or the Drytek RIE) is an isotropic etch. After exposure of the underlying silicon/metal/oxide, the metal/oxide layers must be removed for the subsequent channel etching. Residual material over the silicon could also result in incomplete/blocked channels.

3.8 8th Step: Microfluidic Channel Etching/Resealing

With the patterned parylene serving as a mask, the next step involves isotropic XeF_2 etching of the exposed silicon. In this process, when the silicon is exposed to XeF_2 gas, Xe gas is created along with SiF_4 (a gas). As this reaction occurs, the exposed silicon is etched isotropically, thereby creating an equal-directional etch of silicon with large undercuts. The microfluidic channel patterns are composed of arrays of 8μm x 15μm rectangles which are spaced 10μm away from each other in the desired direction of the microchannel. Before etching via the XeF_2 gas, the microchannel patterns are first etched

via the STS Pegasus DRIE using LNF Recipe #1 for 5 minutes. This allows the microchannels to be deeper, thereby enlarging and reducing flow resistance within the channels. As the XeF_2 reaction etches the exposed silicon isotropically, the undercut underneath the rectangular patterns converge eventually creating a silicon channel with overlying parylene. It is important to note that a more extended XeF_2 is important to allow for a smoother microchannel, however excessive XeF_2 could result in short-circuit connections between microchannels. The microchannel formation is achieved using 5 cycles of 700mTorr XeF_2 each of 1 minute duration. During XeF_2 etching, the chamber must be purged of all impurities through cycles of pumping and nitrogen venting. After exposing the wafer to 700mTorr XeF_2 for 1 minute, the F_2 is consumed and the etching begins to saturate with SiF_4, thereby reducing the etch rate. For this reason, it is better to purge the chamber after 1 minute of XeF_2 etching and start a new cycle. After 5 to 10 cycles of XeF_2 etching, it is important to use a microscope to optically inspect the wafers to determine the etching rate of silicon and to determine if there are any open circuits or broken channels forming. If the rectangular patterns are being properly etched, the exposed silicon should appear gray, at a slightly different focal length, and slightly roughened. As the cycles progress, the etch rate can be determined by measuring the undercut of the rectangular patterns. The target etching is around 25 microns of undercut on both sides of the channels. This amount of undercut would result in a 50 micron diameter half-pipe microchannel. Once this undercut has been achieved, the microfluidic patterns are inspected for completion of etching. Channel undercut between rectangular patterns should be overlapping with no open circuits within the same channel and no short circuits between different channels. The channel at this point is similar to a silicon

half-pipe with patterned parylene covering the top of the channel. The rectangular patterns within the parylene are leak points for the channel and must be sealed to complete the microchannel formation. In order to seal the channels, parylene is again deposited on the wafers to reseal the rectangular patterns. As parylene coats uniformly, parylene will be deposited along the inside surface of the channel and at the rectangular openings until opposing sides of the rectangles join (since the rectangles are 8 microns wide, the sealing off should happen after 4 microns of parylene have been deposited). This will result in a microchannel with 4 micron thick parylene wall. As a result, the 50μm silicon channel will effectively produce a 46μm inner diameter half-pipe parylene channel. Before depositing the second layer of parylene, the first parylene layer must be treated with oxygen plasma (30sccm O_2 gas, 100 Watts, threshold pressure of 200 mTorr, and duration of 90 seconds) to improve the adhesion between the two parylene layers. To ensure that all openings are effectively sealed, 12 microns of parylene (approximately 30 grams of parylene dimer) are deposited on the wafers. Additionally, this second thicker parylene enhances the durability of the flexible interconnecting cables for the completed device. As before, a glass slide should be used to determine the final parylene thickness. Additionally, the microchannels should be observed under optical microscopy to ensure that the parylene within the rectangular patterns has converged.

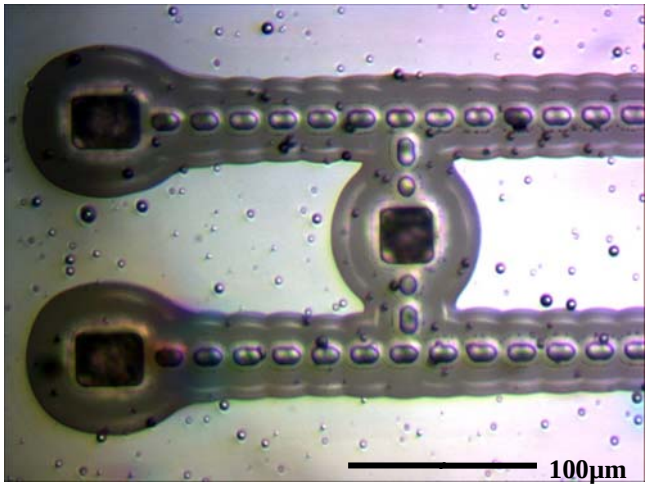

Figure 3-2: Microchannel inlet after XeF2 Etching (before 2nd Parylene Deposition)

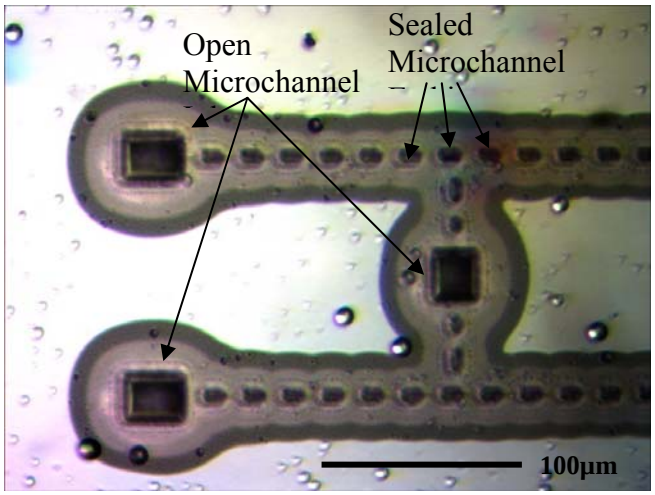

(a)

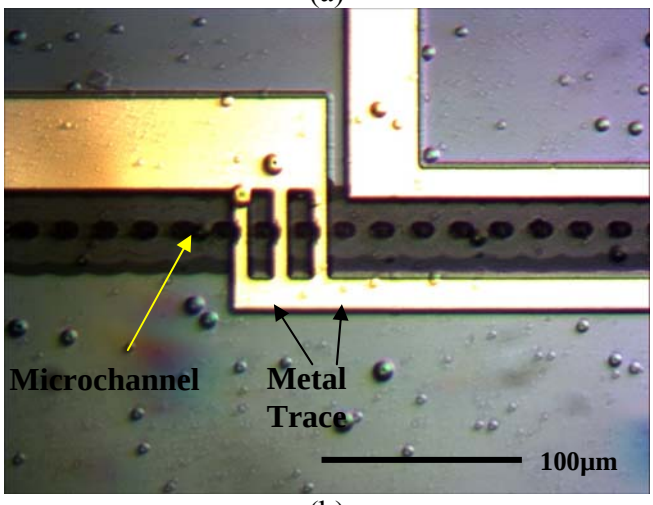

(b)

Figure 3-3: (a) image of microchannel inlet after 2nd parylene layer demonstrating sealed microfluidic channel; (b) image illustrating the crossing of a microchannel and a metal trace

Lessons/Potential Pitfalls: During XeF_2 etching, care must be taken to observe development of any short circuits or open circuits earlier on so that the problem can be resolved before further etching is done. If areas of the microfluidic channel are not etching, additional wet etching may be needed to completely expose the silicon within the rectangular patterns. If open circuits are formed due to some areas being etched slower, more etching time may be adequate to allow for completion of the microfluidic channel, however this may result in constricted flow within the channel which should be avoided if possible. During XeF_2 etching, it was noted that after cycles of 2 minutes of etching, the etch rate per cycle was still the same. This led to the conclusion that 1 minute cycle intervals is adequate to ensure a more uniform etch rate per cycle. It should be noted that etch rate is dependent on amount of exposed silicon. More exposed silicon would increase the consumption of F_2 thus resulting in a slower etch rate. Optical microscopy is the simplest way to determine etch rate during XeF_2 etching. After deposition of parylene, rectangular patterns should again be optically inspected to determine if microfluidic channels are fully sealed. If the parylene mask rectangular patterns were too wide in preceding steps, a larger amount of parylene may need to be deposited, however this will result in longer parylene etching times in later steps.

3.9 9th Step: Front-side shaping/Parylene Patterning

After completion of the microfluidic channels, an additional 12 – 13 microns of parylene will have been deposited on the wafers. To begin shaping the devices and exposing the desired electrodes, an aluminum mask is used to aid in parylene etching. In

this process, an aluminum mask is desirable since the amount of parylene to be etched is rather large (about 15-16 microns) resulting in a prolonged etch time. As a result of the isotropic oxygen plasma etch, the patterns would be considerably enlarged if a photoresist layer were used instead. A metal mask is reflective for the plasma RIE and is therefore less likely to exhibit significant pattern enlargement. In order to improve adhesion of the metal mask to the parylene, the surface is first roughened using oxygen plasma RIE with 30sccm O_2 gas, 100 Watts, and a threshold pressure of 200 mTorr for 90 seconds. The aluminum layer is then deposited using the E-beam evaporator and patterned using standard photolithography. The aluminum mask only serves as a masking layer, so a deposition of 200nm deposited at a rate of 1nm/sec is sufficient. As in previous parylene etching steps, the exposed parylene sites are etched away using the Drytek RIE. Oxygen plasma with 30sccm O_2 gas, 150 Watts, and a threshold pressure of 200 mTorr should be sufficient. In this etch, the silicon adjacent to the devices, the electrode sites and bonding pads, and the microfluidic inlets and outlets must all be uncovered. For the silicon, electrode sites, and bonding pads, 15-16μm of parylene must be etched away. However for the inlets and outlet sites, an additional 4μm parylene wall must be etched away. As parylene is etched at a rate of 1 micron for every 5 minutes using this recipe, 110 minutes should be enough to ensure the parylene is fully etched with a justifiable 10 minute over-etch. In addition, 6sccm CF_4 should be added to the gas mixture in the last 20 minutes to remove any parylene residue on the electrode/bonding pad sites. Completion of parylene etching can be observed through Dektak profilometry and optical inspection. The parylene etch should be complete when etching depth does not change. The surface of the exposed electrode sites can be scratched via a needle-

microprobe to verify that no parylene residue remains on the surface. Additionally, a white-light interferometer may be used to approximate the depth of the inlets/outlets to verify that the inlets/outlets have been opened. After completion of the parylene etch, the patterned parylene should be representative of the final device outline. An AZ4620 8 micron thick photoresist mask is used to protect the exposed gold sites and the inlets/outlets for the following DRIE step. Since this is thicker photoresist, it is more viscous and less likely to clog the inlets/outlets. This photoresist is spun at a rate of 3000rpm for 30 seconds, after which it is soft baked at 100 ^{o}C on the hot plate for 10 minutes. Next, the photoresist is exposed for 80 seconds and developed in 400K Developer solution (mixed with 3 parts DI water) for 2 minutes after which it is optically inspected and subsequently descummed. The wafers are then processed again using the LAM9400 with a dry oxide etch recipe in an effort to remove any residual oxide layers. A timed etch of about 90 seconds should be sufficient. At this point, the only two surface layers should be thick photoresist and silicon, with the silicon exposed at areas adjacent to the parylene front-side patterns. The next stage is etching of the silicon via the STS Pegasus standard DRIE BOSCH process as described during trench etching. For this process, the recipe used is a modified recipe #3 with reduced power. Recipe #3 differs from recipe #1 in that the cycle times are more beneficial for large features and faster etching times. In the reduced power recipe, the RF coil generator is reduced in power by more than half in comparison to the standard recipe #3. The purpose of this reduced power is to reduce the heating effects on the wafer. Additionally, the wafer should be checked at least every 25 minutes to verify proper etching of silicon and to reduce cumulative heating effects. A total of 90 minutes with the reduced power recipe results

in an etching depth of about 200 µm. The Dektak surface profilometer can be used to verify etching depth. After completion of DRIE etching, PR stripper is used along with Drytek descumming (as described earlier) to remove any residual photoresist. Finally, the wafers are immersed in the aluminum etch bath to strip the aluminum mask.

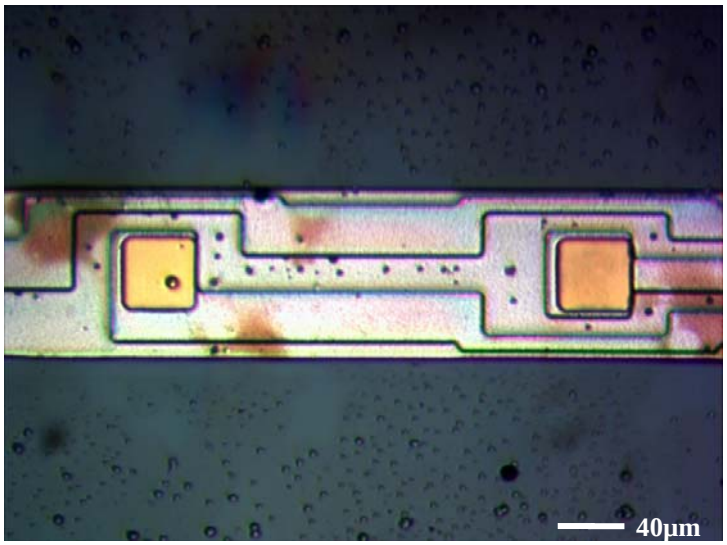

Figure 3-4: After Creating Aluminum mask on Parylene

Lessons/Potential Pitfalls: It was occasionally observed that with standard oxygen plasma etching of parylene, a thin parylene residue remained on the surface of the silicon after a long period of parylene etching. This residue is quite undesirable resulting in an etch stop and black silicon production during the DRIE step. For this reason, CF_4 is added to aid in removal of this residue. Optical microscopy and inspection by scratching the silicon surface is a quick way to determine complete removal of parylene. Instead of using the LAM9400 to etch the residual oxide on the silicon, BHF was originally chosen due to ease of use. However during the BHF dip, the thick photoresist was observed to not provide a complete protection of the aluminum mask. Due to the large step height of the parylene, the step coverage of thick photoresist may be incomplete in protecting the

entire aluminum mask and some areas of aluminum may be attacked by the BHF. During DRIE, etching should be conducted carefully, starting with 2 – 5 minutes and continuing to larger duration cycles as a proper etch rate is observed (should be about 4 microns per minute). This is important because black silicon can be observed earlier and prevented via simple measures such as more RIE etching of parylene or more LAM9400 dry oxide etching. If black silicon is accidently formed, the surface can be treated via XeF_2 isotropic etching for 3 or 4 cycles. This will cause some undercut of the devices (undesirable) however it is necessary in order to proceed with DRIE.

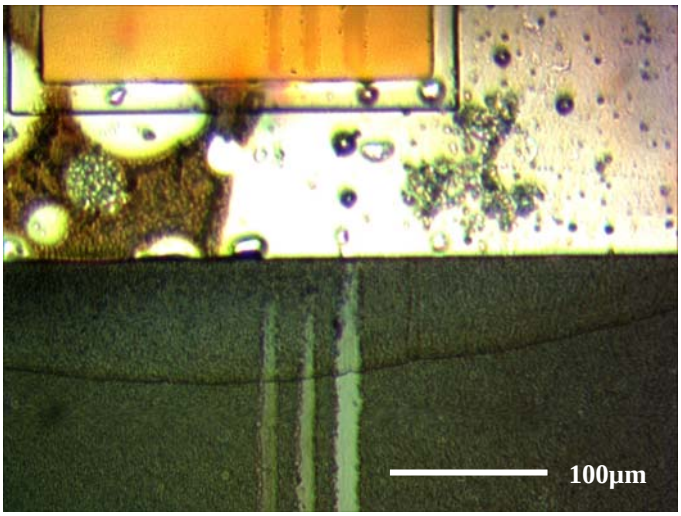

Figure 3-5: Parylene Residue

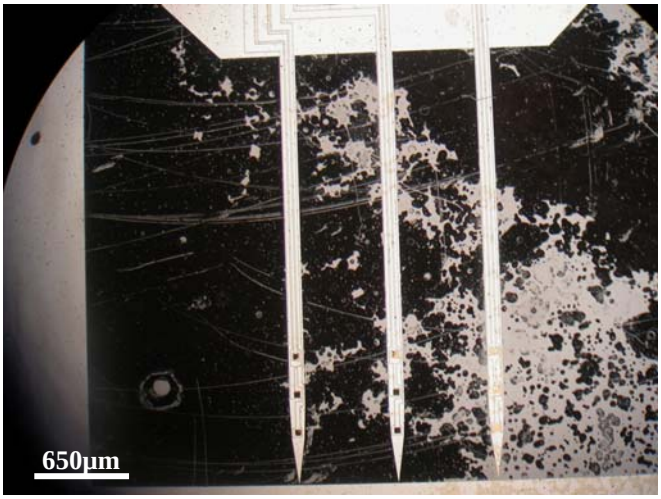

Figure 3-6: Black Silicon During Frontside DRIE

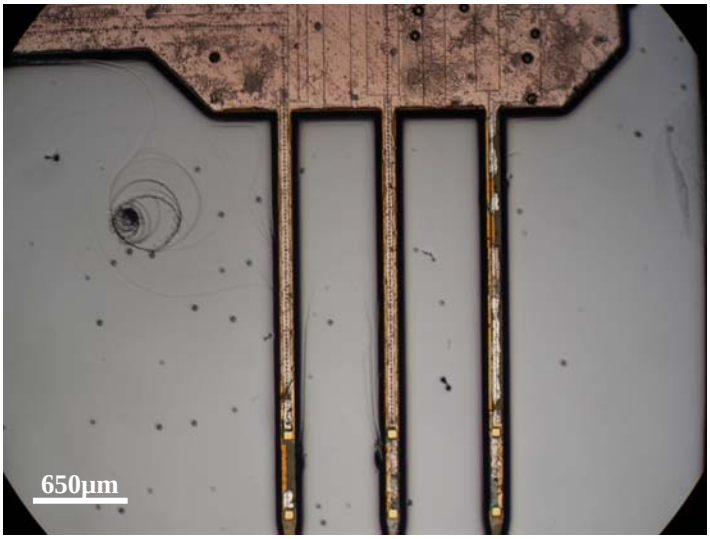

Figure 3-7: After XeF2 and consecutive DRIE

3.10 10th Step: Backside Etch/Device Release

After the devices have been shaped from the front-side of the wafers, the last and final steps involve shaping of the backside of the devices and release of the devices via the Pegasus STS DRIE system. For the majority of the rest of the process, processing will proceed on the backside of the wafers unless otherwise stated. In the front-side etching step, the devices are shaped 200µm into the silicon. In the back-side etching

step, the devices must be shaped into three distinct depths: a non-etched portion corresponding to the thickness of the device islands, a depth equivalent to the thickness of the wafer minus the depth of front-side etching for the device shanks, and a depth corresponding to the entire thickness of the wafer for the completely flexible regions. Since the etching depths are so large, photolithography after the first DRIE etch step would be very difficult. As a result, the patterns for both sets of DRIE etching must somehow be on the wafer before proceeding with any DRIE etching. Photoresist as a mask is easy to work with as no additional etching steps are needed and the photoresist can be removed easily using photoresist stripper solution or acetone. However, this could only work for one of the masks as all photoresist masks would be removed by photoresist stripper solution or acetone. A metal mask such as aluminum could be used, however certain tools restrict the use of metal masks (such as an aluminum mask), including the Pegasus STS DRIE system. The parylene layer on the back-side of the wafer, which was grown from previous parylene deposition steps (which should be 15 micron thick), can be utilized as a good alternative for a metal mask in the DRIE. Since the features for the last mask are quite large, a thick photoresist may be used to pattern the thick parylene layer. AZ9260 photoresist is spun on the backside of the wafer at a speed of 2000rpm to achieve a thickness of about 10μm. This thickness is reasonable as only a few microns of parylene are actually needed to serve as a mask in the DRIE. After the photoresist masked is completely etched away via oxygen plasma, the parylene will be etched uniformly until the originally exposed areas are completely etched. This should result in a 10μm thick parylene mask. To prevent thermal deformation of the parylene on the front-side, the photoresist is baked for 20 minutes at 100^{o}C on a hot plate. The thick

photoresist is then exposed for 55 seconds after which is developed in AZ400K developer solution (1:4 400K:DI water) for about 2:30 minutes. As before, the parylene is etched away using Drytek oxygen plasma (30sccm O_2 gas, 150 Watts, and threshold pressure of 200 mTorr) for 90 - 100 minutes. Near the end of the etch, 6sccm CF_4 can be added to the gas mixture to etch away any parylene residue from the oxygen plasma etching. To ensure the parylene is completely removed from the exposed regions, the wafers can be scratched and observed under optical microscopy. After parylene has been removed, any underlying oxide layer is removed using the LAM9400 oxide etching recipe as in step 4 (utilizing a mixture of C_2F_6 and Argon) for duration of about 2-3 minutes. The Nanospec optical analyzer can be used to ensure removal of the oxide layer. At this point, there should be only exposed silicon and a parylene mask corresponding to the final DRIE mask. Next, we spin another thick photoresist layer as before (AZ9260 10μm thick photoresist) and pattern using the second to last photoresist mask, which corresponds to the completely flexible regions of the devices. Photolithography proceeds as before for patterning of the parylene layer, after which the wafer is descummed using oxygen plasma as in previous steps. After all masks patterning is complete, the wafer can be wafer bonded to a backup wafer using Crystal Bond 555. Crystal Bond 555 is a wafer bonding agent that melts at 60 ^{o}C and is water soluble. First, the backup wafer (a bare silicon wafer) is heated on a vacuum hot plate to 80 ^{o}C, after which the stick of crystal bond is applied to the center of the heated wafer thereby melting crystal bond on the wafer. Next the device wafer is placed with the front-side facing the melted crystal bond of the backup wafer. The vacuum hot plate is then pumped down for 5 minutes after which the chamber is slowly vented and the wafers are removed. After bonding the

wafers to backup wafers, the combined wafers processed in the LAM9400 with the oxide etching recipe for 1 minute to remove any residual oxide layer. As with the front-side etching, the reduced power LNF Recipe #3 is used in an effort to avoid excessive heating effects. Etching continues until a depth of 200μm is achieved (corresponding to the depth of the front-side etching). Etching depth can be measured using the Dektak surface profilometer. After completion of the first DRIE etching process, the remaining thick photoresist is removed via spinning on a photolithography spinner (2000 rpm) using sequential acetone and isopropanol spray until all of the photoresist is removed. This photoresist removal method is preferred compared to the usual photoresist stripper solution dip because it maintains the crystal bond between the device wafer and backup wafer, eliminating the need to first remove the crystal bond and then later reapply it. After photoresist removal, the bonded wafers can be descummed again to remove any residual photoresist. At this point, the device wafer should have exposed patterned silicon with the previously patterned parylene layer still present. The bonded wafers are placed back in the Pegasus STS DRIE and etched using LNF Recipe #3 until the devices are released. Near completion of this final etching step, the underlying front-side shanks and the titanium/gold layers of the flexible parylene cables should start to become visible. After completion of the process, the devices should still be attached to the backup wafer via crystal bond. To release devices, the bonded wafers are placed in hot water (60 ^{o}C) and the devices are carefully removed.

Lessons/Potential Pitfalls: For back-side photolithography, a special spinner chuck is needed for proper spinning of the front-side patterned wafer. The reason for this is the

large front-side features which prevent proper vacuum grip of the normal spinner chuck. The proper chuck to use involves utilization of a rubber ring which elevates the wafer slightly above the surface of the chuck. As the vacuum of the chuck is applied, the space between the wafer and the chuck surface is brought to vacuum thereby gripping the patterned wafer. The process of applying crystal bond also presented various issues in the back-side etch process. The typical process for bonding with crystal bond involves utilizing a few milligram shavings of crystal bond to the heated backup wafer. For device wafers with limited to non-existant front-side features, the amount of crystal bond used is justifiable. However, since there is a 200µm front-side etch, regions within the 200µm-depth regions would not be in direct contact with the backup wafer, thus resulting in heat-isolation and therefore overheating of the devices. Crystal bond 555 is not a very good heat conductor, but it is significantly more conductive than air. Thus, enough crystal bond should be used such that the 200µm depth is sealed but not too much such that there is poor conductivity between the device wafer and the backup wafer. In addition, care must be taken to not allow any air bubbles to be trapped between the two wafers. The vacuum hot plate helps in removing some trapped air, however air can still be trapped underneath the wafer. In fact, during the second DRIE step (etch-through), a complication developed and the middle-portion of the wafer developed a small explosion which damaged many of the devices towards the middle of the wafer. This explosion was likely due to the thermal heating and expansion of trapped gas within the wafer bond during DRIE. In an effort to resolve the problem, crystal bond can be applied to both wafers before the two wafers are bonded together. In this manner, trapped gas within the bond can be avoided, thus avoiding wafer explosion.

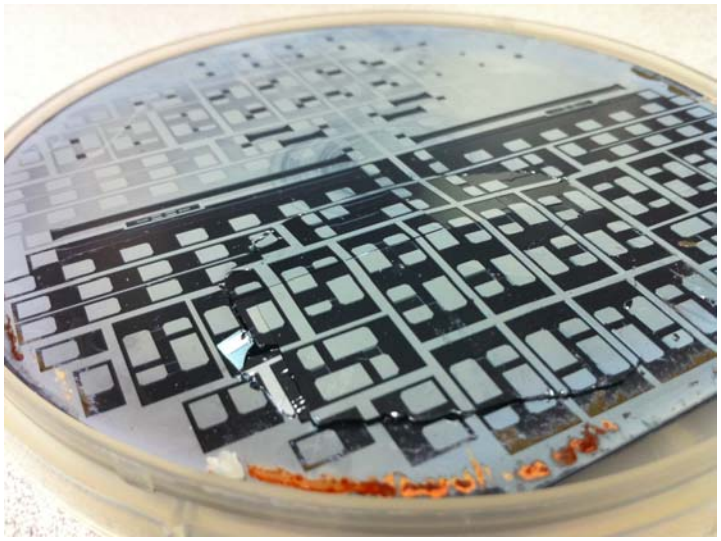

Figure 3-8: Exploded wafer during final backside DRIE

CHAPTER 4: FABRICATION AND PACKAGING RESULTS

4.1 Introduction

As discussed in the design chapter, development of the neural devices was an iterative process. Prototypic devices were designed, analyzed, tested, and then redesigned with modified features. The first prototypic devices demonstrated some of the beneficial features of these devices including multiple islands, flexible interconnects, and integrated microfluidics. The device depicted in Figure 4-1is one of the prototypic devices, having two penetrating probe islands, a planar-electrode island, and wire bonding island, with each island being connected via a completely flexible interconnect. This device, like the other prototypic devices, demonstrated the overall processing technique in developing this neural device technology. However, these devices had a number of issues including clogged microfluidic channels and easily friable island interconnections. In addition, the parylene flexible interconnect was full of intrinsic stress causing the parylene cable to be distorted after fabrication. In an effort to resolve these issues and generate neural devices with relevant device dimensions and parameters, the second generation of neural devices were designed and produced.

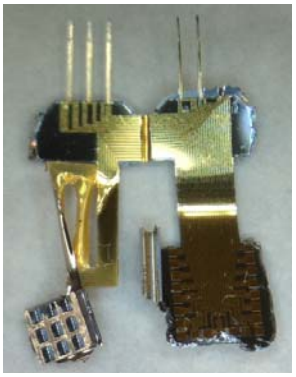

Figure 4-1: Prototypic Neural device with planar and penetrating probe islands

4.2 2nd Generation Neural Devices

These devices were the first batch of neural devices designed to complete a specific task – recording electrical signals occuring at different layers of cortex in the rat brain. As mentioned in the design chapter, six different device designs were created from the 2nd generation of neural devices. Three rigid electrode-only devices were created: a rigid single-island device, a rigid two-island device, and a rigid-three island device (Figure 4-2). As mentioned in the design section, the purpose of creating rigid device designs was to reduce the complexity of the neural devices. The first prototype neural devices often suffered from broken and disconnected flexible interconnections. In addition, the prototypic flexible devices created challenge during implantion of the devices, as the probe islands would be very difficult to manually position due to the ultra-flexible interconnects. To avoid this problem and to allow reliable first-stage device characterization and animal testing, the rigid devices were designed with no flexible interconnection between probe islands and the wire bonding island. Additionally, since there were issues in regards to the functionallity of the microfluidic devices, rigid microfludic devices were also created with no flexible interconnect (Figure 4-3(a). These rigid devices were utilized in the majority of preliminary tests including impedance analysis, fluidic testing, and preliminary animal studies. In addition to the rigid devices, two flexible interconnect devices were created with flanked interfaces between the rigid islands and the flexible regions (Figure 4-3(b) and Figure 4-4). These flanked interfaces were presumed to reduce the likelihood of tearing of the flexible interconnect at the interface. In addition, a 45mm long flexible interconnect device was prototyped,

demonstrating the ability to create device which could potentially interface with a circuit board far away from the site of implantation (Figure 4-4). These 2nd generation devices were also created in two batches with different metalization layers: one was composed of 20nm/200nm chrome/gold and the other was composed of 20nm/200nm titanium/platinum. This allowed comparison studies between the impedance characteristics of both types of devices. One of the platinum devices is depicted in Figure 4-2(b).

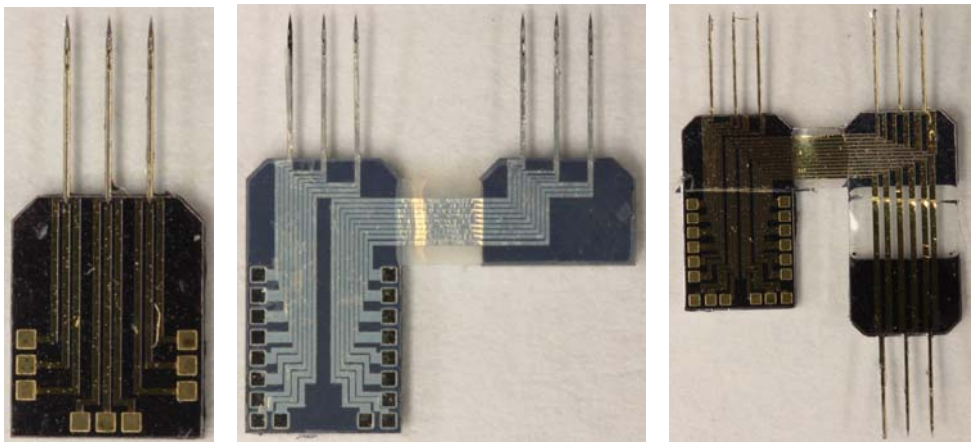

Figure 4-2: (a) rigid (gold) single-island device, (b) rigid (platinum) two-island device, and (c) rigid (gold) three-island device

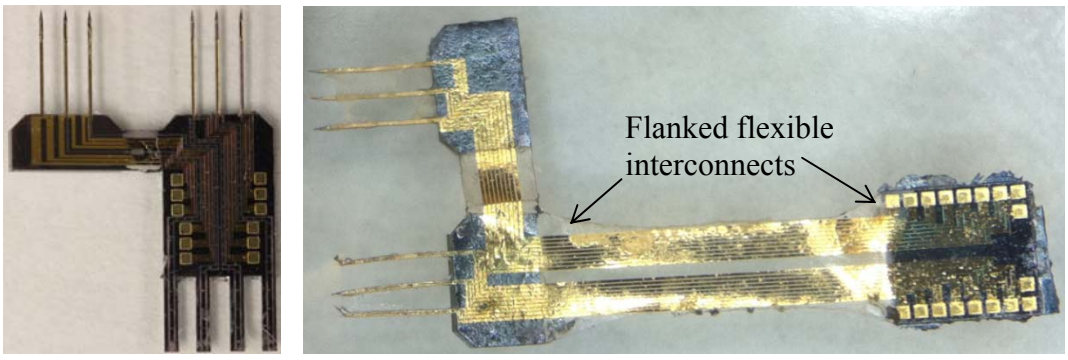

Figure 4-3: (a) a microfluidic device, (b) a prototype flexible interconnect device

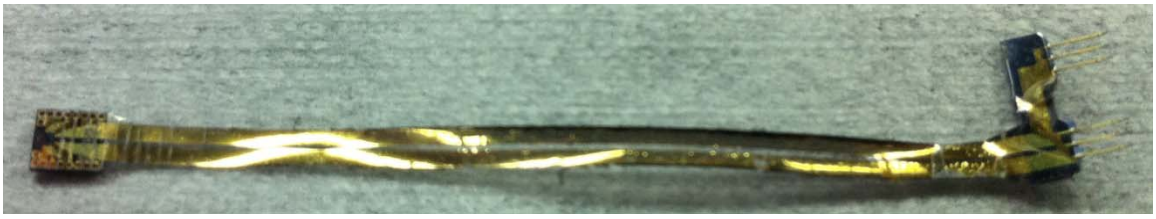

Figure 4-4: Prototypic extra-long (45mm) interconnect device

4.3 Trenches

After development and testing of the 2nd generation of neural devices, trenches were incorporated into the design. One of the major benefits of the trenches was encapsulation of the sidewalls of the silicon shanks. Figure 4-5 shows SEM images of the tip of a probe shank. It can be clearly observed that the sidewalls are encapsulated with parylene thin film. This sidewall encapsulation prevents the top parylene layer from peeling off during implantation. In addition, the electrical isolation of metal traces is also improved, as the parylene on the sidewalls may prevent exposure of the metal traces near the edge of the shanks. Another benefit of the trenches which was realized in later designs was that the parylene trench could serve as an etch stop in the lateral direction. This allowed for the development of completely-flexible and partially-flexible devices.

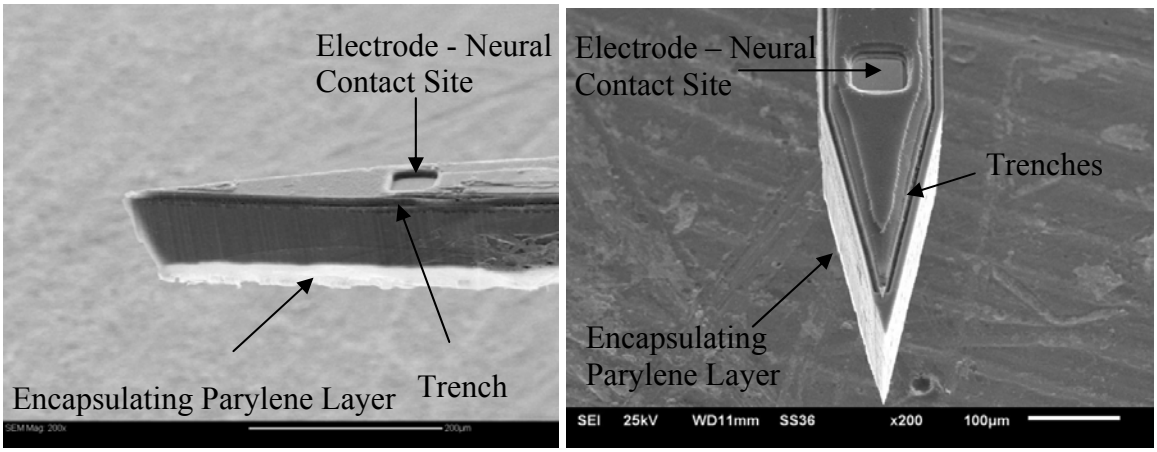

Figure 4-5: Probe tip demonstrating deep trenches and associated encapsulating parylene layer

4.4 Flexible Shank Devices

Upon development of the trenches for encapsulation of the sidewalls, it was understood that the deep trenches could serve as an etch stop in the lateral direction. Thus the concept of creating flexible shanks was created as described in the design section. Flexible shank designs were created for all of the 6 designs used previously. As a means to conserve cost and time while fully demonstrating the technique, metal and oxide layers were not included in this batch of devices. In addition to the flexible shank design concept, microchannels for the purpose of adjusting the stiffness and enhancing the durability of the flexible interconnect cables were also introduced in this design. Two of the flexible shank devices are depicted in Figure 4-6. Figure 4-7 depicts scanning electron microscope (SEM) images of the flexible shanks. Figure 4-8 demonstrates utilization of the flexible shank concept on the chronic device design.

Figure 4-6: Flexible shank devices with (a) two island device with completely flexible shanks and (b) flexible interconnect device with partially flexible probe shanks; devices also demonstrate stiffness-enhancing microchannels

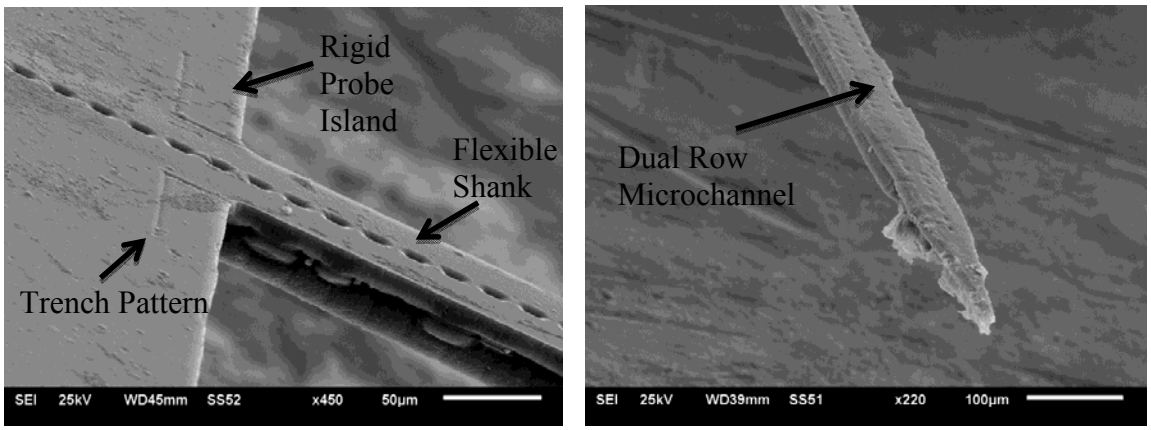

Figure 4-7: SEM images of flexible shanks

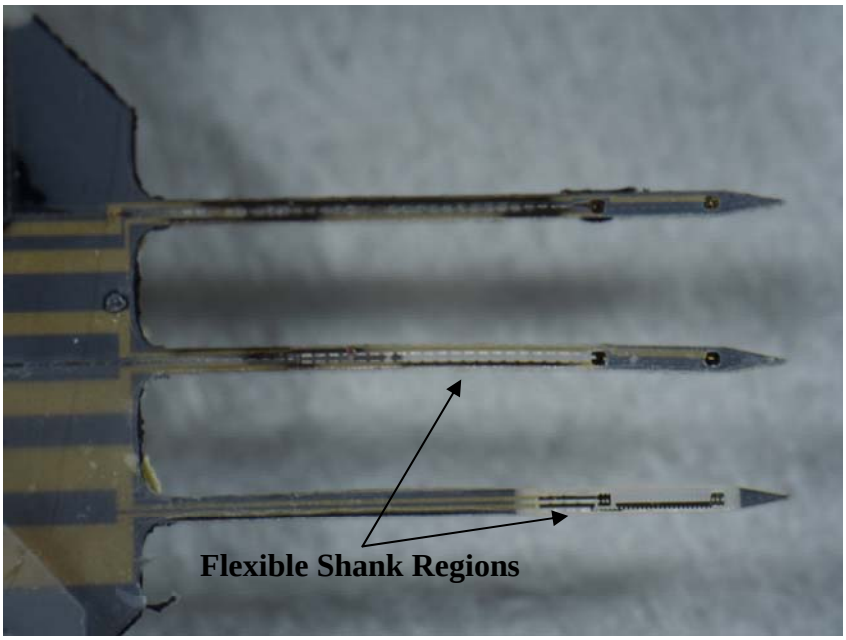

Figure 4-8: A chronic device demonstrating the flexible shank feature

4.5 Chronic Devices

Chronic neural devices with different parameters have been designed and fabricated. Figure 4-9(a) shows a photograph of one fabricated planar device with two shank islands and one interfacing island (with bonding pads). The assembled 3D neural probe with

4×3×2 array of electrodes is shown in Figure 4-9(b). It should be noted that alignment of the probe islands was achieved manually through an optical microscope. Better alignment could be achieved through the use of alignment holes. This feature will be added in future device designs. The folded parylene C layer connecting the Si islands can be clearly observed.

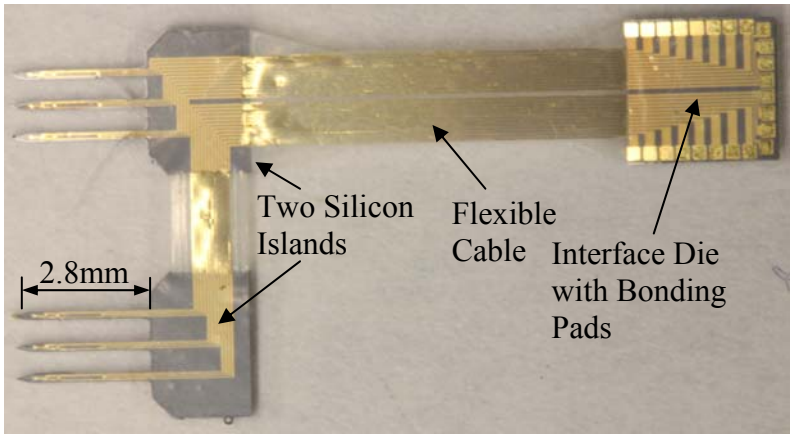

(a)

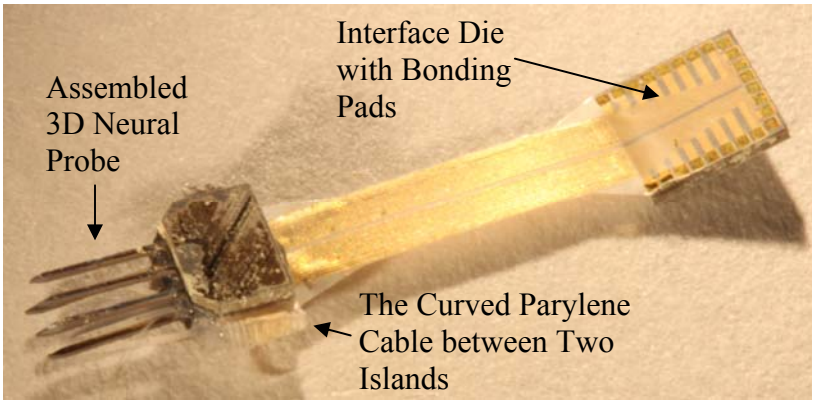

(b)

Figure 4-9: (a) Planar silicon islands structure before folding; (b) One assembled neural probe with 2×3×2 electrode array (2 silicon islands, 3 shanks per island, and 2 electrodes per shank)

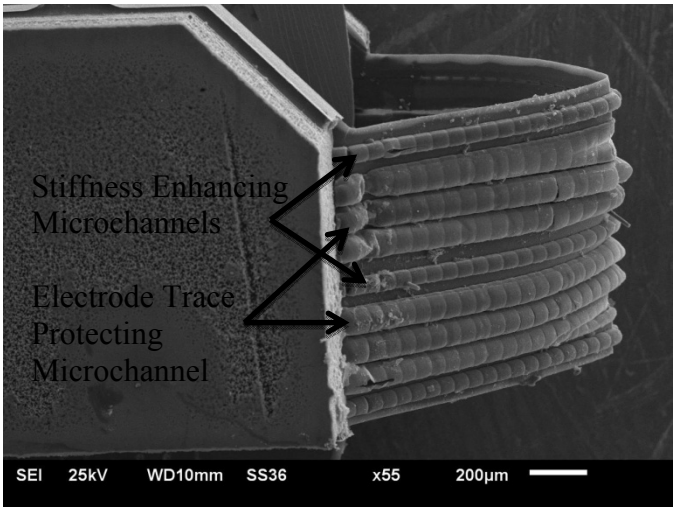

Figure 4-10: SEM image of folded interconnect connecting two probe islands

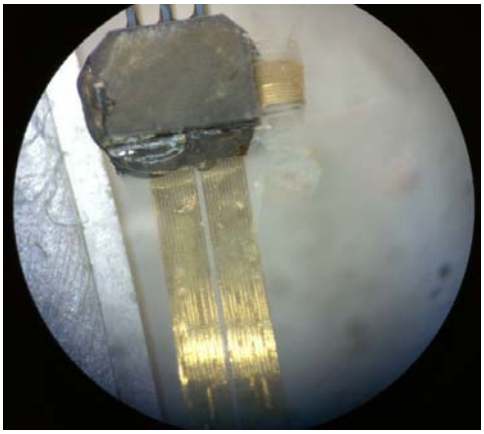

(a)

(b)

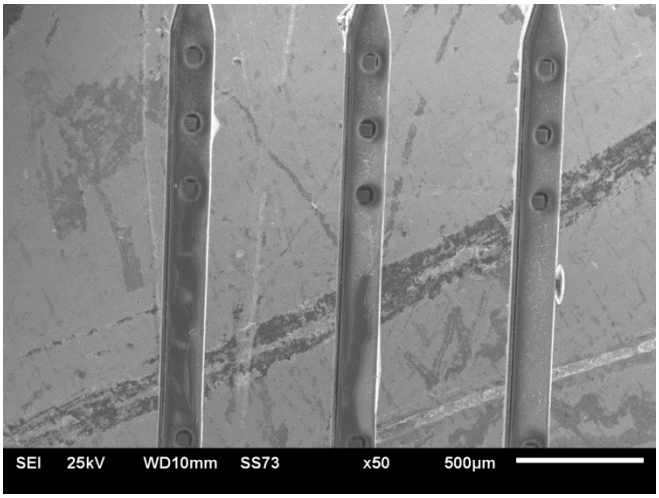

(c)

Figure 4-11: (a) close up view of the flexible interconnections; (b) close up view of aligned probe shanks; (c) probe shanks of electrode-only chronic device

3D chronic neural devices with integrated microchannels have been demonstrated as well. A prototype with a 2×3×2 3D array of electrodes and four microchannels has been developed as shown in Figure 4-12. The four beams on the interfacing die are used to couple external tubing to on-chip microchannels. Figure 4-13 shows an SEM picture of a probe island with six electrodes and two microchannel outlet ports. The SEM image of the backside of a bent parylene cable without trace-protecting microchannels is shown in Figure 4-14(a). Note that both metal traces and microchannels are embedded in the flexible parylene cables. The embedded microchannels and metal traces are clearly observed. No breaks or cracks are observed on the folded microchannels, however some buckling of the channel can be identified. Though this could increase the flow resistance of the channel, this may not cause blockage of the channel. It should be noted that buckling in the folded microchannels can be avoided, as the bending radius can be adjusted by simply lengthening or shortening the flexible interconnect in the device design. The relationship between bending radius and flow rate will be analyzed in future studies. The cross section of a microchannel is shown in Figure 4-14(d). It is clearly seen that the microchannel patterns are sealed completely by the thick parylene.

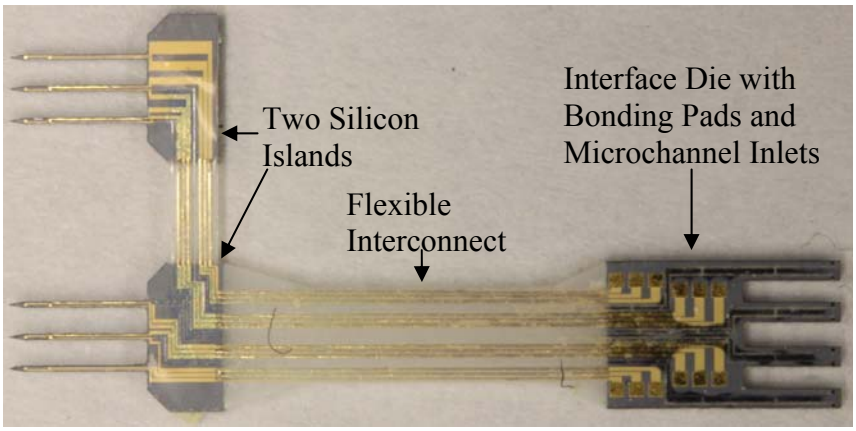

(a)

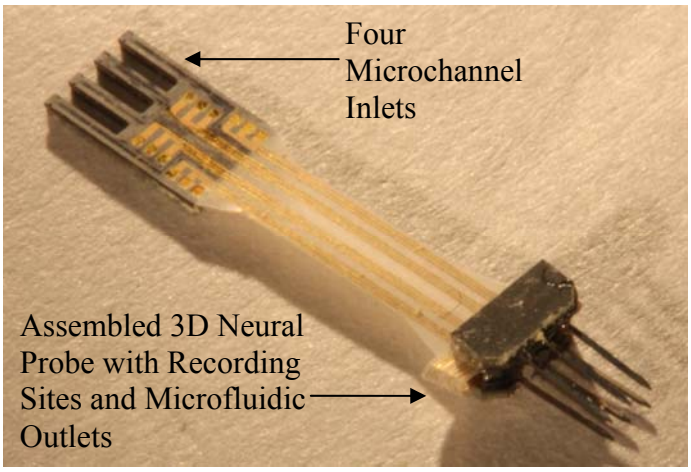

(b)

Figure 4-12: (a) Photograph of a neural probe device with 2 silicon islands and 4 integrated microchannels before folding; (b) photograph of an assembled neural probe device with a 2×3×2 array of electrodes (2 silicon islands, 3 shanks per island and 2 electrode per shank) and 4 integrated microchannels

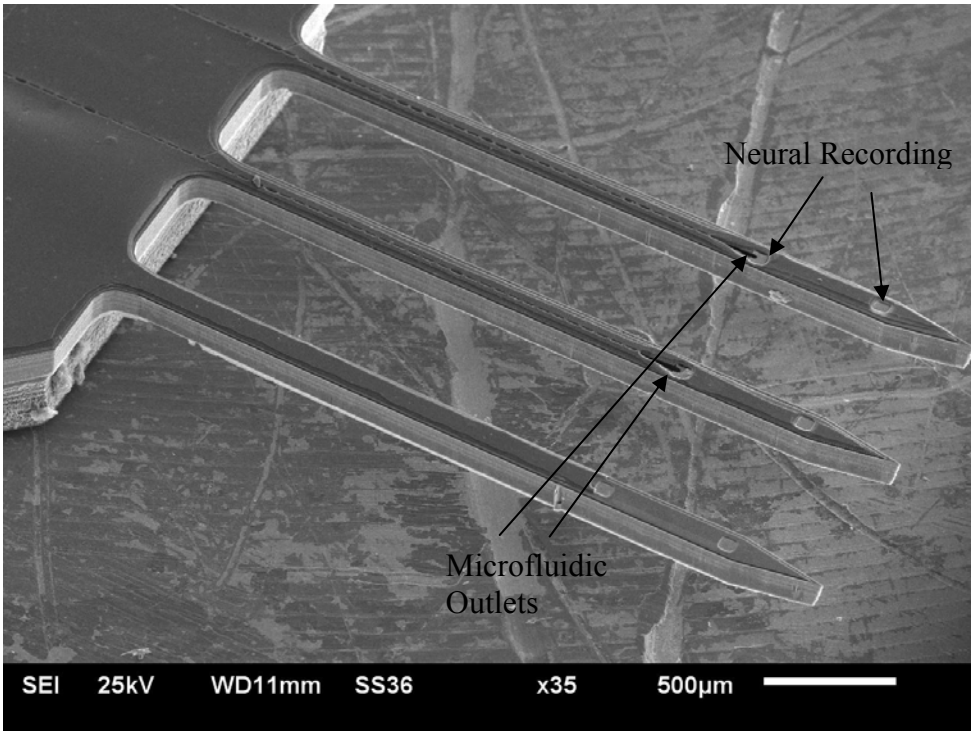

Figure 4-13: Probe island of chronic microfluidic neural device

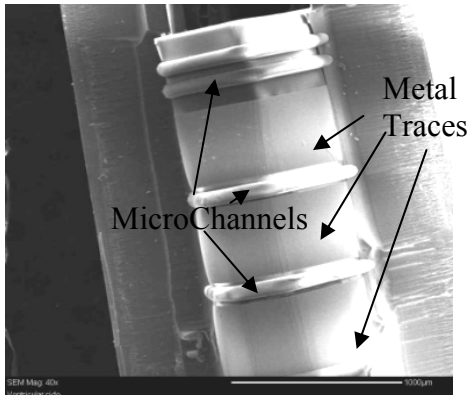

(a)

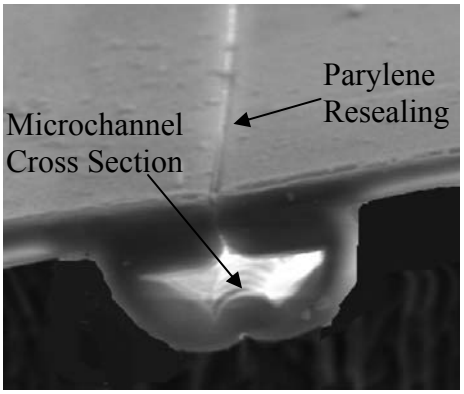

(b)

Figure 4-14: (a) SEM image of the backside of a bent parylene cable between two islands; (b) SEM image of the cross section of a parylene microchannel

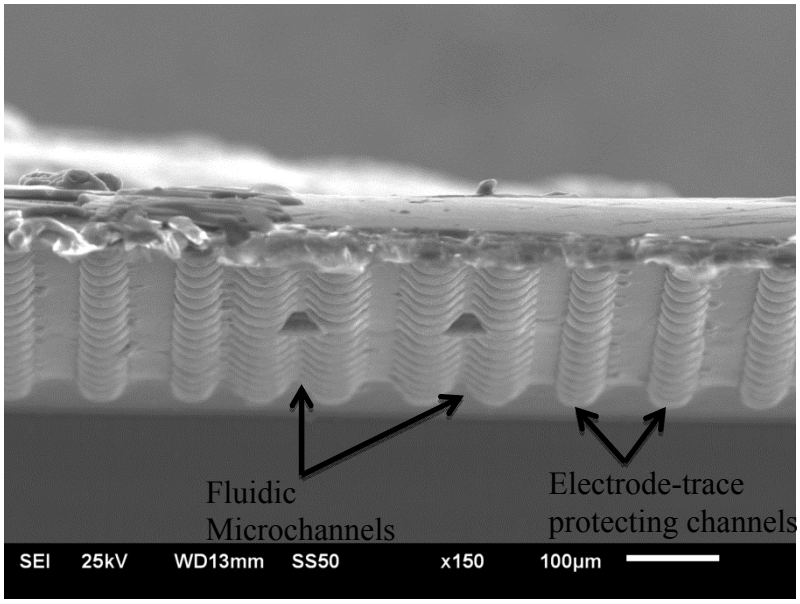

Figure 4-15: Backside of microchannels of flexible interconnect joining the bonding island to the probe islands; fluidic microchannels and electrode-trace protecting microchannels can be identified

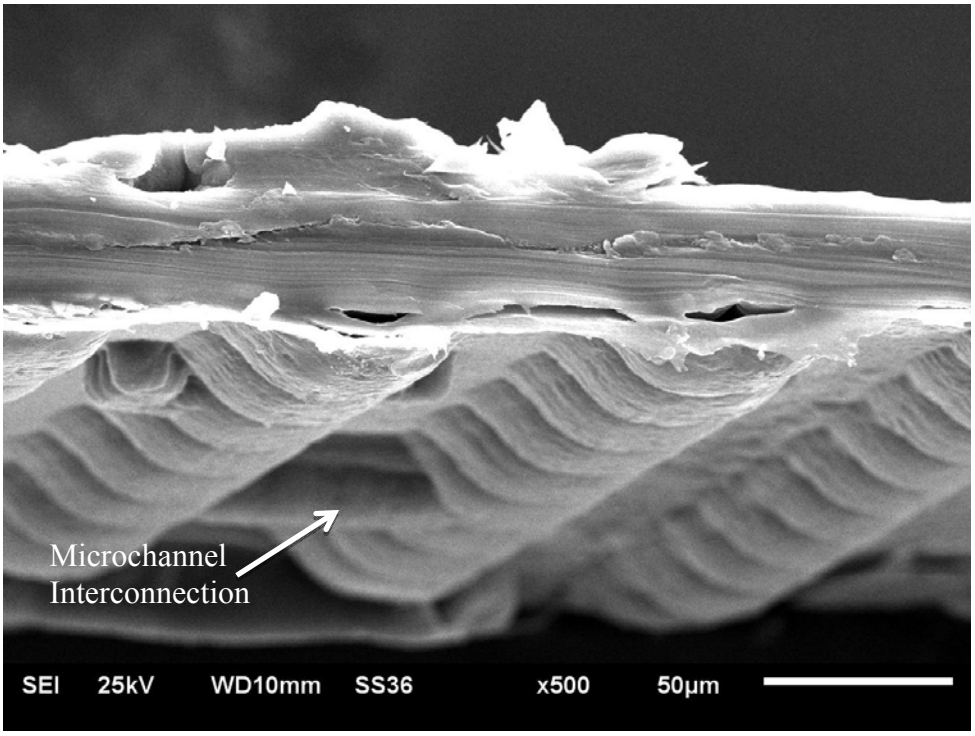

Figure 4-16: Cross-section of flexible interconnect cable; the microchannel cross-section appears smaller due to compression by the razor during cutting of the cable; microchannel interconnections can be identified between fluidic microchannels

Figure 4-17 shows the SEM microscope image of the inlet area on the tip of the coupling beam. The small discrete patterns are marks of openings on the parylene film for the XeF2 undercutting of the silicon substrate. These opening were sealed after depositing another thick parylene layer due to the nature of the conformal coating. Note that the inlets can be formed by either using larger openings or re-opening the inlet ports via RIE. To improve the yield, we used two parallel channels for one microchannel outlet with interconnections between parallel channels (Figure 4-16). Figure 4-18 shows the SEM image of one microchannel outlet. This image demonstrates placement of a microfluidic outlet within an electrode site.

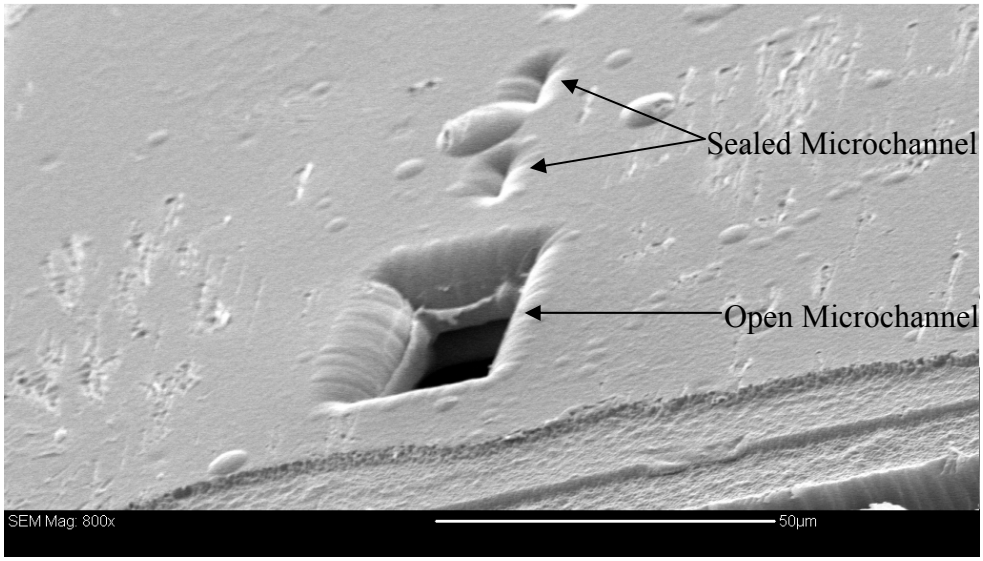

Figure 4-17: SEM image of a microchannel inlet

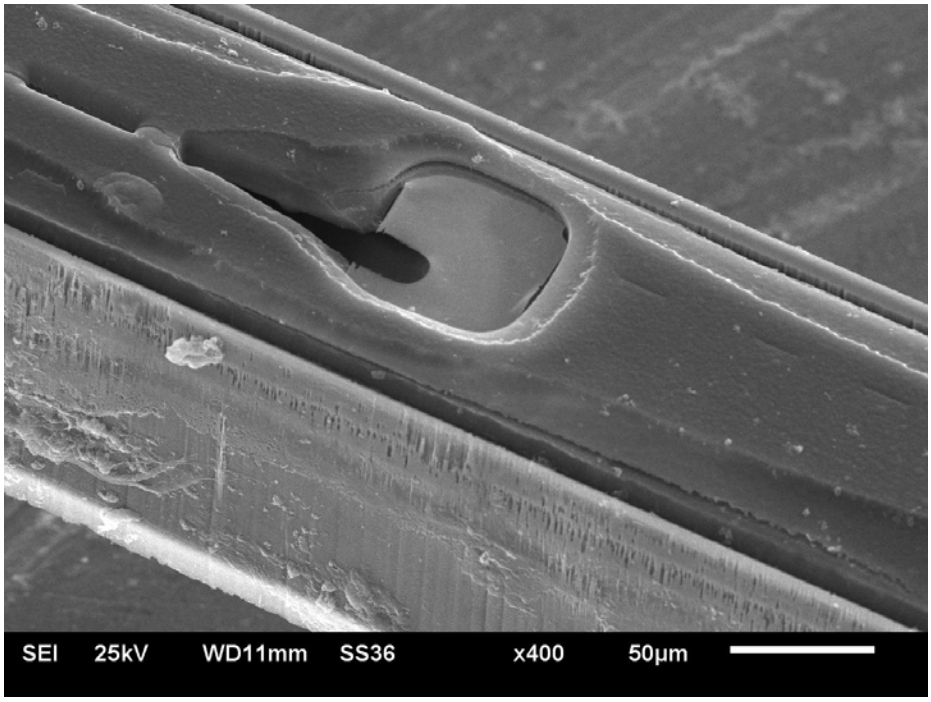

Figure 4-18: SEM image of microfluidic outlet port

4.6 Chronic Device Printed Circuit Board

As described in the design chapter, a customized chronic device printed circuit board (PCB) was designed along with the design for the chronic devices. As such, the spacing of the wire bonding pads on the PCB corresponds directly to the size parameters of the device wire bonding island. The PCB is the platform used to connect the omnetics connector to the chronic neural device. In addition, the board has soldering pads which also allow connection to the device. The final board dimensions are length of .51", width of .458", and thickness of .021". Images of the PCB are depicted in Figure 4-19.

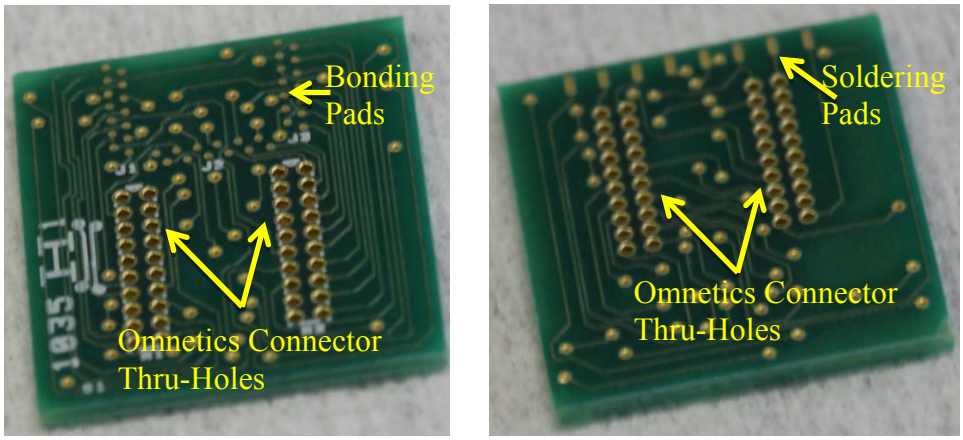

Figure 4-19: Front-side and Back-side of chronic device printed circuit board

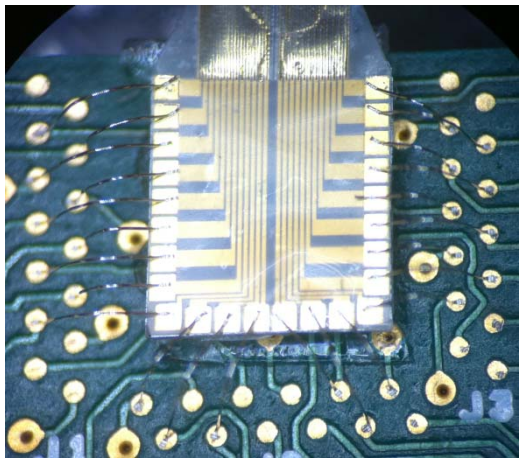

Figure 4-20: wire bonding between device wire bonding pads and PCB wire bonding pads

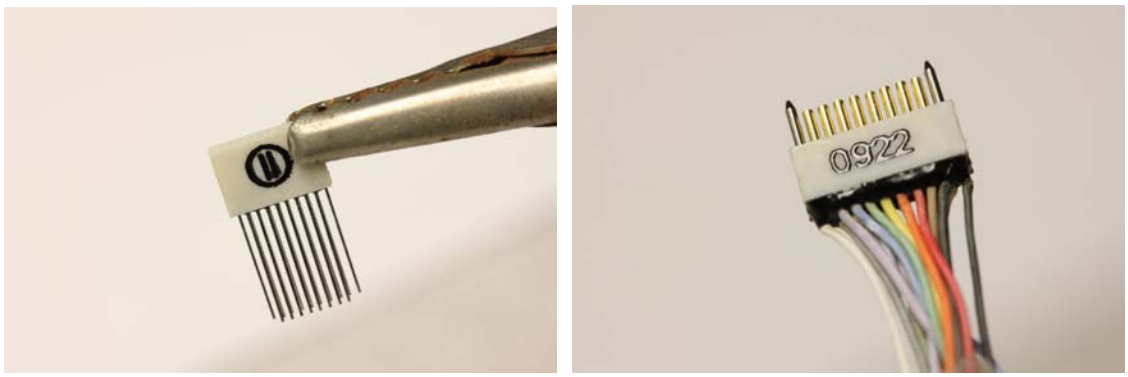

Figure 4-21: Optical images of (left) female Omnetics connector and (right) male Omnetics connector

4.7 Final Packaging of Device Assembly

Final package assembly begins with attachment of the Omnetics connectors to the circuit board. Although the connector can be placed on either the device-side or the soldering pad-side of the PCB, placing the connectors on the device-side of the PCB creates challenges during wire bonding of the device, as the connectors get in the way of the wire bonding tool. For this reason, the connectors are placed on the soldering pad-side of the PCB. The tails of the Omnetics connectors are fed through the thru-holes after which they are soldered at the point of contact between the tails and the thru-holes. It is important to avoid soldering between adjacent thru-holes and adjacent tails, as this creates short-circuits between channels. After soldering, the tails can be trimmed and the connections can be analyzed for any possible short-circuits. The wire bonding island of the chronic neural device is then fixed via double-sided tape or epoxy to the PCB between the wire bonding pads of the PCB. A K&S 4123 wire bonder tool with 1 mil diameter aluminum wire was used to create the wire bonds between the device and PCB wire bonding pads. After wire bonding connections are made, the device should now be tested for identification and verification of functional channels using an impedance

analyzer (see device characterization section). Once the channels are verified, the probe islands are assembled into their 3D assembly. An image of the fully packaged device with wire bond connections is depicted in Figure 4-22. At this point, the channels should be verified again to ensure no channels were lost during the folding process. Once channels are verified, the delicate wire bonding can be protected using a low-viscosity non-conductive epoxy. This epoxy can be placed over the entire device-side of the PCB to serve as a protectant and insulator, as this side will be attached to the skull of the rat. An image of the epoxy-protected assembly is depicted in Figure 4-23.

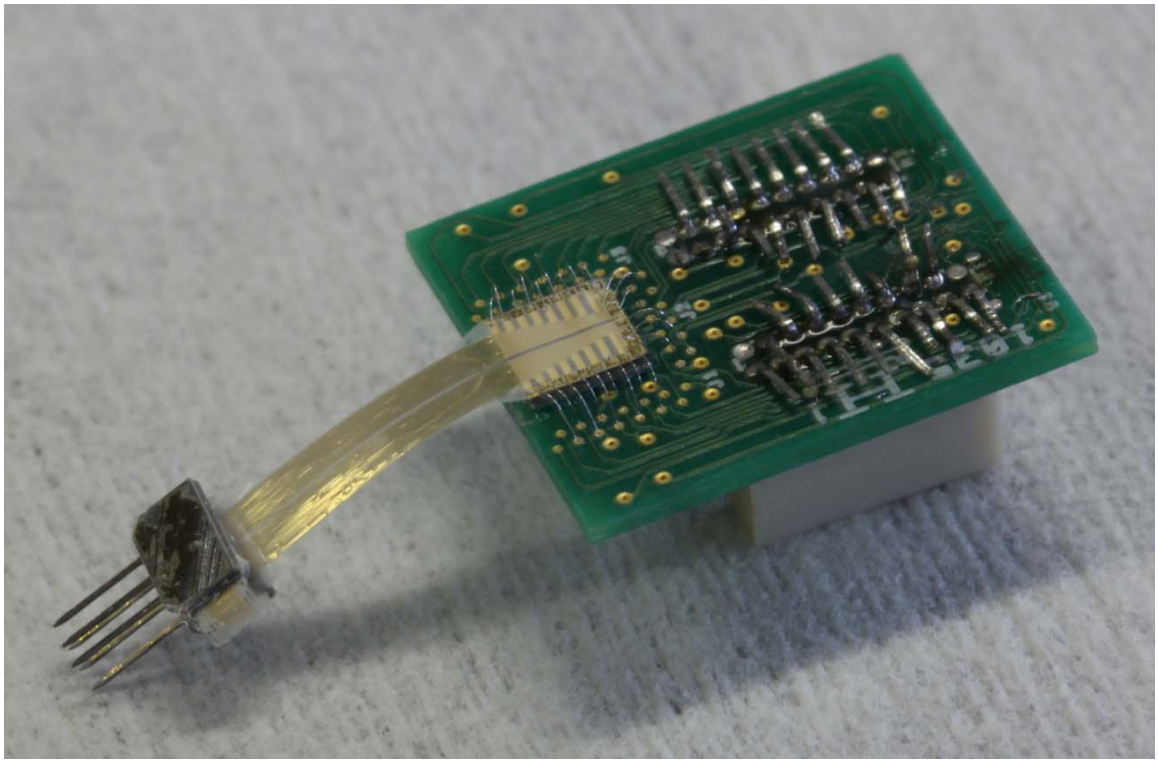

Figure 4-22: Fully packaged 3D neural recording array with, neural multi-electrode device, custom printed circuit board, and Omnetics connector; the device is connected to the board via wire bonding and the board is connected to the connectors via soldering between the tails of the connectors and the thru-holes of the board

Figure 4-23: Epoxy-protected device side of the PCB

4.8 Microfluidic Chronic Neural Device Packaging

As with the electrode-only devices, the microfluidic devices also have a wire-bonding island which fits perfectly within the wire-bonding pads on the PCB. As such, the microfluidic chronic neural devices are assembled similar to the electrode-only chronic device, with the exception of the microfluidic connections. In order to connect to the microfluidic inlets, flexible polyimide tubing (with an inner diameter of 620 μm) was coupled to each microchannel inlet after which they were sealed with marine (water resistant) epoxy at the interface between the microfluidic channels and the base of the inlets (Figure 4-24). After coupling of the tubing to the inlets, the device can be fixed and wire bonded to the PCB as with the electrode-only device. An image of a fully packaged microfluidic chronic device is seen in Figure 4-25. Figure 4-26 depicts an implantation model for animal surgery with black dotted lines representing the exposed surface of the rat skull during surgery. The probe islands are seen with shanks inserted into a model burr hole (3mm diameter). The device is fixed to anchoring skull screws as

utilized during animal surgery. The fluidic tubing can be flexed and cut as needed to properly implant the device

Figure 4-24: Polyimide tubing connected to inlets of microfluidic device

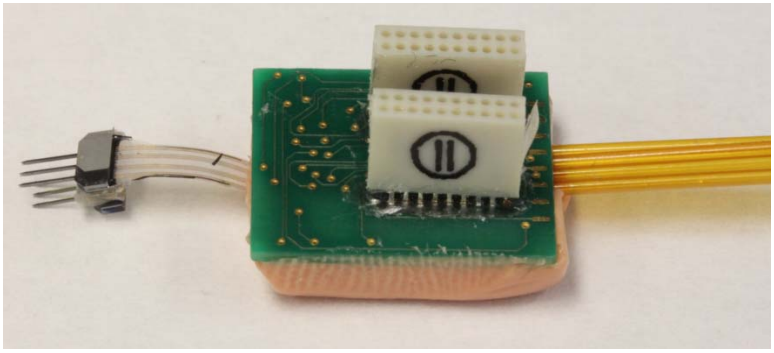

Figure 4-25: Assembly of microfluidic package assembly

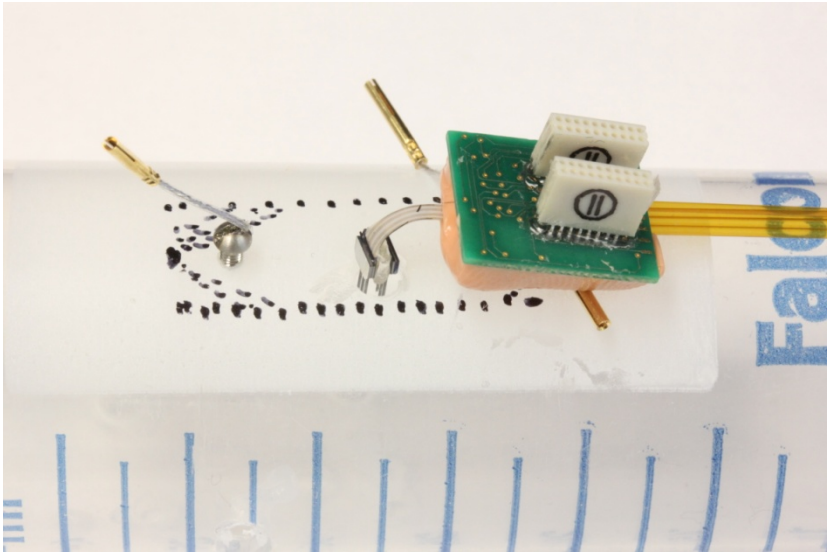

Figure 4-26: Implantation model for animal surgery

CHAPTER 5: DEVICE CHARACTERIZATION

5.1 Introduction

After development of the neural devices, it was important to characterize the devices in the benchtop setting to understand the recording capabilities of the neural devices before being used to record neural signals. In addition, the microfluidic channels were analyzed for flow rate and delivery of liquid substances. These characterization studies were used throughout the device development process as a means to improve the devices as issues arose. Animal studies were also used to improve device design, but this will be discussed in the animal studies chapter.

5.2 Electrode Impedance Analysis in Saline

Impedance of an object is equal to the relation of the potential difference (voltage) across an object divided by the current passing through the object. As such, to detect the very small voltages seen during a neural action potential, it is desirable to record signals from a low-impedance electrode. In accordance with work done in prior work, electrode impedances were measured in diluted Phosphate Buffered Saline solution (PBS) with an HP 4284A Precision LCR (Impedance) meter. 1mm diameter Platinum wire was used as a counter electrode. PBS solution is known to be a good electrolyte which closely resembles the ionic composition of extracellular fluid seen around neurons. The relationship between current across the electrode potential and electrode current within PBS solution can be defined by the following equation [83]:

$$i = i_0 \left[\exp\left(\frac{\alpha e \eta}{kT}\right) - \exp\left(-\frac{(1-\alpha) e \eta}{kT}\right) \right]$$

where η is the change in electrode potential, *i* is the electrode current, *kT/e* ≈ 26mV at room temperature, α is the symmetry factor, and i_o is the exchange current. The symmetry factor is between 0.2 and 0.5 for neural potentials between -200mV and +100mV. The exchange current is a constant which depends on electrode size. As the other variable of the equations are all constant in a constant environment, the impedance can therefore be determined by dividing the measured value of η, the change in electrode potential, by *i*, the electrode current. In addition, the interface can be modeled by a RC circuit with a constant phase element (CPE) as demonstrated in the diagram below (). This demonstrates the relationship between intrinsic capacitance and resistance as frequency changes. The impedance is dominated by the capacitance between the electrode and electrolyte interface. As the electrode surface area increases, the capacitance increases and the impedance decreases [84].

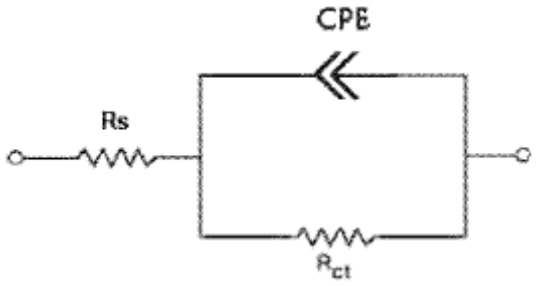

Figure 5-1: Relationship between gold electrodes and phosphate buffered saline in impedance measurements [84]; R_{ct} relates to the charge transfer resistance between the saline and the electrode and R_s relates to the series resistance between saline and electrode

5.3 Electrode Impedance Results

Initial impedance studies were conducted using the rigid single island neural devices. The purpose for using these devices was to measure the impedance of the electrode sites

without any additional complications such as flexible interconnections. The results for six distinct electrodes each with a recording area of 40x40 μm^2 are plotted in Figure 5-2. It can be observed that the impedances for each electrode tended to be less than 60 Kohms at 1 KHz. As mentioned in prior chapters, similar devices were also created using platinum/titanium instead of gold/chrome. For these devices, impedance values were measured to be less than 20 Kohms at 1 KHz (Figure 5-3). For both gold and platinum electrodes, our measured impedance values were smaller than those reported elsewhere [49, 50, 84-86]. This is believed to be due to electrode surface roughening during the DRIE step in our process. Work by other groups reported similar surface roughening caused by RIE [87]. Atomic Force Microscopy was utilized to examine the electrode surface roughness. As a control experiment, parylene was removed over one of the gold electrode tracings and the gold surface was measured underneath the parylene layer, which would not have been attacked by DRIE. Both images are presented in Figure 5-4. It was observed that the gold electrode has an RMS (root mean square) roughness of 196 Å whereas the protected gold has an RMS roughness of 14.3 Å. Such a degree of roughening would likely increase the effective surface area of the electrode, thereby lowering the impedance. It should be noted that while a roughened surface may be more susceptible to erosion upon stimulation, for the purpose of recording neural signals, stimulation-generated surface erosion would not be a major issue. However, further study should be done to determine long-term stability of impedance values.

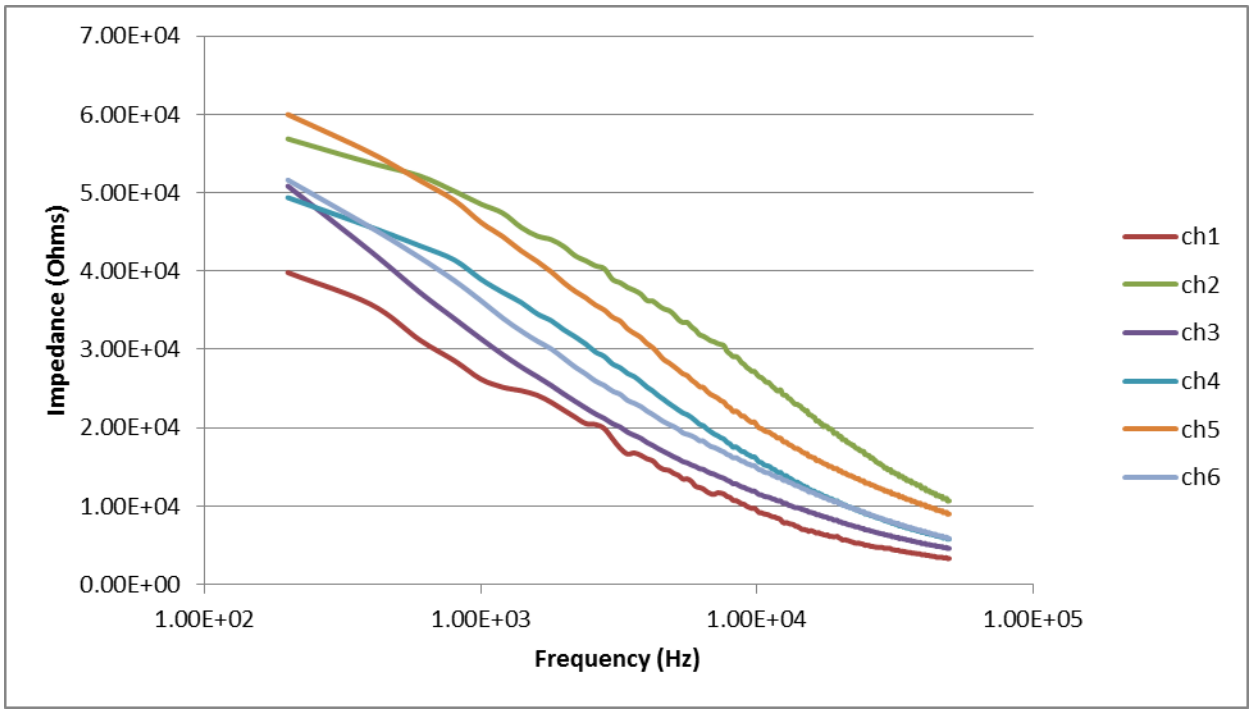

Figure 5-2: Impedances of six distinct gold electrodes (each 40×40 µm^2) from the same device

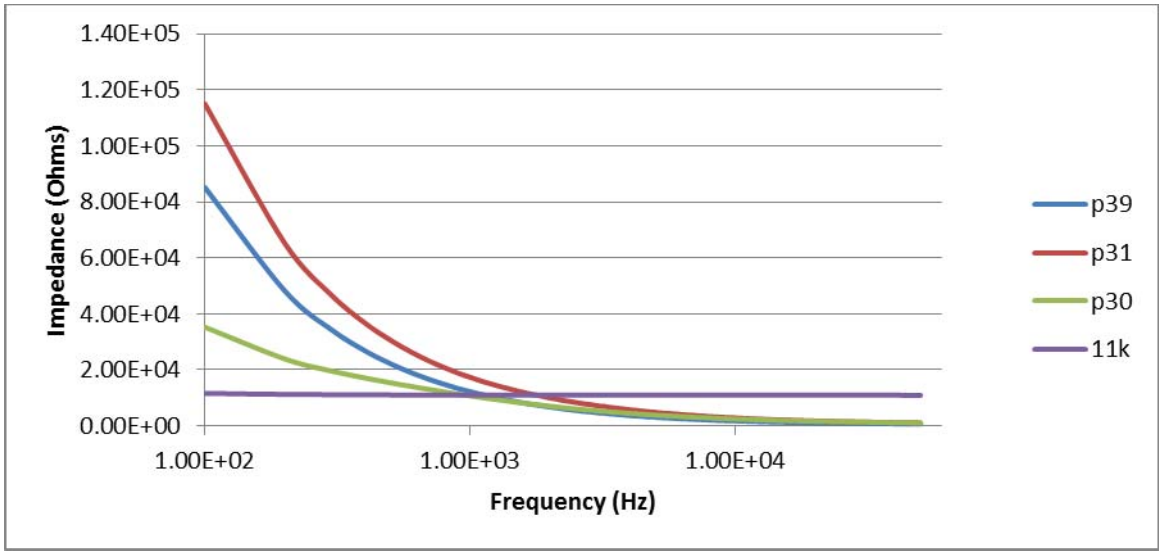

Figure 5-3: Impedances of three distinct platinum electrodes (each 40×40 µm2) from the same device

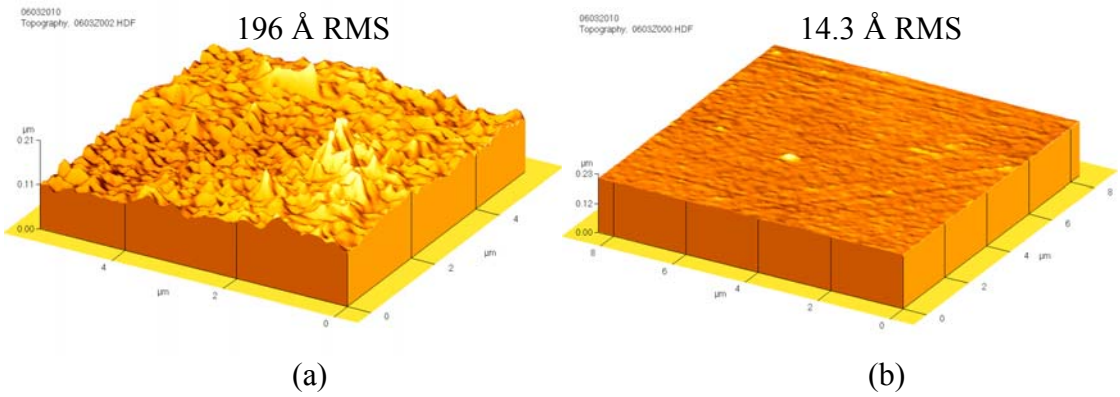

Figure 5-4: Atomic Force Microscopy of (a) the electrode surface and (b) the interconnect surface

5.4 Chronic Device Package Impedance Analysis

Throughout assembly of the chronic device package, the impedance of the device electrodes were analyzed to ensure functionality of all channels. As opposed to the impedance studies done during the rigid device impedance analysis, the chronic device package included a number of additional features which could increase the impedance of the electrodes. The first impedance analysis for the chronic device package was conducted immediately after the device was wire-bonded, but before the probe islands were aligned and packaged in 3D. The next set of impedance data was acquired after aligning and packaging the probe islands in 3D. The final set of impedance data was acquired after using epoxy to seal and protect the wire bonding along with the device side of the PCB (see fabrication/packaging results chapter). See Figure 5-5 for the impedance data for one of the electrodes before and after assembling the probe islands. See Figure 5-6 for the impedance data for the fully packaged and epoxy protected chronic device.

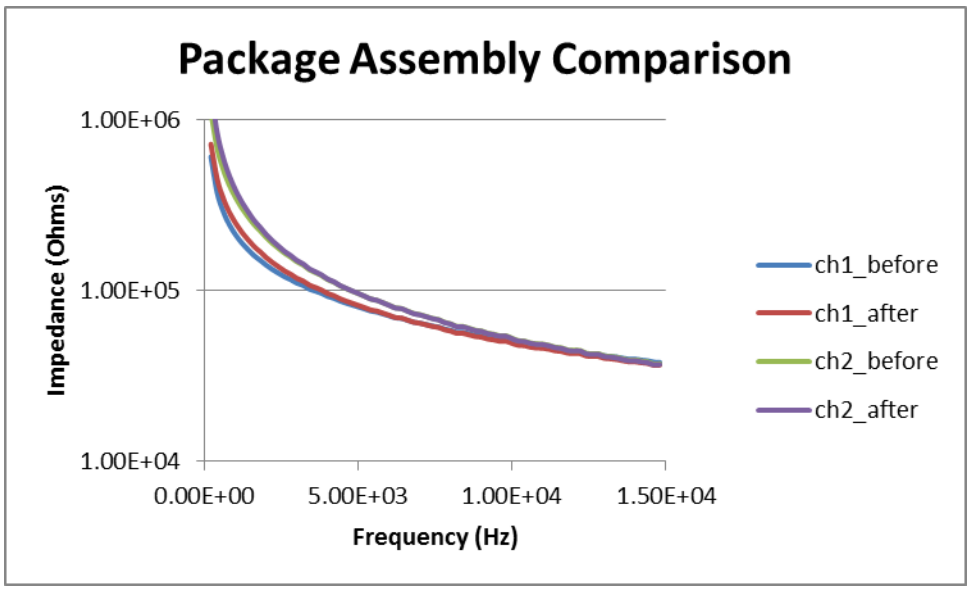

Figure 5-5: Impedance data of two channels before and after assembly of probe islands

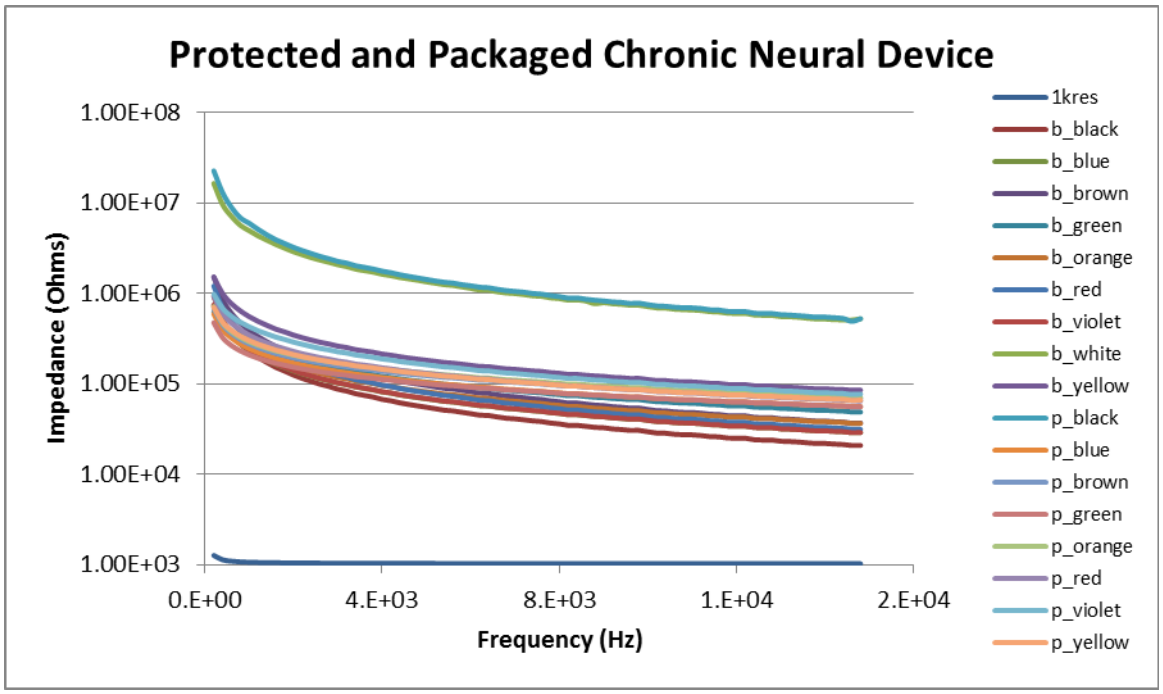

Figure 5-6: Impedance data for epoxy-protected fully packaged device; a 1 Kohm resistor and two unwired connections (p_black and b_white) are included for reference to the working channels

After analysis of the impedance data for a fully packaged device, it was desirable to characterize the change in impedance upon bending of the flexible interconnect

connecting the probe islands to the wire bonding island. In an effort to reduce the complexities of the analysis, an unpackaged chronic electrode-only device was wire bonded to a standard testing printed circuit board. The device was again placed in PBS solution as before and the impedances were measured using the LCR impedance meter. However, in comparison to prior measurements, the angle of the probe island was bent in relation to the interface island at several bending angles from 0 degrees to 150 degrees. The setup of the experiment and the results are displayed in Figure 5-7.

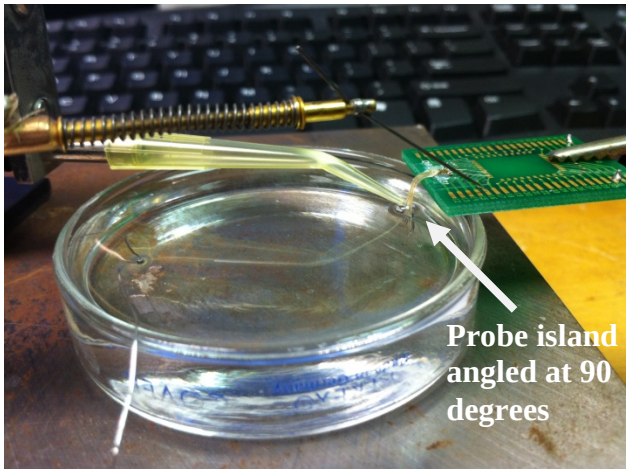

(a)

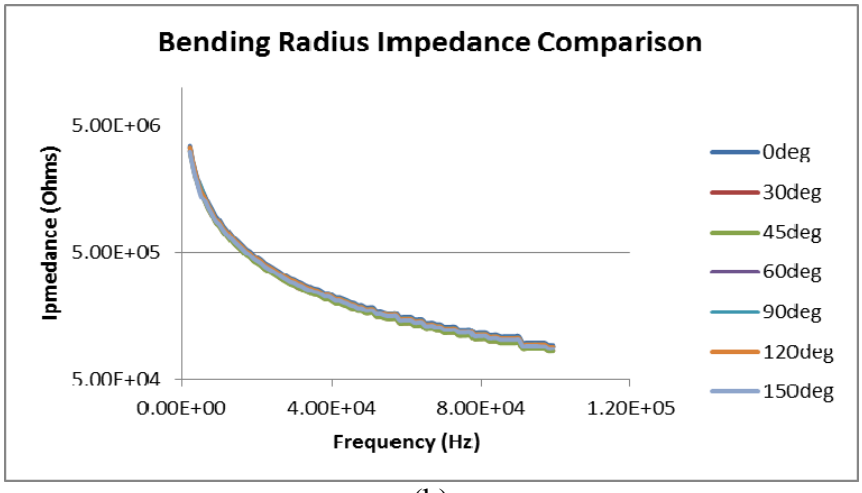

(b)

Figure 5-7: Bending radius impedance characterization (a) experimental setup with probe island bent 90 degrees relative to the wire bonding island and (b) angle results for one of the respective electrode sites

5.5 Microfluidic Channel Analysis

In addition to characterization of the impedance of the electrodes, it was important to characterize the fluid delivery capabilities of the microfluidic channels. The microchannel flow rate was measured using DI (deionized) water. A programmable syringe pump and digital pressure gauge were attached to the tube-connected inlets and were used for dispensing liquid and measuring pressure. Pressure measurements were collected for various flow rate settings programmed into the syringe pump. No leaks were observed on the surface of the microchannels when DI water was pumped into the channel. The flow rate setting as a function of pressure generated was measured and is plotted in Figure 5-8. It should be noted that with the typical pressure of a rat brain being less than 0.1 psi [46], large blood reflux into the microchannel would be unexpected, however further study is needed. Figure 5-9 depicts the flow of DI water traveling through one of the microchannels.

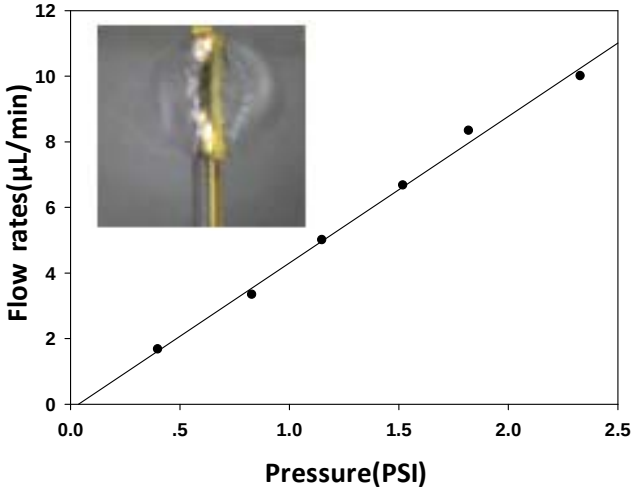

Figure 5-8: The measured relationship between flow rate and pressure. The inset picture shows a liquid droplet emerged from the outlet port of the microchannel at the probe tip.

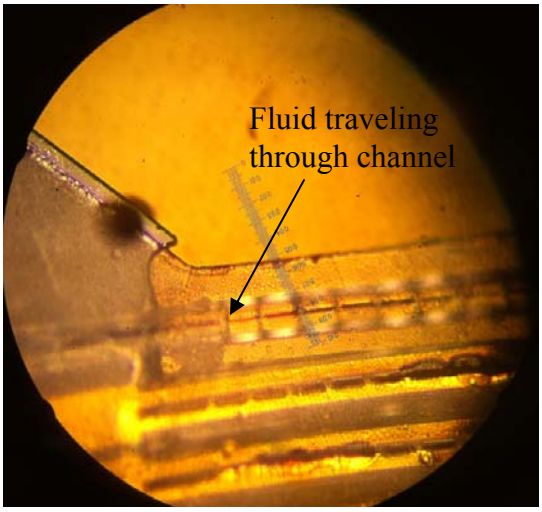

Figure 5-9: Fluid traveling through microfluidic channel

After measurement of the flow rate in relation to applied pressure of the microfluidic channel, it was important to test the functionality of the microchannels within simulated brain-like environments. As demonstrated in previous work [88], agarose gel (0.1% w/v) can be utilized as a brain phantom to simulate the pressure within the brain. As utilized in the study, Evan's blue dye was utilized to test the delivery of fluids through the microfluidic channels. Figure 5-10 depicts a microfluidic probe island before and after injection of Evan's blue dye through the microchannel. Figure 5-11 depicts delivery of the Evan's Blue dye into the Agarose brain phantom.

Figure 5-10: Microfluidic testing via Evan's Blue dye (a) before delivery (b) after delivery

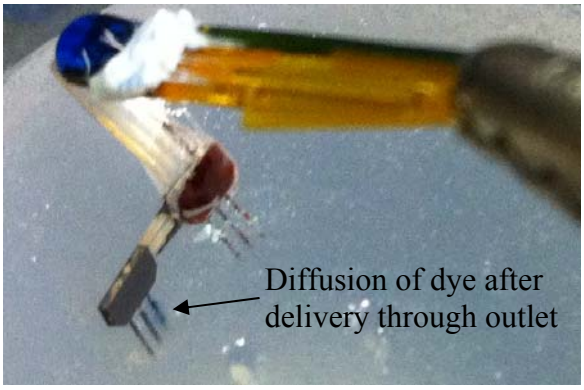

Figure 5-11: Agarose brain phantom with Evan's Blue dye being released into the gel via the microfluidic channel; dye can be seen diffusing via convection after release through the microfluidic outlet

CHAPTER 6: ANIMAL STUDIES

6.1 Introduction

In an effort to study the efficacy of the recording capability of our devices, several in vivo and in vitro animal studies were conducted. The purpose of these studies was simply to verify if these devices could be utilized to gather neural activity data. As such, animal studies were conducted in a progressive manner. Initial studies tested the ability of the devices to record any neural signals, while subsequent steps progressed to the recording of epileptogenic signals in brain slices, acute recording of neural signals in 3D space, and eventually chronic recording of neural signals in 3D space. In addition to the recordings, preliminary biocompatibility studies were conducted to demonstrate the immunologic response to implanted neural devices. All animals used were male, adult (4 months) Sprague-Dawley rats. All protocol for animal studies were pre-approved by the animal investigation committee (AICUC) at Wayne State University.

6.2 Acute Neural Activity

In one of the earlier studies, one of the rigid neural devices was implanted into the auditory cortex of an adult normal rat. The purpose of this study was to mimic a neural signal recording study which utilized microwire arrays to record neural signals related to the perception of sound [89]. The wire bonding pads of the neural device were connected to a printed circuit board composed of wire bonding pads and soldering pads. The

soldering pads of the circuit board were soldered to the lead wires of an Omnetics connector. The counterpart connector was attached to a TDT (Tucker Davis Technologies) recording system, which is a system often utilized to record neural activity from microelectrode arrays [90, 91]. After placing the rat under general anesthesia via ketamine:xylazine (100mg/kg:10mg/kg), the rat was prepared for surgery and placed in a Kopf stereotactic frame with hollow ear bars. A craniotomy was performed in the skull of the rat just above the auditory cortex. With the TDT recording system attached to the device-connector package, the probe shanks of the device were implanted into the auditory cortex. A noise pulse system was then utilized to induce short noise bursts of varying amplitude and frequency into the left external auditory canal of the rat through the hollow ear bars. Neural activity associated with the sensation of hearing in rats was identified by the electrode array. Using a unit sorter program, two distinct neural signals were recorded from the electrode sites as seen in Figure 6-1. This data was seen to be similar to recordings generated via other electrode devices such as the microwire array [89]. In addition, this study demonstrated the ability of the neural devices to be able to acquire and isolate two distinct neural signals.

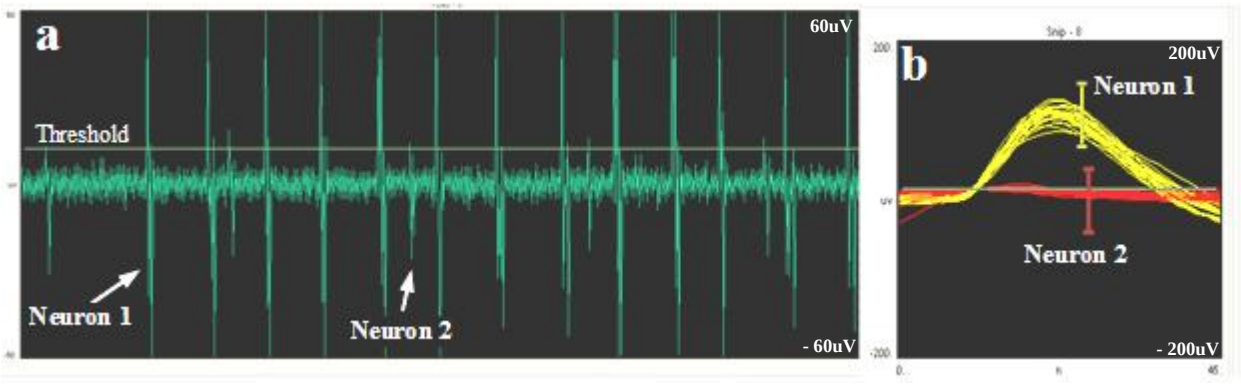

Figure 6-1: (a) Spikes from two neurons recorded from the primary auditory cortex of a rat. Note the difference in amplitude and spike rate between the two neurons. (b) The spikes from the two neurons were well differentiated using a unit sorter program

6.3 Slice Recording Data

After demonstration of the utility of the neural devices in recording noise-induced neural signals within the auditory cortex, it was important to demonstrate acquisition of epileptogenic signals via the devices. Young normal rats (less than 3 months of age) were euthanized via guillotine, after which their brains were harvested and sectioned into 350μm thick cortical slices. Slices were immediately perfused in standard ringer solution (glucose, oxygen, etc.) to maintain viability of the slices for a few hours. Similar to the previous animal study, a rigid neural device was wire bonded to a printed circuit board with wire bonding pads and soldering pads. EEG compatible lead wires were then soldered to the soldering pads, after which they were connected to a Stellate Harmonie EEG recording system. This system had been well utilized in prior studies for recording of epileptogenic neural signals [7, 9]. Cortical slices were placed on a nylon grid and immersed in a perfusion chamber which delivered fresh modified ringer solution at a constant rate. This modified ringer solution differed from standard ringer solution in that magnesium was removed and 4-Aminopyridine was added to the solution. Ringer solutions lacking magnesium and containing 4-aminopyridine have been shown to cause epileptiform activity in rat cortical slices [92, 93]. The probe shanks of the neural device were then penetrated through the cortical slice and the electrode sites of the shanks were positioned within the slice via a micromanipulator. After connection of the EEG lead wires to the system and placement of a reference wire, neural signals were recorded through the Stellate recording system. It should be noted that only some of the electrode sites were in contact with brain tissue as the slice was only thick enough to accommodate

two of the electrodes on a shank. The electrode sites (channels P4 and C4) were located in different regions of cortex and were referenced to a wire within the perfusion solution. As seen in Figure 6-3, epileptiform discharges were observed across both channels. Figure 6-3(a) demonstrates the onset of an epileptic event on channel P4. As can be identified in the data, after an initial neural spike, continuous neural spiking occurs with gradually increasing amplitude. This neural behavior is consistent with what is seen during the beginning of an ictal (seiure) event. Figure 6-3(b) demonstrates cessation of the ictal event after 2.5 minutes. Neural spiking can be seen at the beginning of the recording, but it eventually wanes until very little spiking is seen relative to the background noise. Figure 6-3(c) demonstrates a short ictal event on channel C4. This event is understood to be an ictal event in a different area of cortex compared to what was seen earlier in channel P4. Neural signals were recorded from the cortical slices for approximately 3 hours before neural activity ceased. Although this was an ex vivo neural signal recording study, this study demonstrated the ability of the devices to record epileptiform neural activity similar to what has been seen using conventional seizure recording systems [92, 93].

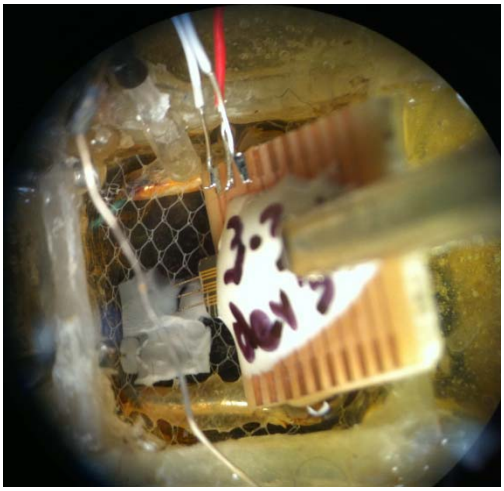

Figure 6-2: Cortical slice recording setup

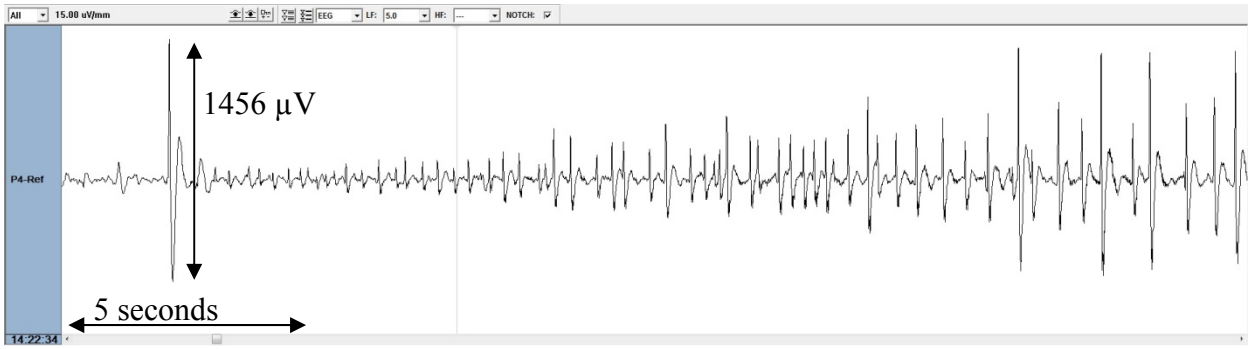

(a)

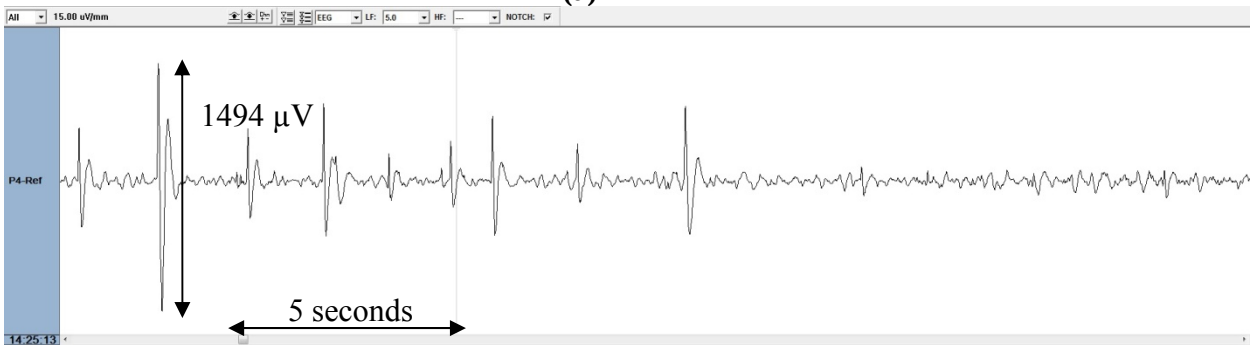

(b)

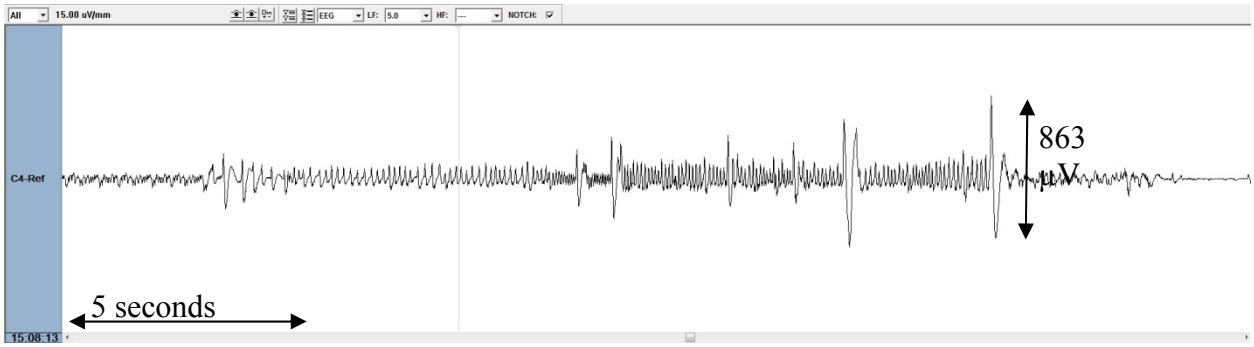

(c)

Figure 6-3: Epileptiform activity from a cortical slice. Channels C4 and P4 refer to electrode sites placed at differing cortical region. (a) Beginning and development of seizure on channel P4; (b) Cessation of seizure event after continuous high spiking activity for around 2.5 minutes; (c) Short seizure event occurring on channel C4

6.4 Acute 3D Neural Recording

The previous animal studies had demonstrated the functionality of the neural devices in recording neural signal data similar to what had been seen in other works. However, recording of neural activity through a 3D array of electrodes had yet to be demonstrated. In one of the first 3D recording studies, a 2 island, 6 shank, 12 electrode neural probe was wire bonded to a printed circuit board with wire bonding pads and soldering pads. Similar to the brain slice recording study, the soldering pads were soldered to EEG compatible lead wires which connected with the Stellate Harmonie EEG recording system. For this study, an adult rat was placed under pentobarbital anesthesia after which it was prepared for surgery and placed in a stereotactic frame. Using proper sterile technique, the scalp was incised and a burr hole was generated using a 3mm diameter drill bit 1mm posteriorly and 3.5mm laterally to Bregma, which corresponds to the region of the somatosensory cortex [76]. The connected 3D neural probe was then lowered into the cortex using a micromanipulator and then fixed in position using dental cement (methyl methacrylate). After placement of a reference wire on the skull and verification

of connections with the Stellate recording system, neural activity was recorded for an hour. Neural activity was observed across 10 channels as seen in Figure 6-6. Two channels were non-functional and were excluded from the recording. To improve the quality of the recorded signals, electrodes were re-referenced differentially to one of the electrodes on the device (electrode C3). After the recording, the animal was properly sacrificed and the device was carefully removed. The device was later re-characterized for impedance to verify functionality of the channels. Two of the electrode impedances are represented in Figure 6-4. This study demonstrated the ability of the devices to record acute neural activity in 3-dimensional space.

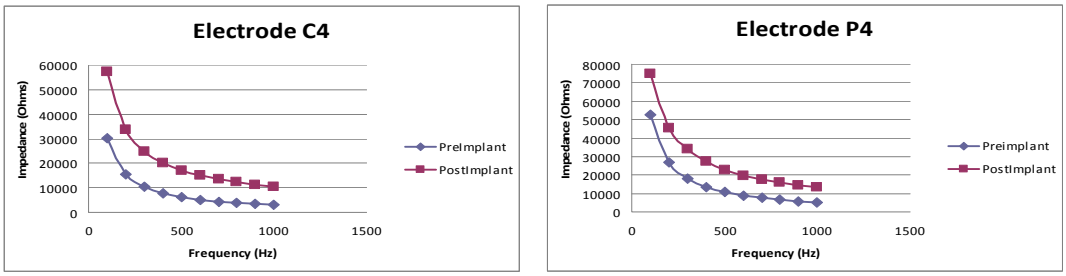

Figure 6-4: Impedance results of two electrodes before and after implantation; the slight increase in impedance is likely due to residual tissue left on the electrode sites

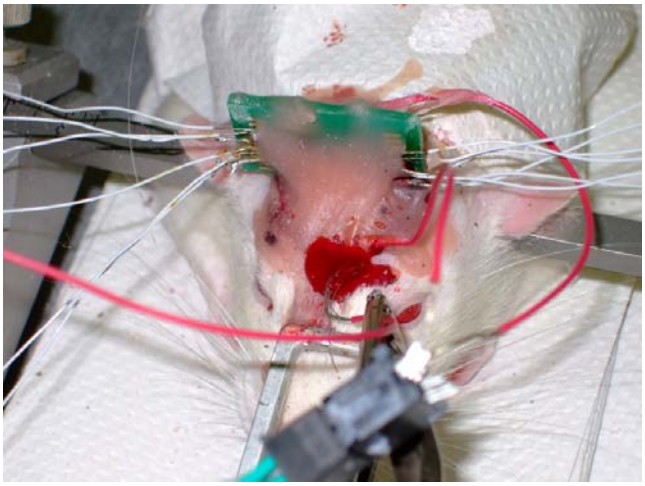

Figure 6-5: Acute 3D Neural Recording

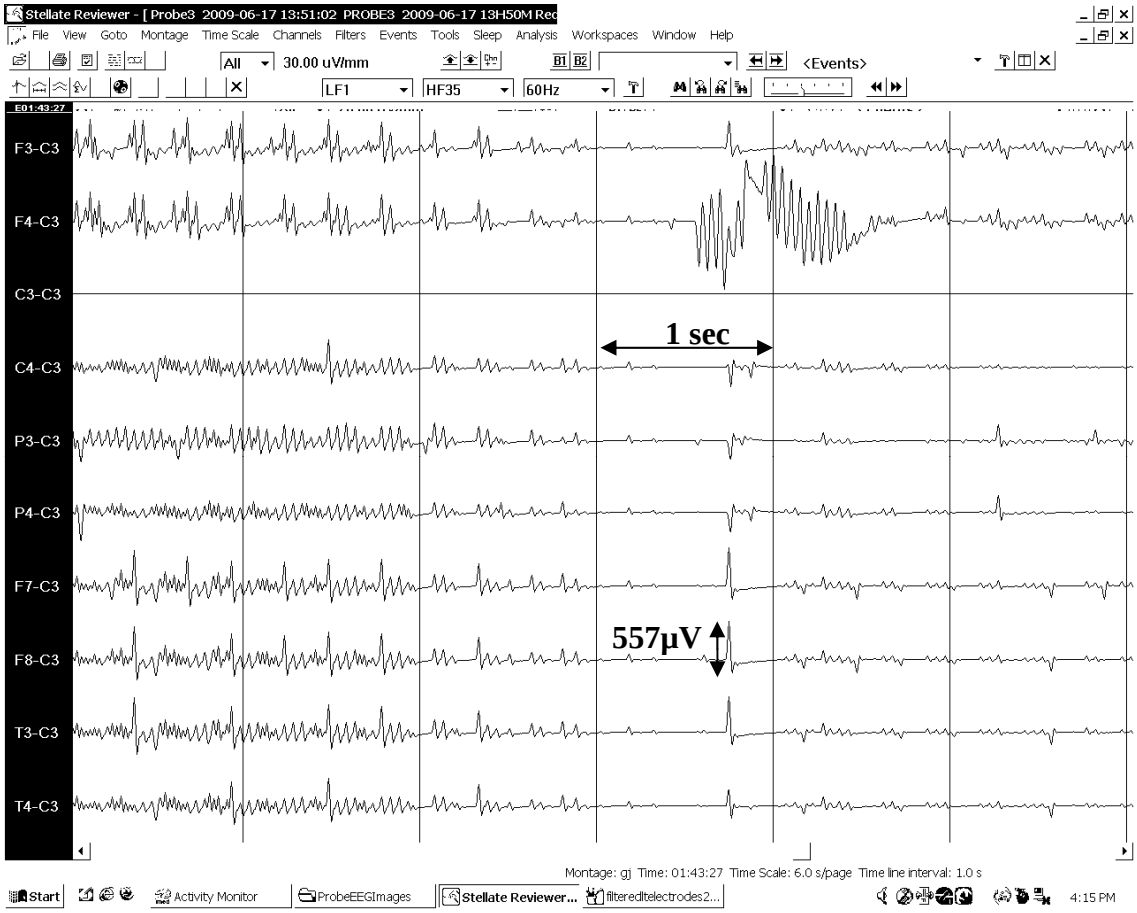

Figure 6-6: In Vivo Acute Rat Cortical Study – rat was placed under pentobarbital general anesthesia and device was implanted at or near the auditory cortex of the rat; Recordings were collected from a Stellate EEG recording system; Device was a two island, 6 shank devices, with each shank having 2 electrodes (2 electrodes were non-functional). The electrodes were referenced differentially to one of the electrodes, electrode C3.

6.5 Biocompatibility study

After completion of the acute 3D neural recording trial, it was important to begin working towards development of a chronic neural device that could be implanted for several weeks. In an effort to determine biocompatibility of the devices after long term implantation, a rigid 9-electrode, single-island device was implanted into the sensory cortex of an adult rat. To avoid complexity during the surgery, the device was not connected to a circuit board. As with the acute animal study, the rat was anesthetized via

pentobarbital, prepared for surgery, and placed in a stereotactic frame. After creating an incision along the midline of the scalp, a 3mm diameter dremel bit was used to create a burr hole after which the device was inserted into the cortex. Adjacent to the device, 5 screw electrodes were inserted into the skull and attached to a 6 pin connector [94]. The purpose of the screw-based electrodes and connector were to provide a means for recording the electrophysiological effect of the implanted device as well as serving as anchor points to secure the entire assembly onto the skull. Dental cement was utilized to bind the screws to the device and fix and protect the entire assembly. The rat was allowed to recover for a week after which the rat was placed in a video EEG recording system for 24 hours. Analysis of the EEG data was insignificant for any electrical spiking normally associated with traumatic brain injury. The rat was recorded again at 2 and 3 weeks post-surgery with no electrical signal change associated with traumatic brain injury. At 4 weeks, the rat was sacrificed and its brain was removed for cortical tissue analysis. After fixing of the brain in 4% paraformaldehyde solution and sucrose solution, the brain was cryosectioned and stained using Glial Fibrillary Acidic Protein (GFAP), which is a stain used for visualization of reactive astrocytes seen during inflammation within the brain [95]. Inspection of the GFAP-stained tissue slices demonstrated only mild inflammation and glial scar formation, which shows promise that the immunologic response to the device is limited. Images of the slices can be seen in Figure 6-7.

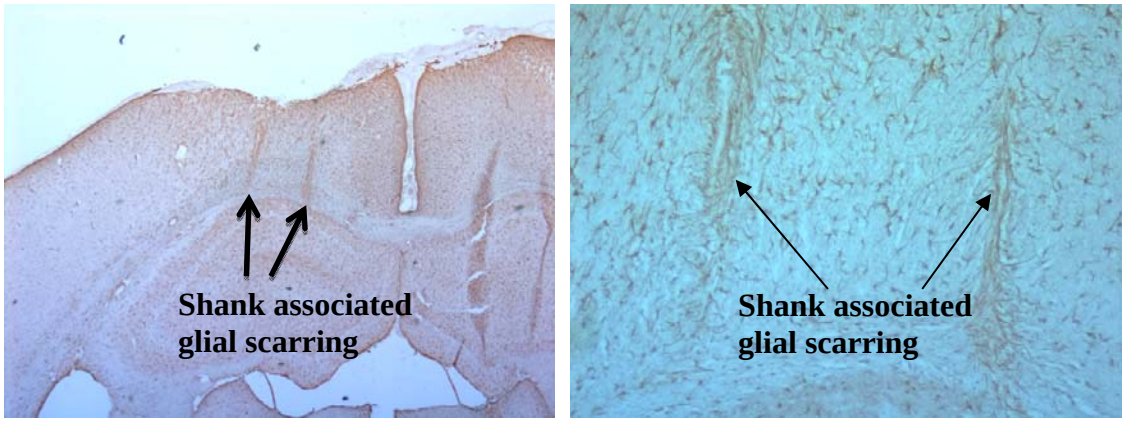

Figure 6-7: GFAP stain of cortical tissue slice demonstrating the gliotic effect of surgical implantation of the devices; devices were implanted for 4 weeks before removal; 2x magnification on left and 10x magnification on right.

6.6 1st Attempt Chronic Neural Device Surgery#

After demonstration of the acute functionality of the device within a live animal, the need was pressing to demonstrate functionality of the devices over a longer period of time. Similar to the device design, the surgical technique was an iterative process which was revised and improved as the design of the device was revised and improved. During the acute 3D neural device surgery, it was quickly understood that the printed circuit board would need to be much smaller in order for the device to be implanted on a freely moving animal (see Figure 6-5). A smaller PCB was designed specifically for the purpose of decreasing the overall package size of the neural device, including the device, the circuit board, and the connector. This circuit board included wire bonding pads and soldering pads, similar to its predecessor, however it was significantly smaller (approximately ¾" by ¾"). This circuit board was wire bonded to a rigid 3D neural device and soldered to a rectangular connector. The rectangular connector had been used in screw-based electrophysiological studies [22]. Similar to the acute neural device surgery, the rat was put under general anesthesia via pentobarbital after which it was

prepared for surgery and placed in a stereotactic frame. Using stereotactic technique, the scalp was incised and reflected, after which a 3mm burr hole was created 1mm posteriorly and 3.5mm laterally to Bregma (somatosensory cortex region) [76]. The device package (neural device, circuit board, and connector) was positioned and implanted via a micromanipulator into the cortex. Dental cement was then applied to the skull and the device package to fix the assembly in place on the skull. Although the assembly was much smaller than the assembly created during the acute animal surgery, the package was still quite large and bulky in relation to the rat's head. Within days after implantation, the entire assembly head cap separated from the rat's skull and the rat needed to be euthanized. An image of the animal after surgery is depicted in Figure 6-8.

Figure 6-8: 1st attempt chronic device implant

6.7 2nd Attempt Chronic Neural Device Surgery#

After the initial attempt at creating and implanting a chronic neural device, it was understood that a more holistic approach would be necessary in achieving reliable

chronic device package. From the first chronic package, it was understood that combination of the printed circuit board, the rigid device, and the large rectangular connector resulted in a structure that was very large (over 1") and unstable for use in a chronic animal study. In addition, the rectangular connector only allowed for 8 possible channels, which limited the amount of channels available for the device and limiting the degree of 3D resolution. From these lessons, the chronic device and device package was re-designed to be much smaller in size while allowing for a larger number of channels. As mentioned in the design chapter, it was realized that the most stable implantation setup would be such that the package is parallel to the plane of the skull, with only the probe islands being perpendicular to the skull implanted into the cortex. In order achieve this, the flexible interconnect design was utilized with the wire bonding island being fixed along with the package to the skull. Via the flexible interconnect between the wire bonding island and the probe islands, the probe islands could be positioned and implanted within the cortex. With this concept in mind, the chronic device printed circuit board and the chronic device were designed and developed. In addition, the Omnetics connectors were chosen to replace the rectangular connectors to decrease the size of the connector and increase the number of available channels. Details of all design procedures and parameters have been discussed in detail in the design chapter.

Considering the change in the overall design of the chronic device package, a new surgical technique was required to successfully implant the neural device packages. For the animal surgery, a 4 month old rat was placed under general anesthesia using a ketamine:xylazine (100mg/kg:10mg/kg), after which it was prepared for surgery and

placed in a stereotactic frame. As before, the scalp was incised at the midline and the skin and underlying tissue was reflected to expose the skull. After proper exposure of the skull, a 3mm burr hole was generated 1mm posteriorly and 3.5mm laterally to Bregma (somatosensory cortex region) [76]. A microscope and fine tip forceps were used to remove any residual skull fragments and peel away the dura mater. After the underlying somatosensory cortex was properly exposed, two screws were implanted posteriorly and one screw was implanted anteriorly to the burr hole. These screws would serve as a base for the package assembly and as anchoring points to fix the assembly to the skull. Using a small amount of partially cured dental cement, the epoxy protected side of the device package was fixed to the posterior skull screws. With the device package fixed to the skull screws, forceps can be used to position the probe islands such that the shanks are within the burr hole, just touching the surface of the cortex. With the proper position and implantation angle verified, the forceps can be used to push the probe shanks into the cortex until the base of the probe shank island touches the skull surface. At this point, the electrodes of the device should be located at the desired cortical positions according to the design parameters (see design chapter). Gel foam, a hemostatic absorbable material, can be utilized to temporarily seal any remaining space within the burr hole surrounding the probe island. After ensuring that the skull surface is reasonable dry, dental cement can be applied to the surface of the skull and the probe island of the device in an effort fix the probe island in place and bind the package with the skull screws. The gel foam should prevent the dental cement from seeping into the burr hole, thus protecting the brain surface. After the dental cement has cured such that the device package is secured in place, additional dental cement can be utilized to fully cover the exposed device

package, thus creating the head cap of the assembly. The skin adjacent to the device package can be stapled via surgical staples to reduce the wound size. Triple antibiotic ointment is applied along the wound surface to prevent bacterial infiltration into the wound site. Post-operative continues as outlined in the animal protocol. After surgery, the rat was monitored and allowed to recover for 5 days before attempting a recording study.

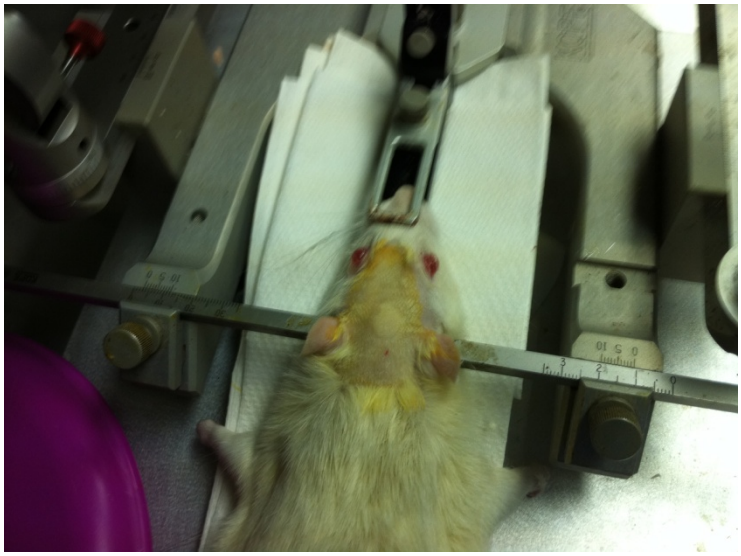

Figure 6-9: Rat placed in stereotactic frame; the ear bars and nose bar prevent motion of the rat's head during surgery

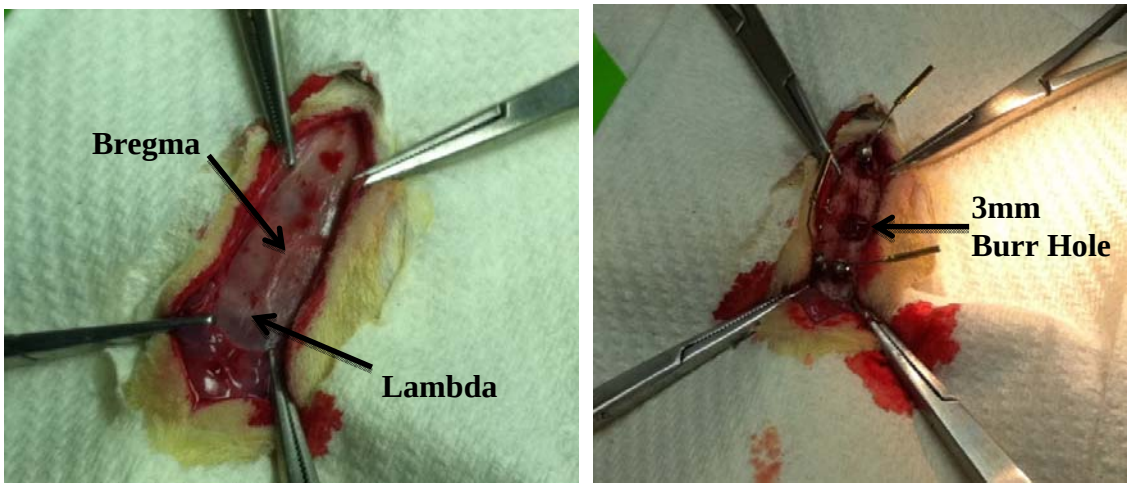

Figure 6-10: Exposed skull with landmarks Bregma and Lambda (b) exposed skull after creation of burr hole and placement of skull screws

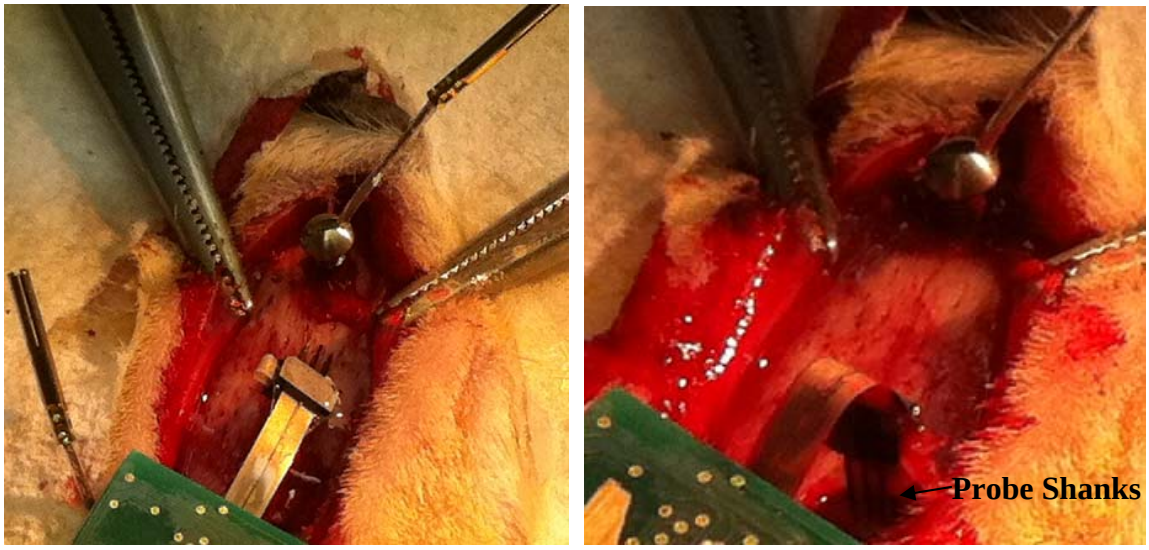

Figure 6-11: Device package after being fixed to skull screws and (b) probe island in burr hole before being inserted into cortex

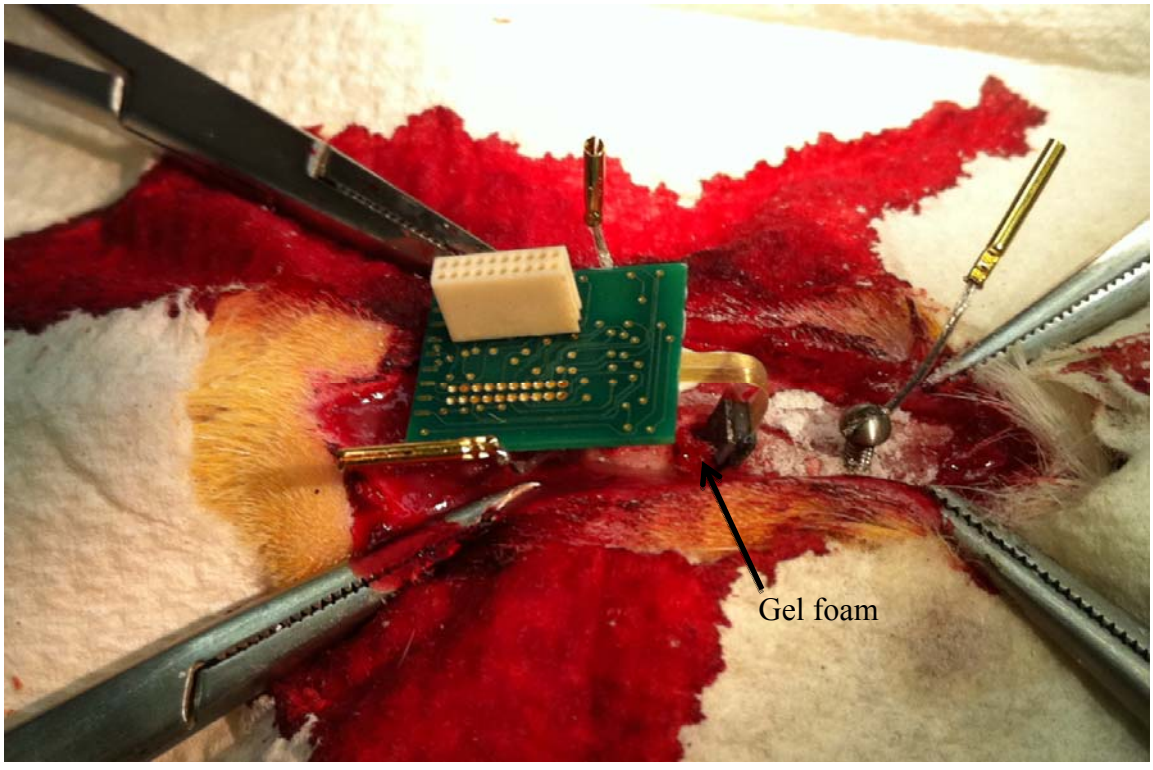

Figure 6-12: Implanted device package with probe island inserted into cortex and Gel foam covering burr hole

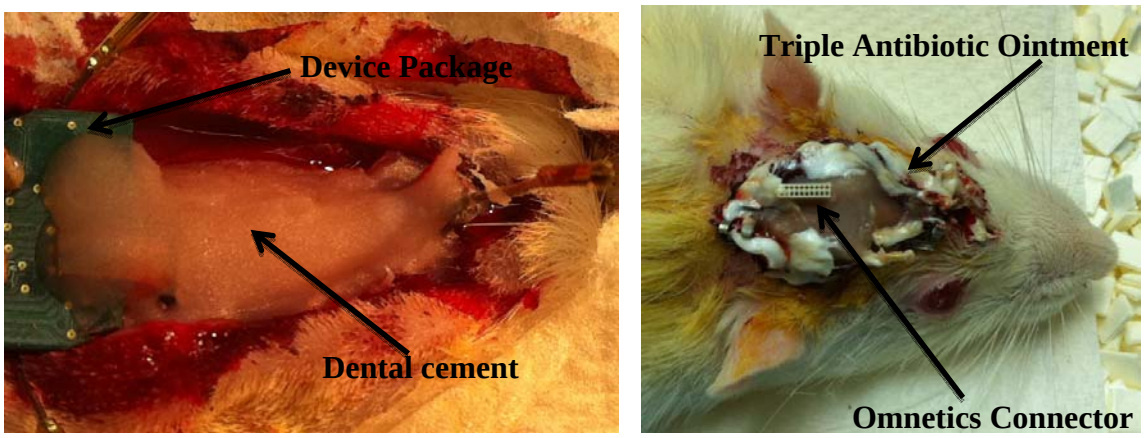

Figure 6-13: (a) Initial application of dental cement which fixes and protects neural device and binds together skull screws and (b) device package head cap after surgery completion

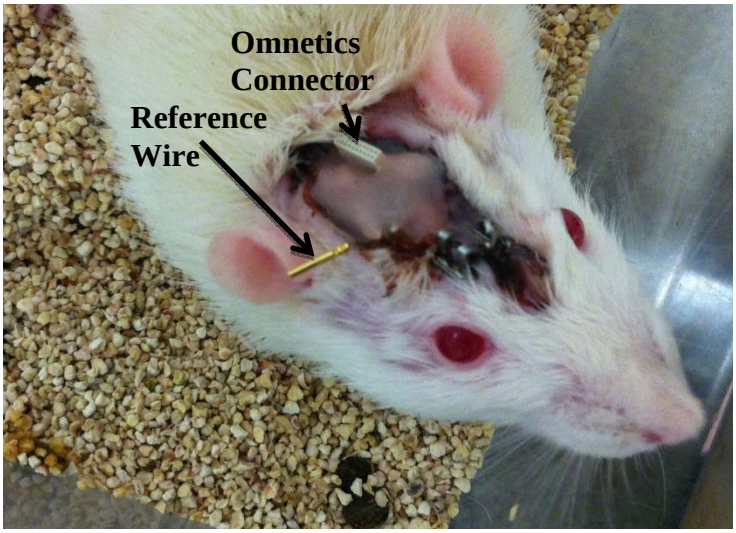

Figure 6-14: Chronic device head cap package after 5 days of recovery; a reference wire was left attached to one of the skull screws to serve as a reference point for the device package

6.8 Chronic Device Neural Signal Recording#

In order to connect with the Stellate EEG recording system, the lead wires of the mating Omnetics connector were soldered to lead wires with EEG-compatible connectors. Due to limitations on the available Stellate EEG recording system, only 6 channels (including 1 reference channel) were available for connection with the 20 possible channels of the neural device. As such, 6 electrode sites were chosen, with 3

corresponding to layers 2/3 and 3 corresponding to layer 4 of the cortex. After ensuring that the wound site was properly healed and the head cap was secure on the rat's head, the mating Omnetics connector was attached to the connector on the rat's head and the EEG connectors were plugged into the EEG recording system. One of the electrode sites (channel 20 of the EEG data) was chosen to serve as a differential reference site to correspond with previous animal recording data. With the animal freely moving in an acrylic cage, neural signals were recorded for one hour. In addition, video of the animal was captured synchronously with the recorded data. Figure 6-16 demonstrates rhythmic neural spiking on channel 21, which supposedly corresponds with layers 2/3 of the somatosensory cortex. Figure 6-17 demonstrates neural signals occurring at different time points across all channels. It is important to note that the neural signals results displayed correspond with time segments when the rat was stationary, thus excluding any erroneous signals that could be due to movement of the animal. The neural probe electrode map to EEG channel correlation is seen below in Figure 6-15.

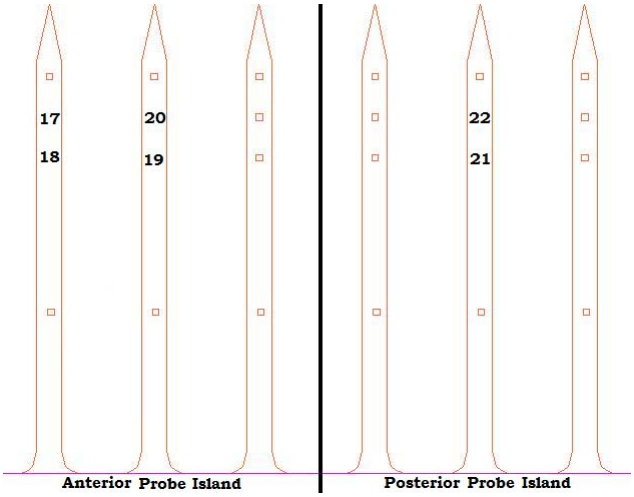

Figure 6-15: Neural electrode map corresponding electrode sites on the neural device to EEG channels in the recording system

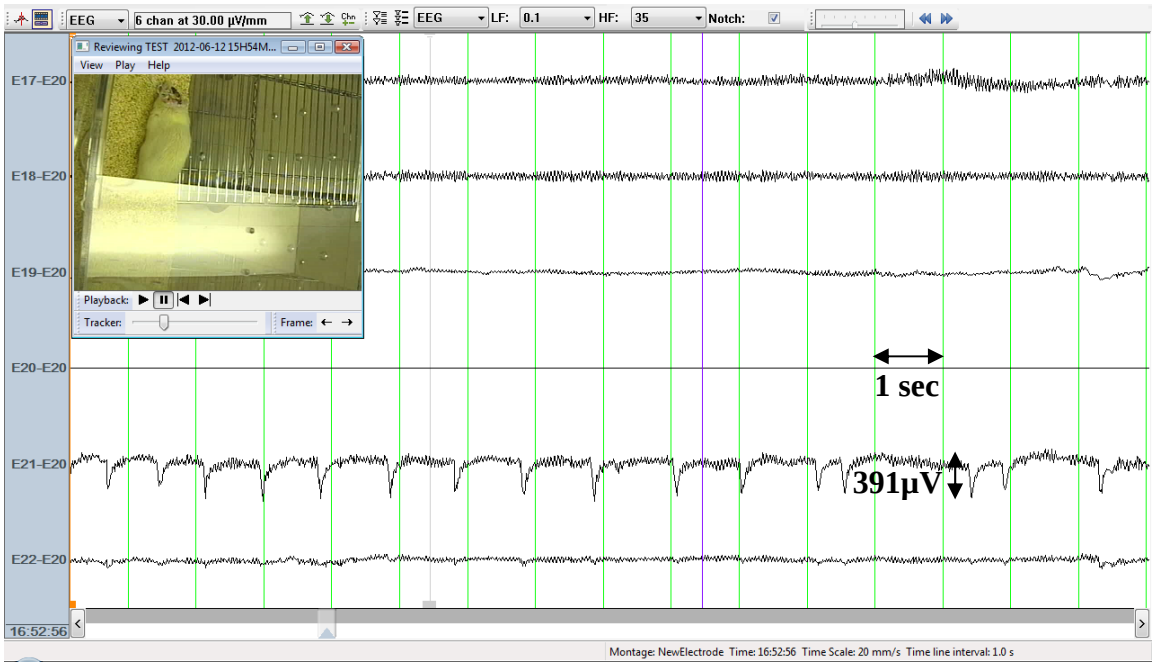

Figure 6-16: Neural recording demonstrating a rhythmic chain of spikes occurring on channel 21 which corresponds to an electrode located at layers 2/3 of the somatosensory cortex

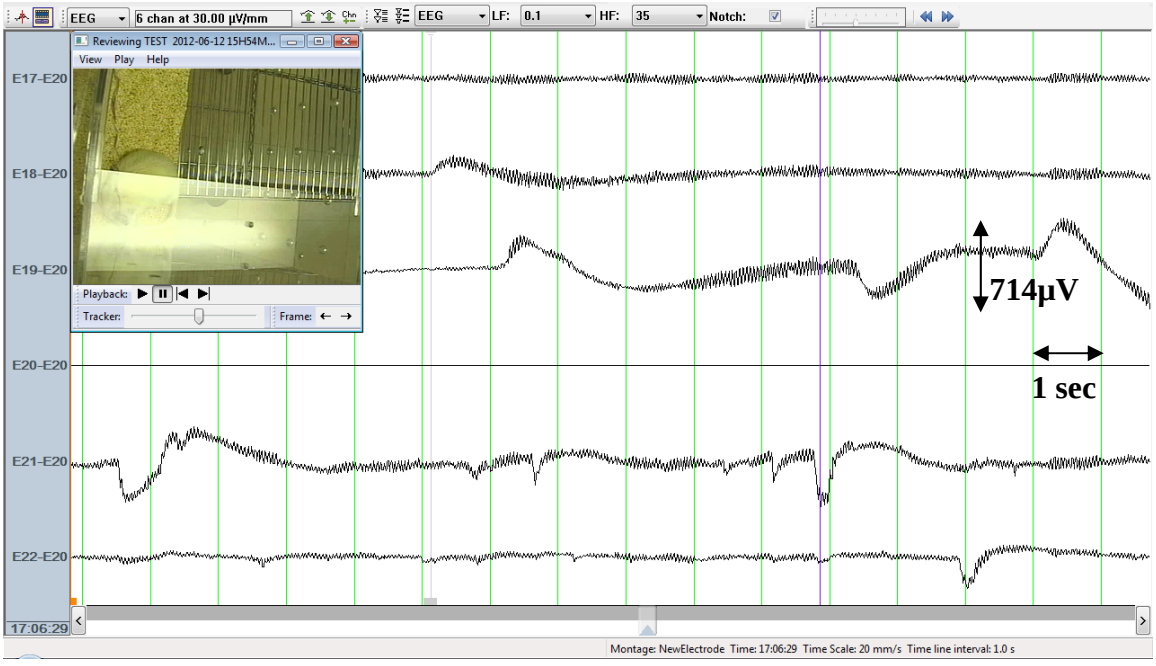

Figure 6-17: Neural recording demonstrating various neural signals across multiple channels occurring at different time points

CHAPTER 7: CONCLUSIONS/FUTURE WORK

In order to better understand neurological diseases such as epilepsy, it is important to develop tools that will enable neuroscientists to observe epileptic pathologies in higher resolution. A novel intracortical neural probe technology based on a silicon island structure and a simple folding process has been proposed and successfully demonstrated. This technology simplifies the fabrication and assembly process, leading to high density 3D arrays of electrodes with integrated microchannels. Neural devices have been designed and developed with parameters specific to a rat model of epilepsy. Characterization studies have demonstrated low impedance, reliable electrode channels and functional, low pressure fluidic channels. Animal studies have demonstrated functionality of the electrode channels in enabling recording of various neural signals. Biocompatibility studies have demonstrated the limited gliosis after implantation of the devices. Reliable chronic 3D devices and chronic device packages have been successfully designed, developed, packaged, and implanted. Preliminary chronic package animal recordings have demonstrated functionality of the recording electrodes.

This work has demonstrated the design, development, and packaging of 3-dimensional intracortical neural interfaces designed towards the study of epilepsy. Now that a reliable chronic device package has been created, much remains to be done. The EEG recording system must be modified to allow for recording of more channels. This will require the integration of some type of commutator that will allow the rat to freely move without getting tangled on any wires. The recording system setup (currently few channels for several animals) may also need modification to enable recording of several

channels for one animal. Further biocompatibility studies are also required to determine the effect of long-term implantation of the devices.

The microfluidic devices must be tested in a live animal for functionality of fluidic drug delivery. Various dyes can be utilized to enable visualization of drug delivery into the cortex. Once the microfluidic functionality is verified, several chronic animal surgeries should be conducted utilizing the tetanus toxin animal model of epilepsy. Utilizing the integrated microfluidic channels, tetanus toxin can be delivered at specific locations after the animal has fully recovered. Immediately after drug delivery, the electrodes can be utilized to enable real-time observation of the progression of the epileptic focus. In addition to its usefulness for the study of epilepsy, these devices can be easily modified for use in the study of various other neurological diseases, such as tinnitus. As with the animal model of epilepsy, the combined ability to deliver fluidic drugs and observe real-time changes in neurological activity may allow elucidation of several other neurological pathologies.

In addition to the potential for various types of neurological studies, further improvements can be added to the current device design. Since the MEMS process is post-CMOS compatible, various on-chip features can be added including amplifiers, filters, and wireless interfaces. Additional features can be added to improve the reliability of the electrode tracings such as spring-based tracing design. Other features may be added to the microchannels including pumps, reservoirs, and flowmeters to enhance delivery of fluidic drugs.

Appendix: Animal Welfare Assurance Form

WAYNE STATE UNIVERSITY

INSTITUTIONAL ANIMAL
CARE AND USE COMMITTEE
101 E. Alexandrine St.
Detroit, MI 48201-2011
Telephone: (313) 577-1629
Fax Number: (313) 577-1941

ANIMAL WELFARE ASSURANCE # A 3310-01

PROTOCOL # A 11-03-08

AMENDMENT # 1

TO: Dr. Jeffrey A. Loeb
Department of Neurology
3122 Elliman Clinical Research Building

FROM: Lisa Anne Polin, Ph.D.
Chairperson
Institutional Animal Care and Use Committee

SUBJECT: Approval of Amendment **# 1** to Protocol # A 11-03-08
"Neocortical epileptogenesis in the rat"

DATE: August 19, 2009

The following requested changes to the above protocol have been reviewed and approved for immediate effect:

Request dated August 17, 2009:

This is an administrative amendment to include Jessin John, MD, PhD, in the list of Research Personnel on this protocol. The IACUC office has verified that Dr. John has completed the required training to work on this animal protocol. The Office of Environmental Health and Safety has been notified of this request and will contact you if additional training is needed.

OEHS Anicon 1080 Form	Verified-12/21/2008
DLAR Species Specific Training on the Rat	Completed-10/15/2008
DLAR Principles of Aseptic Rodent Surgery	Completed-12/18/2008
CITI Responsible Conduct of Research	Completed-10/14/2008
CITI Working with the IACUC	Completed-10/04/2008
CITI Working with the Rat	Completed-12/09/2009
CITI Minimizing Pain & Distress	Completed-12/09/2008
CITI Aseptic Surgery	Completed-12/09/2008

This protocol, as amended, will be subject to annual review on the anniversary date of the initial IACUC review. This protocol was last reviewed on January 20, 2009.

cc: Patricia Denison, DLAR

WAYNE STATE UNIVERSITY

IACUC Annual Review Form

Instructions: Return this form along with any grant progress reports, renewals or proposals via email to Sue Bonarek, sue.bonarek@wayne.edu. Please HIGHLIGHT any corrections that you make to the PRE-FILLED (red) information. Emails must come directly from the Principal or Co-Investigator's official email address (e.g., @wayne.edu, @karmanos.org).

PRINCIPAL INVESTIGATOR: Jeffrey A. Loeb
DEPARTMENT: Department of Neurology
ADDRESS: 3122 Elliman Clinical Research Building
PHONE: (313) 577-9827
EMAIL: jloeb@med.wayne.edu

PROTOCOL NUMBER: A 11-03-08
TITLE: Neocortical epileptogenesis in the rat
FUNDING SOURCE(S): Departmental Funds

All IACUC protocols must be reviewed **annually**. It is the Principal Investigator's responsibility to obtain review and continued approval before the Annual Review deadline.

This communication serves as notification that the above-referenced protocol must receive its annual review by the IACUC prior to November 30, 2009 in order to remain active. To avoid an automatic closure or a delay in your ability to order and use animals, **please return this form no later than SEPTEMBER 29, 2009** so it can be reviewed by the IACUC at a convened meeting.

1. PROTOCOL STATUS

KEEP THE PROTOCOL ACTIVE

- [X] This project is currently being carried out.
- [ ] This project has yet to be initiated. The anticipated start date is: _____

CLOSE THE PROTOCOL

- [ ] The project has been completed or will be completed prior to the required Annual Review deadline of 11/30/2009.
- [ ] The project has never been initiated and no work will be started prior to the expiration date.

2. FUNDING SOURCE

- [ ] The funding source listed above is correct.
- [X] The project is being funded by a different source* List: R01 NS045207
- [ ] The project has been resubmitted to a different funding source* List: _____

Funding Source changes and/or additions must be approved by the IACUC. Grants/Proposals must be submitted with a General Amendment Form so it can be determined if the change is appropriate for approval via amendment.

Protocol #: A 11-03-08

3. EMERGENCY CONTACTS

	Home	Office	Cell/Pager
Dan Barkmeier	(313) 414-9662	(313) 577-5417	(313) 414-9662
Veterinarians DLAR		313-577-1343	(313) 414-9662
Jeffrey A. Loeb	(248) 593-8059	(313) 577-9827	(313) 745-0203 (8958)

a. Has any of the contact information listed above changed?

[X] No

[ ] Yes (highlight corrections in the list above or note below):

4. RESEARCH PERSONNEL

Dan Barkmeier, MD/PhD Student
Jeffrey A. Loeb, Assistant Professor

a. Have any new personnel been added to your research staff?

[ ] No

[X] Yes (list below and submit an amendment if one has not already been submitted*):

Jessin John

All new personnel must be approved by the IACUC via amendment. Complete the Amendment Form to Add Personnel as soon as possible.

b. Have any of the personnel listed above left the laboratory/protocol?

[X] No

[ ] Yes (list below):

5. OCCUPATIONAL HEALTH

In the past year, has anyone involved with this research protocol developed symptoms or sustained injury related to occupational factors (e.g., allergies, bites, rashes, scratches, etc.)?

[X] No

[ ] Yes (describe below and answer follow up question):

Has the Occupational Health Services Clinic and the Occupational Health Nurse in the Office of Environmental Health and Safety been contacted?

[ ] Yes

[ ] No (explain below)

NOTE: The principal investigator is responsible for the day-to-day safety in the workplace regarding occupational health hazards related to this research protocol and encountered by the research employees on this project. This includes identifying and training employees regarding hazards, and supplying appropriate protective clothing and

equipment, if required. For more information consult the Office of Environmental Health and Safety website or call (313) 577-1200.

6. HAZARDOUS WASTE

Have you changed your procedures such that hazardous wastes are now being generated?

X	No
	Yes (describe below and contact the OEHS at (313) 577-1200 immediately if you have not yet done so):

The Principal Investigator, Co-Investigator and/or Faculty Advisor certify the following statements (please mark):

X	My staff and I will comply with all standards for animal care and investigation established in the *Guide for the Care and Use of Laboratory Animals*, and the Federal Animal Welfare Act, and will follow all policies established by the University to assure that these standards are met.
X	All individuals working with the animals on this protocol are qualified by virtue of training or experience to perform proper handling, experimental, and restraint techniques required for the species to be used.
X	No ***alternatives*** are available for proposed painful or distressful procedures.
X	This research does not represent ***unnecessary duplication*** of previous experiments.

IACUC OFFICE USE ONLY

REVIEWER COMMENTS:

☐ **RECOMMENDED FOR APPROVAL**

Lisa Anne Polin, IACUC Chairperson — Date

REFERENCES

1. Hauser, W.A., J.F. Annegers, and W.A. Rocca, *Descriptive epidemiology of epilepsy: Contributions of population-based studies from Rochester, Minnesota.* Mayo Clinic Proceedings, 1996. **71**(6): p. 576-586.
2. Scheffer, I.E. and S.F. Berkovic, *Genetics of the epilepsies.* Current Opinion in Pediatrics, 2000. **12**(6): p. 536-542.
3. Noebels, J.L., *The biology of epilepsy genes.* Annual Review of Neuroscience, 2003. **26**: p. 599-625.
4. Steinlein, O.K., *Genetic mechanisms that underlie epilepsy.* Nature Reviews Neuroscience, 2004. **5**(5): p. 400-408.
5. Babb, T.L. and J.K. Pretorius, *Pathologic Substrates of Epilepsy*, in *The Treatment of Epilepsy: Principles and Practices*, E. Wyllie, Editor 1993, Lea & Febiger: Philadelphia. p. 55-70.
6. Annegers, J.F., *Epidemiology and genetics of epilepsy.* Neurol Clin, 1994. **12**(1): p. 15-29.
7. Asano, E., et al., *Quantitative interictal subdural EEG analyses in children with neocortical epilepsy.* Epilepsia, 2003. **44**(3): p. 425-34.
8. Rakhade, S.N., et al., *A common pattern of persistent gene activation in human neocortical epileptic foci.* Ann Neurol, 2005. **58**(5): p. 736-47.
9. Rakhade, S.N., et al., *Activity-dependent gene expression correlates with interictal spiking in human neocortical epilepsy.* Epilepsia, 2007. **48 Suppl 5**: p. 86-95.

10. Coulter, D.A., *Epilepsy-associated plasticity in gamma-aminobutyric acid receptor expression, function, and inhibitory synaptic properties.* Int Rev Neurobiol, 2001. **45**: p. 237-52.

11. Doherty, J. and R. Dingledine, *The roles of metabotropic glutamate receptors in seizures and epilepsy.* Curr Drug Target CNS Neurol Disord, 2002. **1**(3): p. 251-60.

12. Mody, I., *Ion channels in epilepsy.* Int Rev Neurobiol, 1998. **42**: p. 199-226.

13. Najm, I., et al., *Mechanisms of epileptogenicity in cortical dysplasias.* Neurology, 2004. **62**(6 Suppl 3): p. S9-13.

14. Becker, A.J., et al., *Correlated stage- and subfield-associated hippocampal gene expression patterns in experimental and human temporal lobe epilepsy.* Eur J Neurosci, 2003. **18**(10): p. 2792-802.

15. Baybis, M., et al., *mTOR cascade activation distinguishes tubers from focal cortical dysplasia.* Ann Neurol, 2004. **56**(4): p. 478-87.

16. Miyata, H., A.C. Chiang, and H.V. Vinters, *Insulin signaling pathways in cortical dysplasia and TSC-tubers: tissue microarray analysis.* Ann Neurol, 2004. **56**(4): p. 510-9.

17. Elliott, R.C., M.F. Miles, and D.H. Lowenstein, *Overlapping microarray profiles of dentate gyrus gene expression during development- and epilepsy-associated neurogenesis and axon outgrowth.* J Neurosci, 2003. **23**(6): p. 2218-27.

18. French, P.J., et al., *Seizure-induced gene expression in area CA1 of the mouse hippocampus.* Eur J Neurosci, 2001. **14**(12): p. 2037-41.

19. Nilsen, K.E., M.C. Walker, and H.R. Cock, *Characterization of the tetanus toxin model of refractory focal neocortical epilepsy in the rat.* Epilepsia, 2005. **46**(2): p. 179-87.

20. Benke, T.A. and J. Swann, *The tetanus toxin model of chronic epilepsy.* Adv Exp Med Biol, 2004. **548**: p. 226-38.

21. Jefferys, J.G., *Chronic epileptic foci induced by intracranial tetanus toxin.* Epilepsy Res Suppl, 1996. **12**: p. 111-7.

22. Barkmeier, D.T., *The Interictal State In Epilepsy And Behavior*, in *Molecular Biology and Genetics*2010, Wayne State University: Detroit.

23. Stanford University. Stanford Electronics Laboratories. SEL-77-027., et al., *Feasibility study of a pocket sized gas chromatographic air analyzer*1977. 104p.

24. Reyes, D.R., et al., *Micro total analysis systems. 1. Introduction, theory, and technology.* Analytical Chemistry, 2002. **74**(12): p. 2623-2636.

25. West, J., et al., *Micro total analysis systems: Latest achievements.* Analytical Chemistry, 2008. **80**(12): p. 4403-4419.

26. Macis, E., et al., *An automated microdrop delivery system for neuronal network patterning on microelectrode arrays.* Journal of Neuroscience Methods, 2007. **161**(1): p. 88-95.

27. Lim, M.W.K. and T.P. Fan, *A "pancreatic tooth" design best accommodates the limitations of current artificial pancreas technology.* Medical Hypotheses, 2007. **69**(4): p. 741-745.

28. Nissenson, A.R., et al., *The human nephron filter: Toward a continuously functioning, Implantable artificial nephron system.* Blood Purification, 2005. **23**(4): p. 269-274.

29. Staples, M., et al., *Application of micro- and nano-electromechanical devices to drug delivery.* Pharmaceutical Research, 2006. **23**(5): p. 847-863.

30. Wise, K.D., *Silicon microsystems for neuroscience and neural prostheses.* Ieee Engineering in Medicine and Biology Magazine, 2005. **24**(5): p. 22-29.

31. Wise, K.D., *Micromachined interfaces to the cellular world.* Sensors and Materials, 1998. **10**(6): p. 385-395.

32. Wise, K.D., et al., *Wireless implantable microsystems: High-density electronic interfaces to the nervous system.* Proceedings of the Ieee, 2004. **92**(1): p. 76-97.

33. Stieglitz, T., *Neuro-technical interfaces to the central nervous system.* Poiesis & praxis : international journal of ethics of science and technology assessment, 2006. **4**(2).

34. HajjHassan, M., V. Chodavarapu, and S. Musallam, *NeuroMEMS: Neural Probe Microtechnologies.* Sensors, 2008. **8**(10): p. 6704-6726.

35. Cheung, K.C., *Implantable microscale neural interfaces.* Biomedical Microdevices, 2007. **9**(6): p. 923-938.

36. Campbell, P.K., et al., *A silicon-based, 3-dimensional neural interface - manufacturing processes for an intracortical electrode array.* IEEE Transactions on Biomedical Engineering, 1991. **38**(8): p. 758-768.

37. Badi, A.N., et al., *Development of a novel eighth-nerve intraneural auditory neuroprosthesis.* Laryngoscope, 2003. **113**(5): p. 833-842.

38. Vetter, R.J., et al., *Chronic neural recording using silicon-substrate microelectrode arrays implanted in cerebral cortex.* Ieee Transactions on Biomedical Engineering, 2004. **51**(6): p. 896-904.

39. Pearce, T.M. and J.C. Williams, *Microtechnology: Meet neurobiology.* Lab on a Chip, 2007. **7**(1): p. 30-40.

40. Heiduschka, P. and S. Thanos, *Implantable bioelectronic interfaces for lost nerve functions.* Progress in Neurobiology, 1998. **55**(5): p. 433-461.

41. Motta, P.S. and J.W. Judy, *Multielectrode microprobes for deep-brain stimulation fabricated with a customizable 3-D electroplating process.* Ieee Transactions on Biomedical Engineering, 2005. **52**(5): p. 923-933.

42. Normann, R.A., et al., *A neural interface for a cortical vision prosthesis.* Vision Research, 1999. **39**(15): p. 2577-2587.

43. Ensell, G., et al., *Silicon-based microelectrodes for neurophysiology, micromachined from silicon-on-insulator wafers.* Medical & Biological Engineering & Computing, 2000. **38**(2): p. 175-179.

44. Norlin, P., et al., *A 32-site neural recording probe fabricated by DRIE of SOI substrates.* Journal of Micromechanics and Microengineering, 2002. **12**(4): p. 414-419.

45. Kewley, D.T., et al., *Plasma-etched neural probes.* Sensors and Actuators a-Physical, 1997. **58**(1): p. 27-35.

46. Kindlundh, M., P. Norlin, and U.G. Hofmann, *A neural probe process enabling variable electrode configurations.* Sensors and Actuators B-Chemical, 2004. **102**(1): p. 51-58.

47. Takeuchi, S., et al., *3D flexible multichannel neural probe array.* Journal of Micromechanics and Microengineering, 2004. **14**(1): p. 104-107.

48. Rousche, P.J., et al., *Flexible polyimide-based intracortical electrode arrays with bioactive capability.* IEEE Trans Biomed Eng, 2001. **48**(3): p. 361-71.

49. Lee, K.K., et al., *Polyimide-based intracortical neural implant with improved structural stiffness.* Journal of Micromechanics and Microengineering, 2004. **14**(1): p. 32-37.

50. Blum, N.A., et al., *Multisite Microprobes for Neural Recordings.* Ieee Transactions on Biomedical Engineering, 1991. **38**(1): p. 68-74.

51. Oh, S.J., et al., *A high-yield fabrication process for silicon neural probes.* Ieee Transactions on Biomedical Engineering, 2006. **53**(2): p. 351-354.

52. Pang, C., *Parylene technology for neural probes applications*, in *Electrical Engineering*2007, California Institute of Technology: Pasadena.

53. Tanghe, S.J., K. Najafi, and K.D. Wise, *A Planar Iro Multichannel Stimulating Electrode for Use in Neural Prostheses.* Sensors and Actuators B-Chemical, 1990. **1**(1-6): p. 464-467.

54. Jones, K.E., P.K. Campbell, and R.A. Normann, *A Glass Silicon Composite Intracortical Electrode Array.* Annals of Biomedical Engineering, 1992. **20**(4): p. 423-437.

55. Rousche, P.J. and R.A. Normann, *Chronic intracortical microstimulation of cat auditory cortex using a 100 penetrating electrode array.* Journal of Physiology-London, 1997. **499P**: p. P87-P88.

56. Yao, Y., et al., *A microassembled low-profile three-dimensional microelectrode array for neural prosthesis applications.* Journal of Microelectromechanical Systems, 2007. **16**(4): p. 977-988.

57. Chen, J.K., et al., *A multichannel neural probe for selective chemical delivery at the cellular level.* IEEE Transactions on Biomedical Engineering, 1997. **44**(8): p. 760-769.

58. Li, Y., *An Integrated Drug-Delivery Probe with In-Line Flow Measurement*2006. 1 v.

59. Williams, J.C., et al., *Multi-site incorporation of bioactive matrices into MEMS-based neural probes.* J Neural Eng, 2005. **2**(4): p. L23-8.

60. Fukang, J., et al. *A flexible MEMS technology and its first application to shear stress sensor skin*. in *Micro Electro Mechanical Systems, 1997. MEMS '97, Proceedings, IEEE., Tenth Annual International Workshop on*. 1997.

61. Xu, Y., et al., *Flexible shear-stress sensor skin and its application to unmanned aerial vehicles.* Sensors and Actuators a-Physical, 2003. **105**(3): p. 321-329.

62. Jiang, F.K., et al., *A flexible micromachine-based shear-stress sensor array and its application to separation-point detection.* Sensors and Actuators a-Physical, 2000. **79**(3): p. 194-203.

63. Xu, Y., et al., *IC-integrated flexible shear-stress sensor skin.* Journal of Microelectromechanical Systems, 2003. **12**(5): p. 740-747.

64. Engel, J., J. Chen, and C. Liu, *Development of polyimide flexible tactile sensor skin.* Journal of Micromechanics and Microengineering, 2003. **13**(3): p. 359-366.

65. Katragadda, R.B. and Y. Xu, *A novel intelligent textile technology based on silicon flexible skins.* Sensors and Actuators a-Physical, 2008. **143**(1): p. 169-174.

66. Kipke, D.R., et al., *Advanced Neurotechnologies for Chronic Neural Interfaces: New Horizons and Clinical Opportunities.* Journal of Neuroscience, 2008. **28**(46): p. 11830-11838.

67. Ruther, P., et al. *The NeuroProbes Project – Multifunctional Probe Arrays for Neural Recording and Stimulation*. in *the 13th Annual Conf. of the IFESS*. 2008. Freiburg, Germany.

68. Cheung, K.C., et al., *Implantable multichannel electrode array based on SOI technology.* Journal of Microelectromechanical Systems, 2003. **12**(2): p. 179-184.

69. Metz, S., et al., *Flexible polyimide probes with microelectrodes and embedded microfluidic channels for simultaneous drug delivery and multi-channel monitoring of bioelectric activity.* Biosensors and Bioelectronics, 2004. **19**(10): p. 1309-1318.

70. Li, Y., R. Katragadda, and Y. Xu. *3D neural probes based on a simple folding process*. in *The 38th Neural Interfaces Conference (NIC)*. June 16-18, 2008. Cleveland, OH.

71. Li, Y., et al., *3D neural probes with combined electrical and chemical interfaces*, in *Hilton Head Workshop 2010: A Solid-State Sensors, Actuators and Microsystems Workshop* 2010: Hilton Head Island, SC

72. John, J., et al., *Microfabrication of 3D neural probes with combined electrical and chemical interfaces.* Journal of Micromechanics and Microengineering, 2011. **21**(10): p. 105011.

73. Xu, Y., et al. *Underwater flexible shear-stress sensor skins*. in *IEEE International Conference on Micro Electro Mechanical Systems (MEMS)*. 2004. Maastricht, The Netherlands.

74. Xu, Y., et al., *Flexible shear-stress sensor skin and its application to unmanned aerial vehicle.* Sensors & Actuators, 2003. **105**(3): p. 321-329.

75. Xu, Y., et al., *IC-integrated flexible shear-stress sensor skin.* Journal of Microelectromechanical Systems, 2003. **12**(5): p. 740-747.

76. Paxinos, G. and C. Watson, *The rat brain - In stereotaxic coordinates - Preface: Fourth edition.* Rat Brain in Stereotaxic Coordinates, Fourth Ed., 1998: p. ix-+.

77. Maikos, J.T., R.A. Elias, and D.I. Shreiber, *Mechanical properties of dura mater from the rat brain and spinal cord.* Journal of neurotrauma, 2008. **25**(1): p. 38-51.

78. Mao, H.J., et al., *MATERIAL PROPERTIES OF ADULT RAT SKULL.* Journal of Mechanics in Medicine and Biology, 2011. **11**(5): p. 1199-1212.

79. *The cerebral cortex of the rat*, ed. B. Kolb and R.C. Tees1990, Cambridge, MA, US: The MIT Press. xii, 645.

80. Lee, K., et al. *Fabrication of implantable polyimide based neural implants with flexible regions to accommodate micromovement*. in *TRANSDUCERS, Solid-State Sensors, Actuators and Microsystems, 12th International Conference on, 2003*. 2003.

81. Kipke, D.R., et al., *Silicon-substrate intracortical microelectrode arrays for long-term recording of neuronal spike activity in cerebral cortex.* Ieee Transactions on Neural Systems and Rehabilitation Engineering, 2003. **11**(2): p. 151-155.

82. Kang, C.K., et al., *The fabrication of patternable silicon nanotips using deep reactive ion etching.* Journal of Micromechanics and Microengineering, 2008. **18**(7): p. -.

83. Wise, K.D., J.B. Angell, and A. Starr, *An Integrated-Circuit Approach to Extracellular Microelectrodes.* Biomedical Engineering, IEEE Transactions on, 1970. **BME-17**(3): p. 238-247.

84. McAdams, E.T., et al. *Characterization of gold electrodes in phosphate buffered saline solution by impedance and noise measurements for biological applications*. in *Engineering in Medicine and Biology Society, 2006. EMBS '06. 28th Annual International Conference of the IEEE*. 2006.

85. Kindlundh, M. and P. Norlin, *A gel-based wafer-level testing procedure for microelectrodes.* Sensors and Actuators B: Chemical, 2005. **107**(2): p. 557-562.

86. Drake, K.L., et al., *Performance of planar multisite microprobes in recording extracellular single-unit intracortical activity.* IEEE Transactions on Biomedical Engineering, 1988. **35**(9): p. 719-732.

87. Kee-Keun, L., et al. *Benzocyclobutene (BCB) based intracortical neural implant*. in *International Conference on MEMS, NANO and Smart Systems*. 2003.

88. Neeves, K.B., et al., *Fabrication and characterization of microfluidic probes for convection enhanced drug delivery.* Journal of Controlled Release, 2006. **111**(3): p. 252-262.

89. Zhang, J. and X. Zhang, *Electrical stimulation of the dorsal cochlear nucleus induces hearing in rats.* Brain Research, 2010. **1311**(0): p. 37-50.

90. Hoa, M., et al., *Tonotopic responses in the inferior colliculus following electrical stimulation of the dorsal cochlear nucleus of guinea pigs.* Otolaryngology - Head and Neck Surgery, 2008. **139**(1): p. 152-155.

91. Olsson, R.H., III, M.N. Gulari, and K.D. Wise. *Silicon neural recording arrays with on-chip electronics for in-vivo data acquisition*. in *Microtechnologies in Medicine & Biology 2nd Annual International IEEE-EMB Special Topic Conference on*. 2002.

92. Siniscalchi, A., et al., *Epileptiform discharge induced by 4-aminopyridine in magnesium-free medium in neocortical neurons: physiological and pharmacological characterization.* Neuroscience, 1997. **81**(1): p. 189-197.

93. Dóczi, J., et al., *Effect of a glutamate receptor antagonist (GYKI 52466) on 4-aminopyridine-induced seizure activity developed in rat cortical slices.* Brain Research Bulletin, 1999. **49**(6): p. 435-440.

94. Barkmeier, D.T., et al., *Electrical, molecular and behavioral effects of interictal spiking in the rat.* Neurobiology of Disease, 2012. **47**(1): p. 92-101.

95. Schmidt-Kastner, R., et al., *Immunohistochemical staining for glial fibrillary acidic protein (GFAP) after deafferentation or ischemic infarction in rat visual system: Features of reactive and damaged astrocytes.* International Journal of Developmental Neuroscience, 1993. **11**(2): p. 157-174.

ABSTRACT

3-DIMENSIONAL INTRACORTICAL NEURAL INTERFACE FOR THE STUDY OF EPILEPSY

by

JESSIN KOSHY JOHN

May 2014

Advisor: Dr. Yong Xu

Major: Electrical Engineering

Degree: Doctor of Philosophy

Epilepsy is a chronic disease characterized by recurrent, unprovoked seizures, where seizures are described as storms of uncontrollable neuro-electrical activity within the brain. Seizures are therefore identified by observation of electrical spiking observed through electrical contacts (electrodes) placed on the scalp or the cortex above the epileptic regions. Current epilepsy research is identifying several specific molecular markers that appear at specific layers of the epilepsy-affected cortex. However, technology is limited in allowing for live observation of electrical spiking across these layers. The underlying hypothesis of this project is that electrical interictal activity is generated in a layer- and lateral-specific pattern.

This work reports a novel neural probe technology for the manufacturing of 3D arrays of electrodes with integrated microchannels. This new technology is based on a silicon island structure and a simple folding procedure. This method simplifies the assembly or packaging process of 3D neural probes, leading to higher yield and lower cost. Various types of 3D arrays of electrodes, including acute and chronic devices, have been successfully developed. Microchannels have been successfully integrated into the 3D

neural probes via isotropic XeF_2 gas phase etching and a parylene resealing process.

This work describes in detail the development of neural devices targeted towards the study of layer-specific interictal discharges in an animal model of epilepsy. Devices were designed utilizing parameters derived from the rat model of epilepsy. The progression of device design is described from 1st prototype to final chronic device. The fabrication process and potential pitfall are described in detail. Devices have been characterized by SEM (scanning electron microscope) imaging, optical imaging, various types of impedance analysis, and AFM (atomic force microscopy) characterization of the electrode surface. Flow characteristics of the microchannels were also analyzed. Various animal tests have been carried out to demonstrate the recording functionality of the probes, preliminary biocompatibility studies, and the reliability of the final chronic device package. These devices are expected to be of great use to the study of epilepsy as well as various other neurological diseases.

AUTOBIOGRAPHICAL STATEMENT: Jessin John

Educational Background:
Bachelors of Science in Electrical Engineering, Wayne State University, May 2006
Masters of Science in Electrical Engineering, Wayne State University, May 2010
Doctor of Philosophy in Electrical Engineering, Wayne State University (2006 – Present)
Doctor of Medicine, Wayne State University School of Medicine (2006 – Present)

Professional Experience:
Student Assistant – WSU Department of Biology, Anatomy and Physiology (2002 – 2005)
Research Assistant – WSU Smart Systems and Integrated Microsystems Program (2003 – 2006)
Graduate Research Assistant – WSU Department of Electrical Engineering (2007 – Present)
Graduate Teaching Assistant - WSU Department of Electrical Engineering (2009 – 2011)
Electronics 1 Professor – WSU Department of Electrical Engineering (Winter 2010)

Honors/Awards/Recognition:
Michigan Merit Award 2000
Dean's Scholarship 2001
Allison Memorial Fund 2002
Howard and Mary Kehrl Scholarship 2003
Charles Devlieg Foundation 2004
Anderson Consulting Merit Scholarship 2005
Robert G. Wingerter Award 2006
Outstanding Community Service Award 2003 and 2005
Dean's List 2003 – 2006
Raymond R. Margherio Endowed Memorial Award 2009
1st Place, Graduate Exhibition Poster Competition 2010
IOP Select Publications 2011

Memberships in professional societies:
Tau Beta Pi (The Engineering Honor Society)
Institute of Electrical and Electronic Engineers
American Medical Association
Aesculapians (Medical Service Honor Society)

Publications/Posters:
1. Jessin John, Yuefa Li, Jinsheng Zhang, Jeffrey Loeb, and Yong Xu, "*Microfabrication of 3D Neural Probes with Combined Electrical and Chemical Interfaces,*" Journal of Micromechanics and Microengineering. 2011.
2. Jessin John, Yuefa Li, Dan Barkmeier, Jeffrey Loeb, and Yong Xu, "*High Density Microelectrode Arrays for the Study and Treatment of Epilepsy*," 2009 Engineering Principles in Biological Systems Conference, Cold Spring Harbor Laboratory, Hinxton, UK
3. Jessin John, Yuefa Li, Dan Barkmeier, Jeffrey Loeb, and Yong Xu, "*High Density Microelectrode Arrays for the Study and Treatment of Epilepsy*," Graduate Exhibition 2010 Conference, Wayne State University, Detroit, MI
4. Yuefa Li, Jessin John, Xueguo Zhang, Jinsheng Zhang, Jeffrey Loeb and Yong Xu, "*3D neural probes with combined electrical and chemical interfaces*," Hilton Head Workshop 2010: A Solid-State Sensors, Actuators and Microsystems Workshop, Hilton Head Island, SC, June 6-10, 2010.